2017

Wideband Low Side Lobe Aperture Coupled Patch Phased Array Antennas

Dhruva Poduval
University of South Carolina

WIDEBAND LOW SIDE LOBE APERTURE COUPLED PATCH PHASED ARRAY ANTENNAS

by

Dhruva Poduval

Bachelor of Engineering
Fr. C. Rodrigues Institute of Technology, University of Mumbai, 2010

Submitted in Partial Fulfillment of the Requirements

For the Degree of Master of Science in

Electrical Engineering

College of Engineering and Computing

University of South Carolina

2017

Accepted by:

Mohammod Ali, Director of Thesis

Grigory Simin, Reader

Cheryl L. Addy, Vice Provost and Dean of the Graduate School

ACKNOWLEDGEMENTS

I am very grateful to my thesis advisor Dr. Mohammod Ali for his patience, advice and encouragement throughout this endeavor. Without his support this research would not have been possible.

I would also like to thank my colleague Dr. Chamok Nowrin Hasan for all the help and assistance that he provided me with when I just started working on this thesis. I have got to learn a great deal from him.

Lastly, I would like to thank my parents for all their blessings and financial support which has enabled me to attend graduate school.

ABSTRACT

Low profile printed antenna arrays with wide bandwidth, high gain, and low Side Lobe Level (SLL) are in great demand for current and future commercial and military communication systems and radar. Aperture coupled patch antennas have been proposed to obtain wide impedance bandwidths in the past. Aperture coupling is preferred particularly for phased arrays because of their advantage of integration to other active devices and circuits, e.g. phase shifters, power amplifiers, low noise amplifiers, mixers etc. However, when designing such arrays, the interplay between array performance characteristics, such as gain, side lobe level, back lobe level, mutual coupling etc. must be understood and optimized under multiple design constraints, e.g. substrate material properties and thicknesses, element to element spacing, and feed lines and their orientation and arrangements with respect to the antenna elements. The focus of this thesis is to investigate, design, and develop an aperture coupled patch array with wide operating bandwidth (30%), high gain (17.5 dBi), low side lobe level (20 dB), and high Forward to Backward (F/B) ratio (21.8 dB). The target frequency range is 2.4 to 3 GHz given its wide application in WLAN, LTE (Long Term Evolution) and other communication systems. Notwithstanding that the design concept can very well be adapted at other frequencies.

Specifically, a 16 element, 4 by 4 planar microstrip patch array is designed using HFSS and experimentally developed and tested. Starting from mutual coupling minimization a corporate feeding scheme is designed to achieve the needed performance.

To reduce the SLL the corporate feeding network is redesigned to obtain a specific amplitude taper. Studies are conducted to determine the optimum location for a metallic reflector under the feed line to improve the F/B. An experimental prototype of the antenna was built and tested validating and demonstrating the performance levels expected from simulation predictions. Finally, simulated beam scanning in several angles of the array is shown considering specific phases for each antenna element in the array.

TABLE OF CONTENTS

LIST OF TABLES

LIST OF FIGURES

Chapter 1: Introduction

1.1 Motivation for Work

Broadband antennas have been an active area of research for some decades now. Applications for broadband antennas range from high speed WLAN systems, radars, remote sensing, cognitive radio, etc. Most of these applications require antennas that are compact and have a conformal design which can very easily be inserted or placed on to the surface of a vehicle or aircraft. In this regard, microstrip antennas [1-5] are preferred compared to other bulky broadband antennas like horn antennas and helical antennas. But these low-profile antennas have a major disadvantage due to their inherently narrow bandwidth. This problem can be overcome though by using techniques like creating stacks and changing the feeding technique. One simple way to achieve a wider bandwidth is feeding the antenna through an aperture, the merits and demerits of which have been discussed in the next chapter. But when designing an antenna for a high data rate communication system or radar or sensing applications bandwidth is not the only key parameter. A high level of directivity, narrow beamwidth and low levels of sidelobe radiation are also needed. A broadband high gain antenna with a narrow beamwidth and low sidelobes enables the user to transmit a large amount of data over greater distances with a high level of spatial selectivity. One of the problem which come along with using

an aperture coupled feed is the high levels of backlobe radiation. A high level of backlobe radiation is almost always unacceptable for any kind of communication system. Not only does it decrease antenna efficiency, it also causes a great deal of power to be transmitted to regions which might be sensitive to electromagnetic radiations. This is caused due to the apertures radiating in both the forward and backward direction and must be addressed.

Considering all the above mentioned requirements and concerns, a broadband aperture coupled phased array antenna has been proposed in this thesis. Specifically a 4 by 4 rectangular aperture coupled phased array antenna has been designed, simulated, fabricated and tested. The array was designed with a target operating frequency range of 2.4 to 3 GHz given its wide application in WLAN, LTE and other communication systems. The array design is scalable so the same design concepts can be used to create an array that works at a different frequency range. A corporate feed with appropriate power taper profile is used to feed the array. The amplitude taper is designed to obtain a SLL of 25dB. An appropriately placed metal reflector plate blocks the backlobe radiation and helps boost the F/B ratio of the antenna array. A phased array antenna has been proposed in the end and simulation results for various different scan angles have been presented.

1.2 Overview of Thesis

The first chapter goes over the objectives and motivation behind the work presented and also gives an outline of the thesis and the scope of each chapter. A single element aperture coupled patch antenna and the design metrics affecting its performance

are described in the second chapter. It also goes over the various techniques for optimizing antenna performance factors like the bandwidth and radiation pattern characteristics. The array factor, a linear four element aperture coupled patch antenna array and a planar 4X4 aperture coupled antenna array are discussed in chapter three. The main goal while designing this array was to obtain a wideband response with high directivity which is consistent throughout the bandwidth. The fourth chapter looks at aperture coupled corporate feed networks which are a widely used feeding technique for linear and planar arrays. This chapter also deals with the affect the corporate feed has on the antenna performance and looks at measures to be taken so as to obtain reasonable radiation characteristics. Techniques to minimize the sidelobe radiation of the array have been discussed in the subsequent chapter. It goes over the various amplitude tapering techniques that are used and different means of implementing them as part of a corporate feed network. Chapter five also tackles the issue faced by all aperture coupled arrays, which is high backlobe radiation caused due to apertures radiating in the backward direction. A solution in the form of a strategically placed metal reflector below the array has been presented. Chapter six deals with the fabrication, test and measurement of the antenna array. The reflection coefficients and radiation patterns of the arrays are measured and compared with the simulation results. The phased array antenna is described in the seventh chapter, the required phasing, beam steering concepts and the various simulation results are presented in this section, which is then followed by the conclusion and future scope of this work.

Chapter 2: Aperture Coupled Patch

2.1 Introduction

The rapid development of patch antenna technologies began in the 1970s [6]. By the early 1980s microstrip patch antenna technology was fairly well developed and researchers were looking at techniques to improve and optimize the performance features like gain and bandwidth and were looking to increase the applications of this technology. Microstrip patch antennas seemed to be the ideal candidate for integrated phased array systems as it was very easy to incorporate printed circuits with the Microwave Integrated Circuit (MIC) or Monolithic Microwave Integrated Circuit (MMIC) transmit/receive, phase shifting, biasing and other circuitries of the system.

The first aperture coupled microstrip antenna was fabricated and tested by a graduate student, Allen Buck, on August 1, 1984, in the University of Massachusetts Antenna Lab [7] and since then it has piqued the interest of researchers and engineers around the globe and has undergone a considerable amount of research and development to improve its performance features. Some of the advantages and recent developments in aperture coupled patch technologies are listed below [8]:

- High impedance bandwidth, ranging from 5% to 50%
- Freedom to choose different substrates for antenna and feed sections
- Isolation of the feed network from the antennas via the ground plane

- Increased substrate space for antenna elements and feed lines
- Minimal cross-polarization in the principal planes
- Ease of integration for active arrays
- Higher degree of freedom in terms of deciding patch shape, feed line lengths, aperture size and shape, radomes, etc.
- Extension of these techniques to aperture coupled microstrip line couplers, waveguide transitions, dielectric resonators, etc.

2.2 Slot Fed Patches

The figure below represents the basic structure of an aperture coupled patch antenna. It usually consists of two substrates, one being the antenna substrate and the other being the feedline substrate. The two substrates are separated by a ground plane with an aperture cut out. This aperture helps in coupling the electromagnetic waves from the feedlines to the patch antenna and the resonant frequency of the patch and the slot are chosen in close proximity if a wider bandwidth is desired. The figure below represents the simplest aperture coupled patch antenna design. Many modifications like extra layers, altered aperture shapes, antenna shapes, etc. are possible with the aperture coupling technique so as to achieve the desired radiation pattern characteristics.

Some of the important parameters that effect the antenna performance are as follows:

- Antenna Substrate: The substrate's loss tangent affects the radiating efficiency of the antenna. To avoid efficiency losses one should try to use a substrate with the lowest loss tangent possible. The substrate permittivity affects the dimensions of the radiating patch at the resonant frequency. Lower permittivity also reduces

surface waves. The permittivity of the antenna substrate is usually lower than that of the feed substrate. The thickness of the antenna substrate affects the bandwidth and coupling of the antenna. Thicker substrate increases impedance bandwidth but reduce coupling between the feed line and the radiating patch. It also reduces the resonant frequency of the patch.

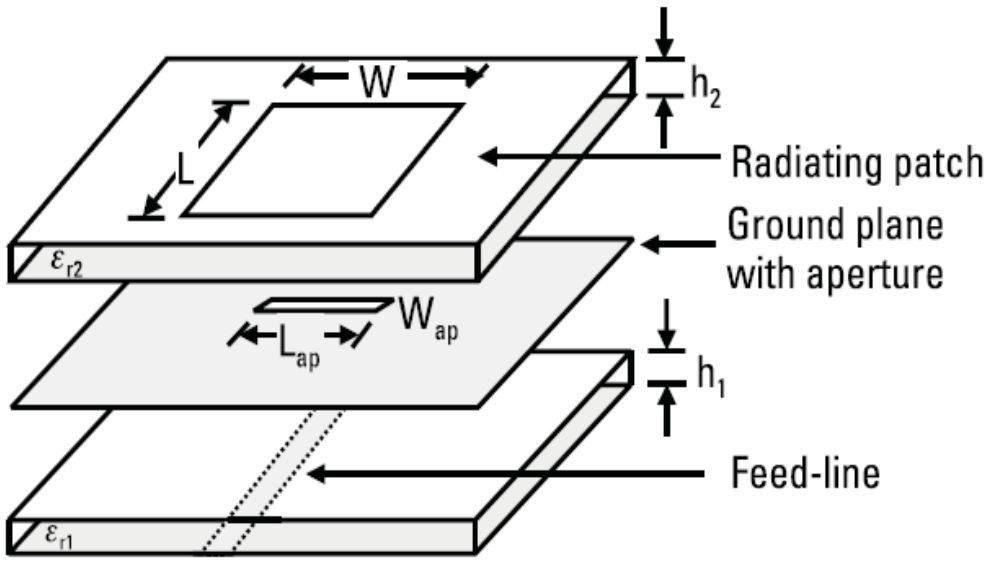

Figure 2.1: Aperture coupled array.

- Microstrip Patch Length and Width: The length determines the resonant frequency of the patch. The width controls the resonant resistance of the patch. Wider patch gives a lower resistance.
- Ground Plane Size: The size of the ground plane needs to insure that there will be no back radiation or unwanted currents on the edge of the ground plane which could also radiate.

- Feed Substrate: Low loss tangent is needed to avoid any loss in efficiency in the coupling between the microstrip transmission line and the aperture. Substrate permittivity and height determine the width of the microstrip transmission line for given impedance. Higher permittivity and thinner substrates result in a stronger coupling [7].
- Aperture Length and Width: For resonant slots the length is comparable to half the wavelength of the antenna. The length governs the coupling level and can be used to increase the impedance bandwidth of the antenna. Generally the ratio of the slot length to width is kept around 10:1 [7]. The input resistance at resonance increase as the ratio increases.
- Position of the Slot with respect to Patch: The slot should be centered under the patch. The magnetic field of the patch is maximum at the center therefore that leads to maximum coupling.
- Feed Line Width: Determines the characteristic impedance of the feed line.
- Stub Length: Shorter stubs move the impedance circle clockwise toward capacitive part of the Smith chart. The stub can be used to tune the reactance of the aperture [7].
- Position of Feed Line with respect to Slot: The feed line should be perpendicular to the center of the slot.

2.3 Design and Optimization of Single Element Aperture Coupled Patch Antenna

We initially looked into various antenna substrates that could be used as our antenna substrate and feedline substrate. Preliminary simulations were conducted with FR4, Duroid 5880, polyethylene and RO4003c. All simulations were carried out using

ANYSYS HFSS and we finally decided to use RO4003c (ε_r=3.55, tanδ=0.002) for both the antenna substrate and also the feedline substrate.

As it is known, the bandwidth of a resonant antenna is inversely proportional to its Quality-factor [9], so one of the techniques used to improve the impedance bandwidth of an aperture coupled patch antenna is to use thicker antenna substrates with very low permittivity, with air being the most ideal material. Doing this eliminates and/or reduces the generation of surface waves which minimizes dielectric losses. On the other hand the efficiency of the antenna is found to be inversely proportional to the relative permittivity of the antenna substrate. This relationship between the antenna bandwidth and the substrate thickness and also the relationship between the relative permittivity of the substrate with the radiation efficiency has been studied in detail in [10-11]. Since the patches cannot be placed in air, low permittivity foams are used. The design being used by us is very similar to the SSFIP (Strip-Slot-Foam-Inverted Patch) design used in [12-13]. The only difference being that the antenna substrate layer is not inverted, but uses a very thin layer of non-inverted dielectric. The foam being used is a high performance, high frequency foam which was provided to us by ROHACELL and is called ROHACELL 71HF (ε_r=1.075, tanδ<0.0002). Further details can be found at [14].

Fig. 2.2 shows the cross-sectional view of the designed antenna and Fig. 2.3 shows us the top view. The length and width of the patch were calculated theoretically [9] at an operating frequency of 2.45GHz and were backed up by simulation. The patch has a length of L=41.4mm and width of W=33.1mm. The antenna substrate thickness is denoted as t_a, the feedline substrate thickness is denoted as t_f and the thickness of the foam spacer required is h_a. We represent the length and width of the slot as l_s and w_s

respectively. Another important parameter that must be determined is the length of the open circuit stub that is needed to tune the feedline so as to obtain the maximum possible coupling between the feedline and the patch. This length is represented as l_{oc} and the separation of the patch from the edge is S=62.5mm ($\lambda/2$).

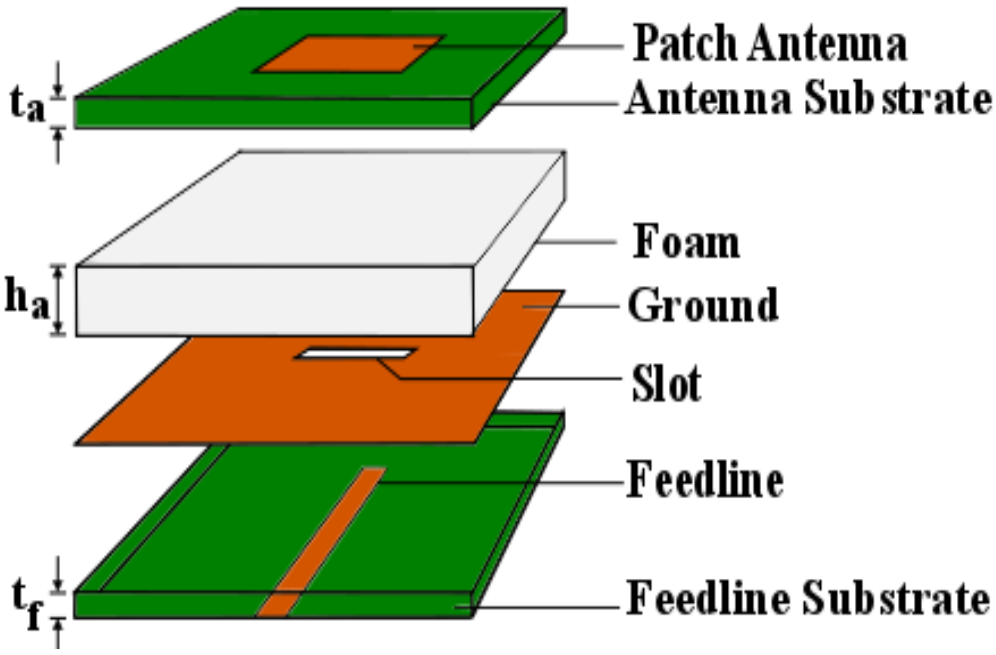

Fig. 2.2: Cross-sectional view of antenna.

To determine the optimum thickness for each layer, multiple parametric simulations were run to optimize the design. The aperture size and the feedline length were also tuned to get the maximum possible coupling between the feedline and the patch antenna. In the section below we look at the various parametric simulations used to optimize the s_{11} performance of the aperture coupled patch so as to obtain a wide bandwidth. To find the best possible configuration of all parameters and which of them work together best, all parameters discussed below were varied simultaneously in a very large simulation setup. Then from this large group the best performing configurations

were selected and then each parameter was individually tuned to obtain optimum results and this reduced set has been presented in the section below as it would be very laborious and unproductive to discuss all of it.

2.3.1 Optimizing the Thickness of the Antenna Substrate

The antenna substrate thickness needs to be optimum so as to maximize the impedance bandwidth while at the same time it also needs to allow good coupling between the slot and the patch. Fig. 2.4 compares the S_{11} performance of the aperture coupled patch when the antenna substrate thicknesses is varied from 0.2mm to 1.4mm in steps of 0.4mm, while all other parameters were kept constant. Simulations were carried out for a larger range of thicknesses with smaller step sizes, but only a small number of them are presented in each of these cases for the sake of brevity. We see that the best S_{11} performance at 2.45GHz, and also the best impedance bandwidth is obtained when the substrate thickness t_a=1mm.

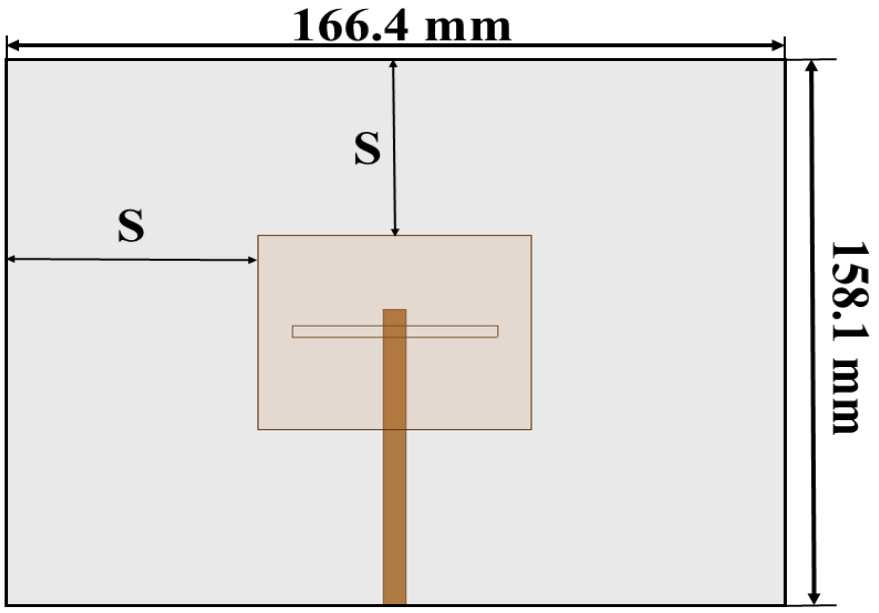

(a)

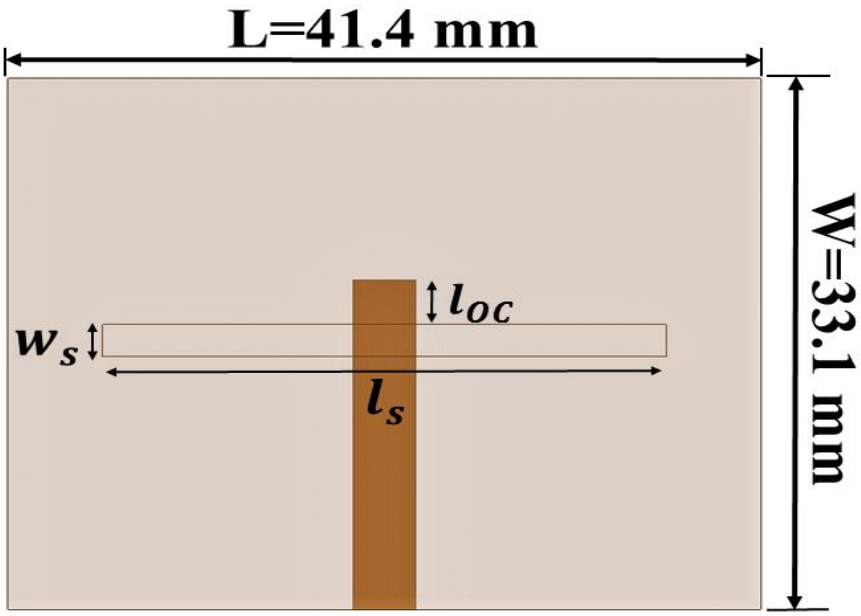

(b)

Fig. 2.3: (a) Top view of antenna, (b) Top view of patch.

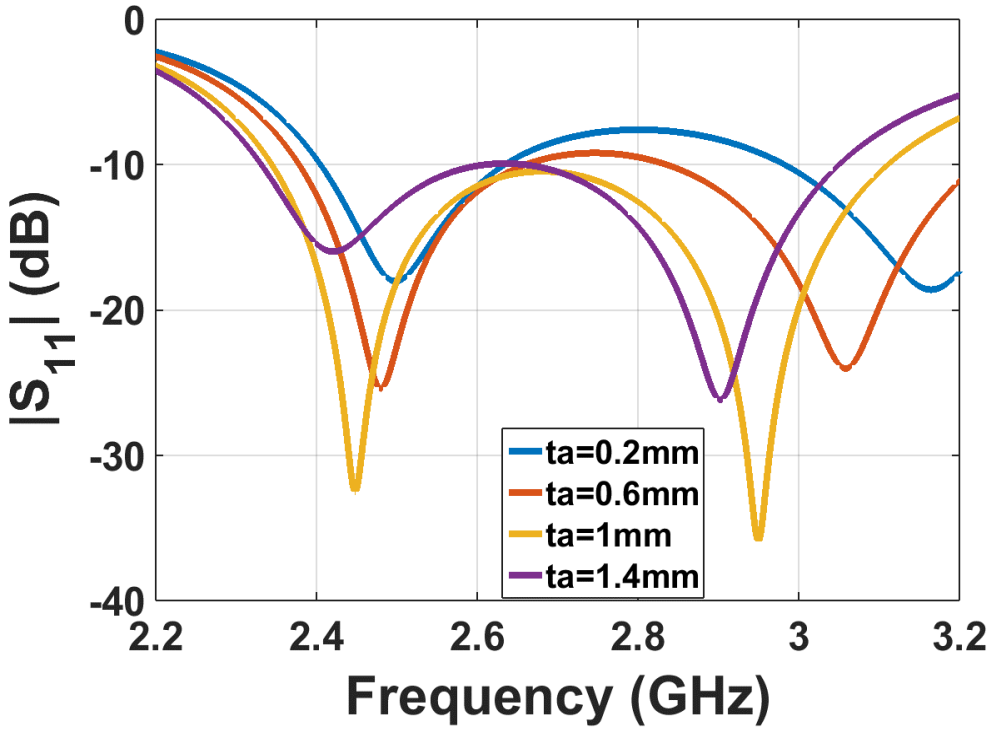

Fig. 2.4: S_{11} response when thickness of antenna substrate is varied.

2.3.2 Optimizing the Thickness of the Foam

As mentioned earlier, a layer of foam is used to separate the antenna substrate from the ground plane. The main role of this foam is to help increase the thickness of the antenna substrate while keeping the relative permittivity low so that we can try to achieve a wide bandwidth while maintaining a high level of radiation efficiency. And the foam being used comes as close to air as possible with a relative permittivity of 1.075 and has virtually no loss. To obtain the best case scenario where we obtain a high bandwidth with a high gain, the thickness of the foam spacer is very crucial. The S_{11} response obtained when the thickness of the foam is varied from 9mm to 11mm can be seen in Fig. 2.5. No major variation is observed in the S_{11}, but we see that we obtain a relatively wider band response when the foam spacer thickness is h_a=10mm.

2.3.3 Optimizing the Thickness of the Feedline Substrate

Thinner feedline substrates help in better coupling between the lines and the slot. The thickness and permittivity also play an important role in the size of the microstrip lines being used. The Fig. 2.6 shows how the S_{11} changes with the change in thickness of the feedline substrate. The optimum S_{11} plot is obtained when the thickness of the lower substrate is 1.52mm. This high difference is seen mainly due to the impedance of the line changing as we change the thickness of the substrate. It is possible for us to match the feedline at these various thicknesses and obtain a better S_{11} performance at each of these substrate sizes. We see that for the current configuration the best match is found when the feedline substrate is t_f=1.5mm thick and the feedline used is 3.5mm wide (50Ω

characteristic impedance). But the actual thickness of commercially available RO4003c is 1.52mm and this value will be used henceforth.

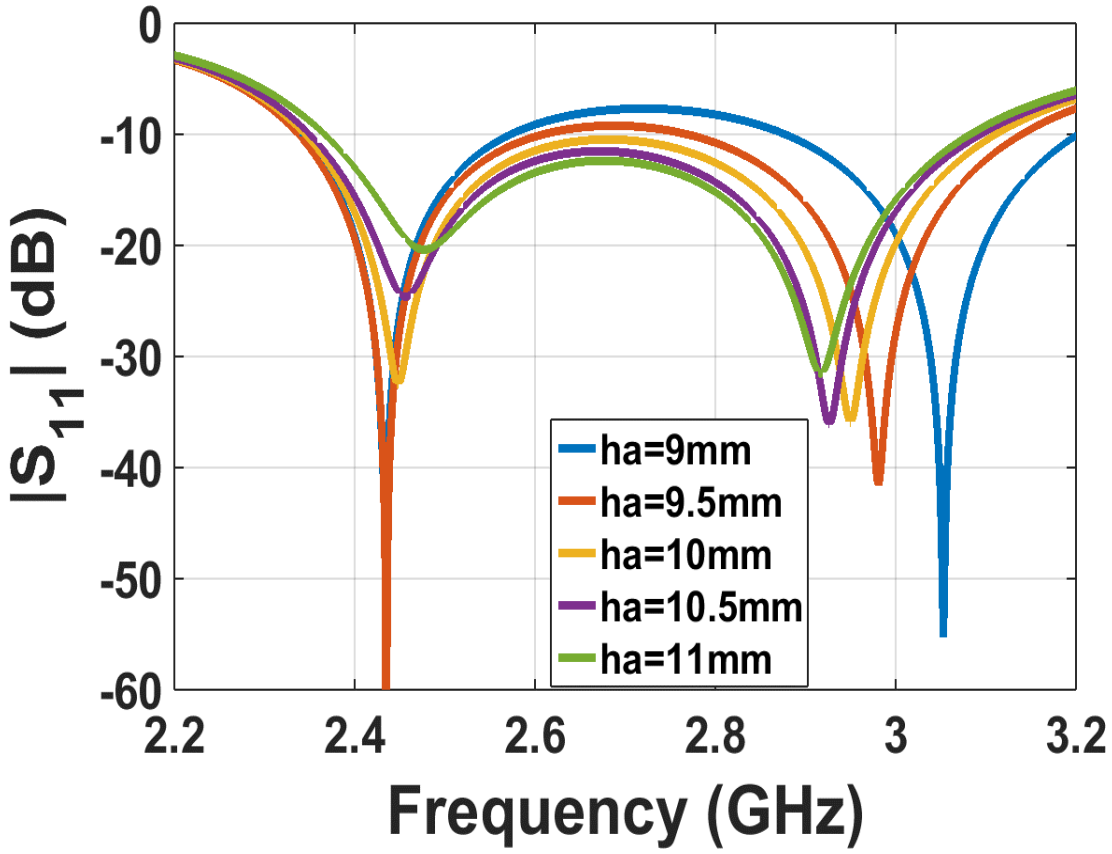

Fig. 2.5: S_{11} response when thickness of foam spacer is varied.

2.3.4 Tuning the Feedline Stub Length

Fig. 2.7 below shows the S_{11} in dB as a function of the feedline stub length. The feedline is aligned such that it passes through the center of the aperture and the aperture is placed right in the middle of the patch so as to maximize the energy coupled. This input feedline is then followed by an open circuit stub. The function of this stub is to tune the feedline and the patch. The length of the stubs are measured from the center of the

aperture. The best coupling is obtained when the stub is of length l_{oc}=3.75mm, measured from the center of the slot.

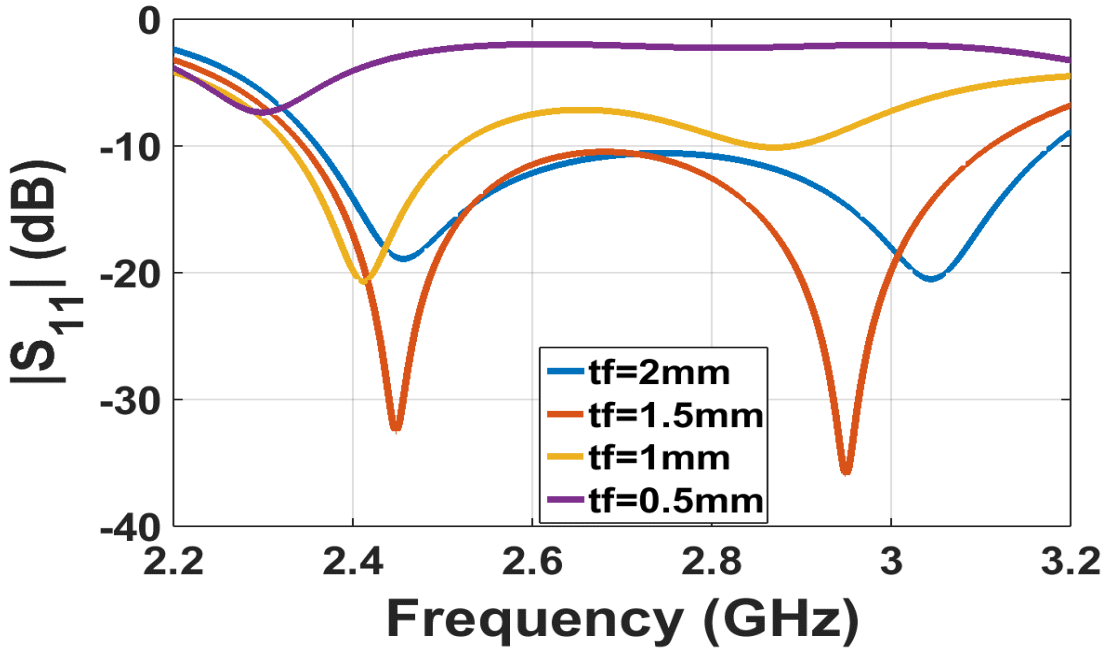

Fig. 2.6: S_{11} response when thickness of feedline substrate is varied.

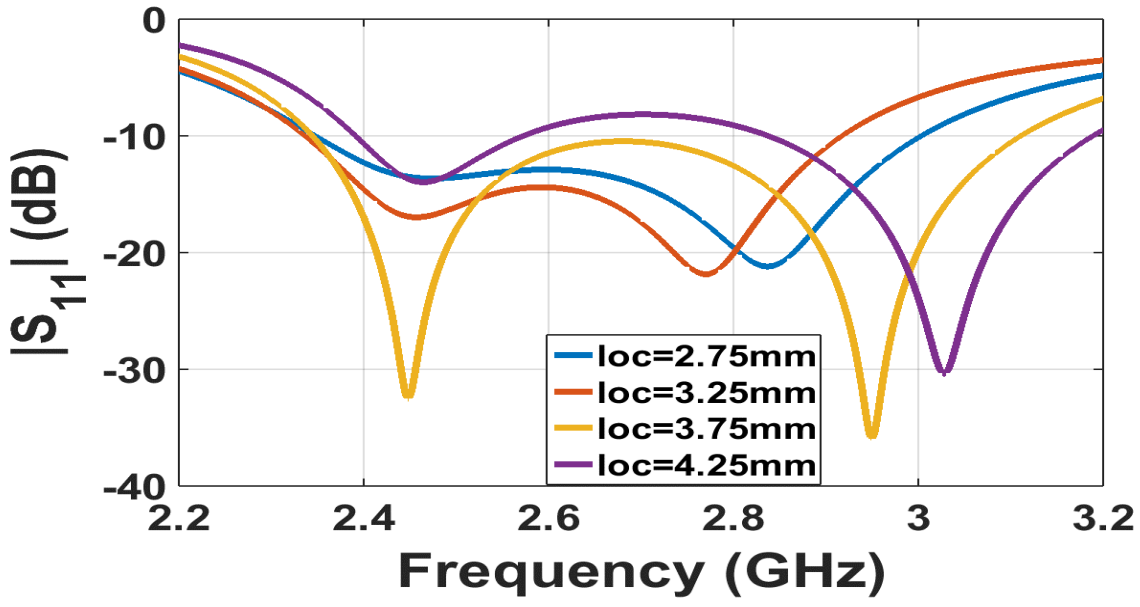

Fig. 2.7: S_{11} response as a function of the length of OC stub at the end of feedline.

2.4 Design of Single Element Patch Antenna

From the various parametric simulations a patch design was finalized, the parameters of which are listed in the table below.

Table 2.1: Antenna parameters.

Parameter	Dimensions
Length of Patch	41.4 mm
Width of Patch	33.1 mm
Antenna Substrate Thickness	1 mm
Feedline Substrate Thickness	1.52 mm
Thickness of Foam	10 mm
Length of Stub	3.75 mm
Aperture Size	31 mm X 2 mm

The S_{11} response of the selected antenna is as shown in Fig. 2.8 below. The impedance bandwidth ranges from 2.34GHz to 3.1GHz, which is a 27.9% bandwidth. And the value of S_{11} at 2.45GHz is -32.3dB. The radiation pattern for this aperture coupled patch antenna has been plotted out in Figure 2.9. The radiation pattern plots have been shown at 2.45GHz, 2.65GHz, 2.85GHz and 3.05GHz to show that the antenna works across the entire bandwidth. Each plot shows the radiation pattern in the $\Phi=0^o$ plane and also the radiation pattern in the $\Phi=90^o$plane. The z-axis lies along the broadside of the antenna, the positive x lies along the width whereas the y-axis lies along the length of the patch antenna.

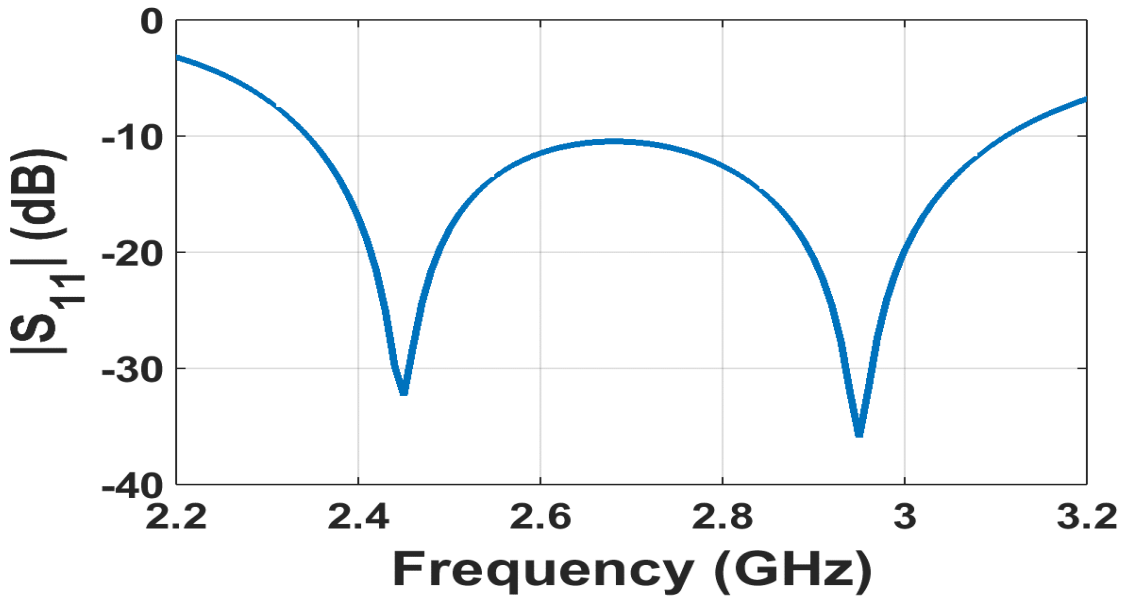

Fig. 2.8: S_{11}.

The maximum realized gain of this antenna at the four shown frequencies are 8.9, 9.1, 9.7 and 9.5 dBi respectively. The main lobe is normal to the plane of the patch antenna, hence it is a broadside antenna. One of the unwanted side-effects of using aperture coupling based feeding techniques is a high level of back lobe radiation. This is caused by the aperture and patch resonating at frequencies which lie very close to each other [12] which causes the slot to radiate in both directions of the ground plane. The back lobe radiation for this single element antenna at the four frequencies are -1.2, -8.5, -18 and -7.5 dBi respectively, which puts the Front to Back (F/B) ratios at 10.1, 17.5, 27.3 and 17 dB. There is a significant increase in the back lobe radiation when using an array of aperture coupled antennas and this can sometimes be unacceptable in certain applications depending on the level of backlobe radiation. This problem of high levels of radiation in the backlobe is discussed and steps to mitigate this have also been developed in later chapters.

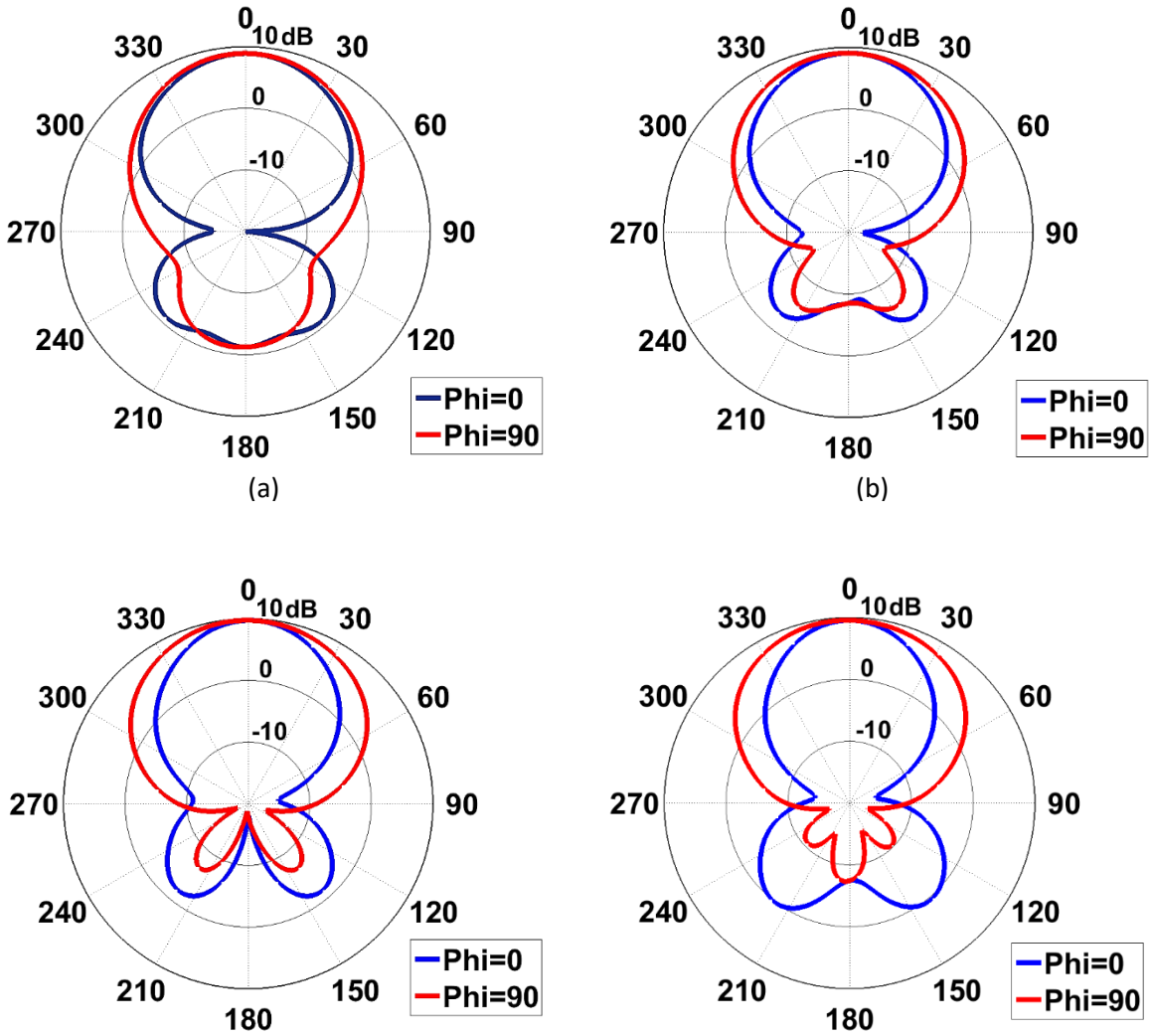

Fig. 2.9: Radiation pattern plots at (a) 2.45 GHz, (b) 2.65 GHz, (c) 2.85 GHz, (d) 3.05 GHz.

Chapter 3: Linear and Planar Array Antennas

3.1 Introduction

This chapter discusses one dimensional linear arrays and planar array antennas and introduces the array factor, which is one of the characteristic properties that is used to define an antenna. We can determine the radiation pattern of an array of antennas by knowing the radiation pattern of a signal element in the array and then multiplying it with the array factor. Chapter three also goes over the design procedure of a four element linear array and a 16 element, 4X4 planar array of aperture coupled patch antennas. We look at simulation results obtained for the S-parameters of these antennas, their radiation patterns (Realized gain) and their directivities. The main design goals currently in this section are to obtain the maximum possible impedance bandwidth around 2.45GHz, to obtain the maximum possible realized gain while keeping the back lobe radiation as low as possible.

3.2 The Array Factor

Antennas with a known radiation pattern can be organized in various different configurations to yield different radiation patterns. The single most important advantage of creating an antenna array is that it boosts the directivity. We have several design variables at our disposal which can be altered to manipulate the radiation pattern as we desire. The array design variables are,

- Geometric arrangement of elements (linear, circular, planar, stacked, etc.)
- Inter-element spacing
- Excitation amplitude of the individual elements
- Excitation phase of the individual elements
- Radiation pattern of elements

The first design presented in this chapter is a linear array of four identical rectangular patches of dimensions 33.1mm by 41.4mm which are spaced uniformly and the second design discussed is a planar 16 element antenna array with uniform spacing and identical design parameters as before. When given an antenna array of identical elements, the radiation pattern of the array can be found using the principle of pattern multiplication [9]. Pattern multiplication theorem means that the radiation pattern of an array is the product of the radiation pattern of a single element in the array times the Array factor, *i.e.*

Array Pattern = Pattern of array element x Array factor (AF)

Without going into the derivation, the Array factor for a linear array of 'N' identical elements with an inter-element spacing of "d" is given by [15],

$$AF = \sum_{i=1}^{N} w_i e^{jb_i} \quad \ldots (3.1)$$

And,

$$w_i = e^{jkidcos\theta_d} \quad \ldots (3.2)$$

Here w_i is the weight assigned to the i^{th} element, b_i is the phase of the i^{th} element and θ_d is the angle at which we want our antenna to radiate. In this case we are assuming a uniform amplitude of excitation for each element. By changing the progressive phase shift between the elements of an array we can electronically steer the antenna main beam to any angle we desire. And by optimizing the excitation amplitude of each element we can manipulate the main lobe gain and the side lobe level of the antenna array. We get the maximum realized gain for an array when the elements have a uniform amplitude and phase excitation. For a non-uniform amplitude broadside array with even number of elements the array factor can be simplified and written as [16],

$$AF = \sum_{i=1}^{N} w_i \cos\left[\frac{(2i-1)}{2} kd\cos\theta\right] \quad \ldots (3.3)$$

Where $k = \frac{2\pi}{\lambda}$ and d is the inter-element spacing. We can extend the same argument to a two-dimensional planar array. Now, if we consider that M such linear arrays are placed together with a separation of d between them, we obtain an N X M planar array, whose array factor can be expressed as,

$$AF = \sum_{i=1}^{N} \sum_{j=1}^{M} w_{ij} e^{jb_i} e^{jb_j} \quad \ldots (3.4)$$

A more simplified form of the normalized array factor for a planar array can be written as [9, 16],

$$AF(\theta,\varphi) = \left\{\frac{\mathrm{Sin}\left(\left(\psi_x\frac{M}{2}\right)\right)}{M\mathrm{Sin}\left(\left(\frac{\psi_x}{2}\right)\right)}\right\}\left\{\frac{\mathrm{Sin}\left(\left(\psi_y\frac{N}{2}\right)\right)}{N\mathrm{Sin}\left(\left(\frac{\psi_y}{2}\right)\right)}\right\} \quad \ldots (3.5)$$

Here, ψ_x and ψ_y are defined as follows,

$$\psi_x = kd_x\sin\theta\cos\phi + \beta_x \quad \ldots (3.6)$$

$$\psi_y = kd_y\sin\theta\sin\phi + \beta_y \quad \ldots (3.7)$$

In the above expression, we are assuming M is the elements placed along the x-axis whereas N is the number of elements that lie along the y-axis. Generally the inter-element spacing between the elements along the x-axis and y-axis is kept as low as possible without causing significant mutual coupling of antenna elements. But the inter-element spacing cannot be an integral multiple of the wavelength as this will give rise to grating lobes [9] which are generated due to constructive interference of the individual radiation patterns of each element causing a significant radiation pattern in a direction other than the main lobe. If we want our antenna to act as a phased array, we can steer the beam by determining the progressive phase shift required in the x- and y-directions by setting ψ_x and ψ_y equal to zero and then solving for β_x and β_y which represent the phase angle progression required in the x and y directions respectively, to move the main beam to our desired position. The inter-element separation plays a significant role when determining the maximum angle the antenna can be electronically steered while maintain acceptable levels of radiation pattern performance. We will discuss the effects of amplitude tapering, phase tapering and other nuances associated with it in detail in the chapters to come.

3.3 Four Element Linear Array

The four element linear array antenna uses the same patch lengths, widths, substrate thicknesses, and feedline and slot dimensions as the optimized single element aperture coupled patch antenna discussed in the previous chapter. The inter-element separation chosen initially is d=62.5 mm (which is $\lambda/2$). Fig. 3.1 shows the cross-sectional and top view of the antenna under study.

In this design, each element of the array is individually fed with a separate feedline. Each patch is excited with the same amplitude and phase. The S-parameters obtained from the simulation are plotted in Figs. 3.2. In this design, each element of the array is individually fed with a separate feedline. Each patch is excited with the same amplitude and phase. The S-parameters obtained from the simulation are plotted in Figs. 3.2. The four element linear array antenna has an operating frequency approximately from 2.36 GHz to 3.18 GHz, which gives us a bandwidth of 0.82 GHz which is a 29.6% bandwidth if we consider 2.45GHz as the operating frequency. The mutual coupling observed in the four plots below are seen to be quite low. This can be seen by looking at the S_{12}, S_{13} and S_{14} for the first antenna, whose values lie below -20dB almost all over the entire operating frequency. The reflection coefficient and mutual coupling coefficients seen at the other three ports follow a very similar trend due to the symmetry and simplicity of the circuit.

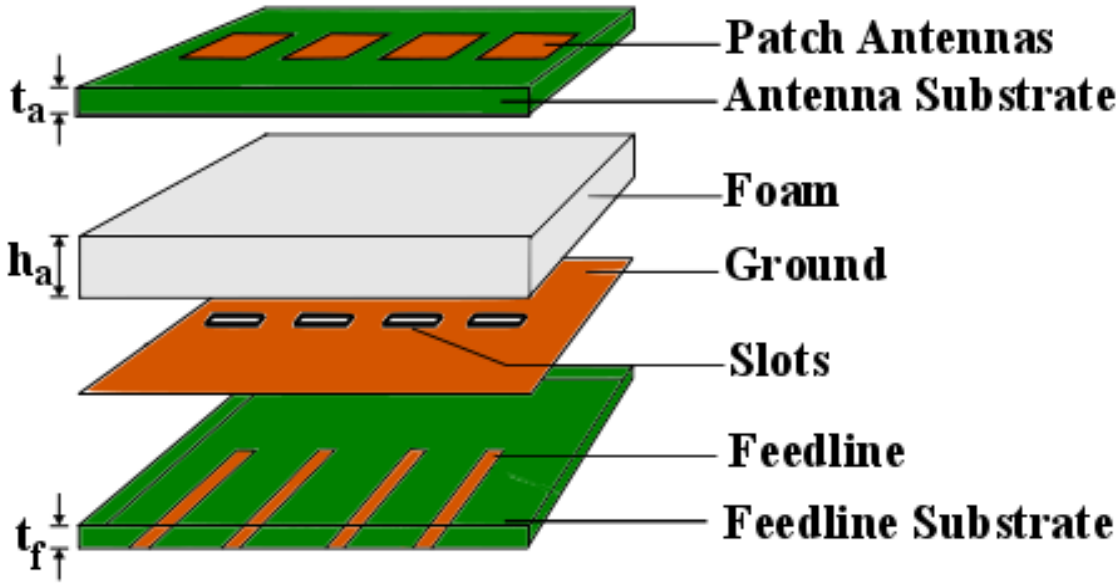

(a)

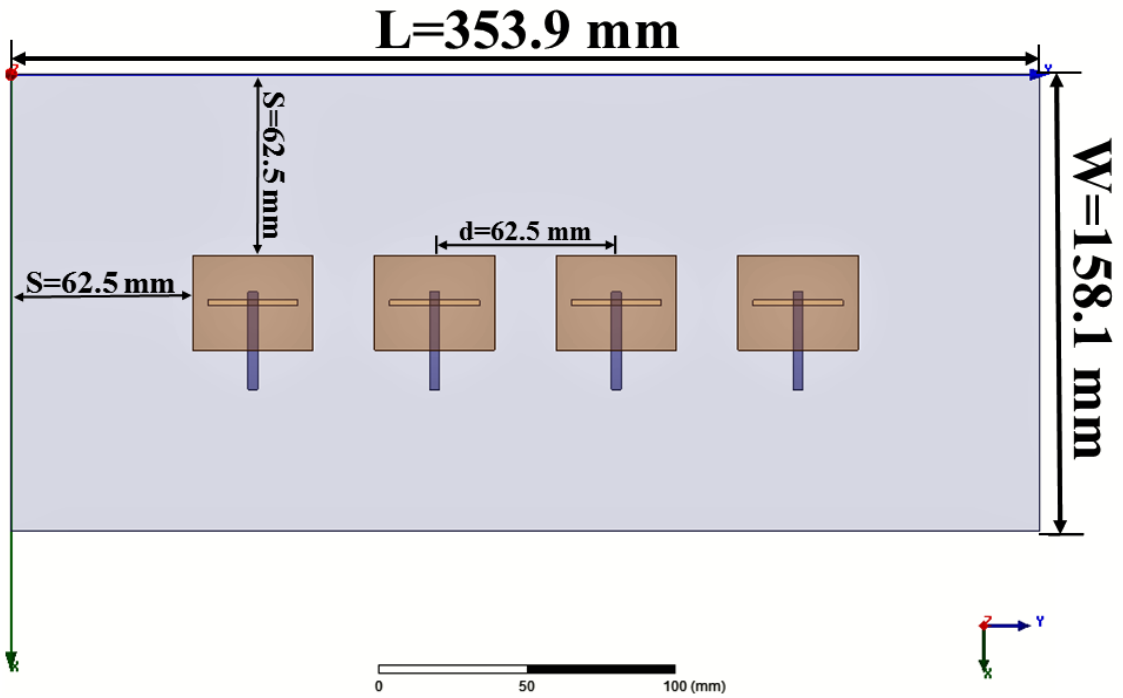

(b)

Figs 3.1: Linear array, (a) Cross-sectional view, (b) Top view.

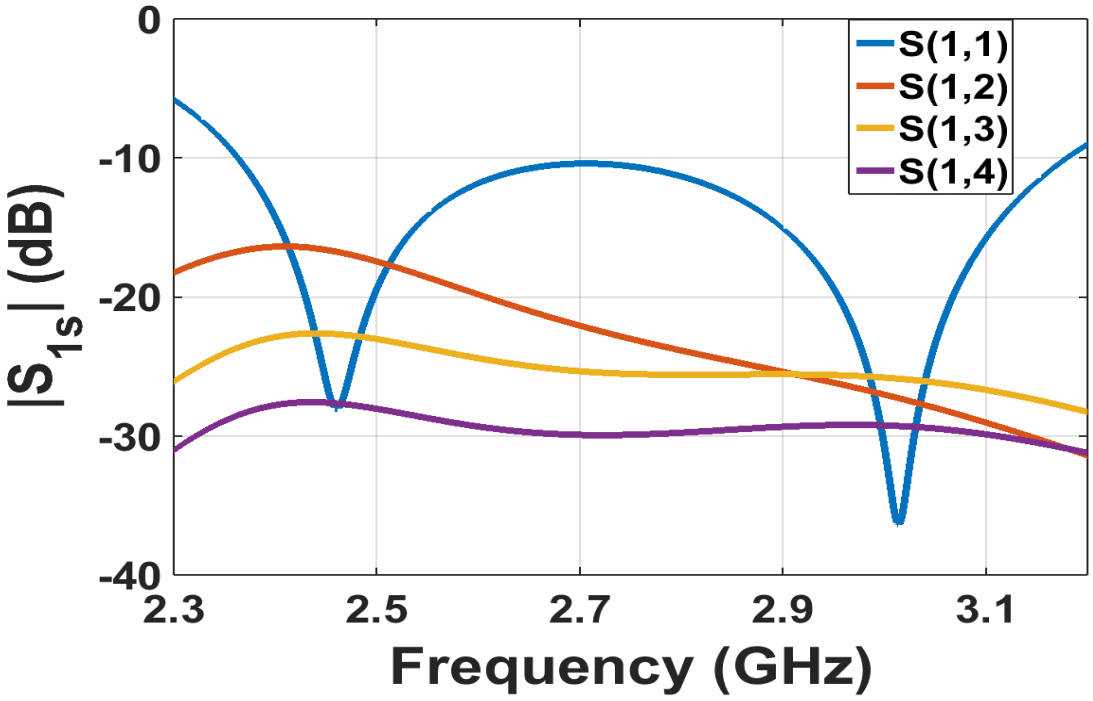

(a)

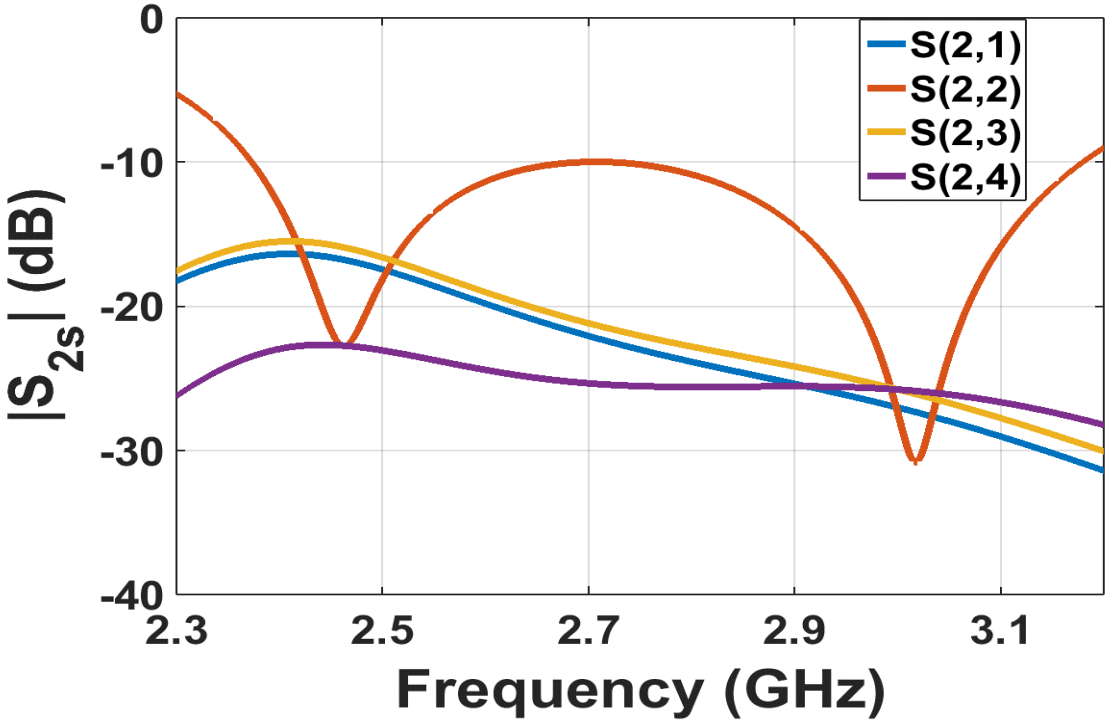

(b)

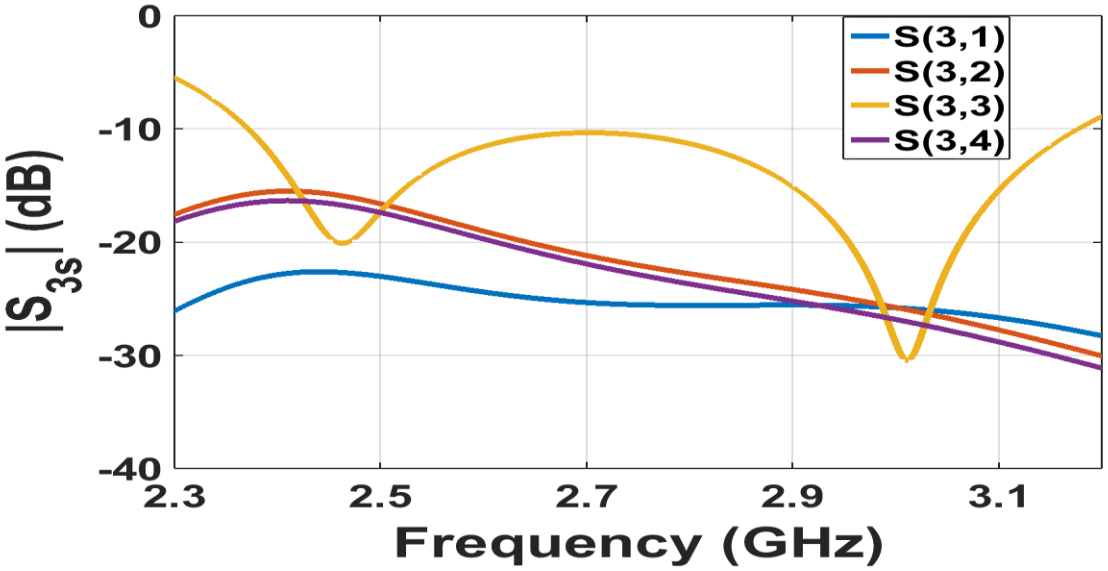

(c)

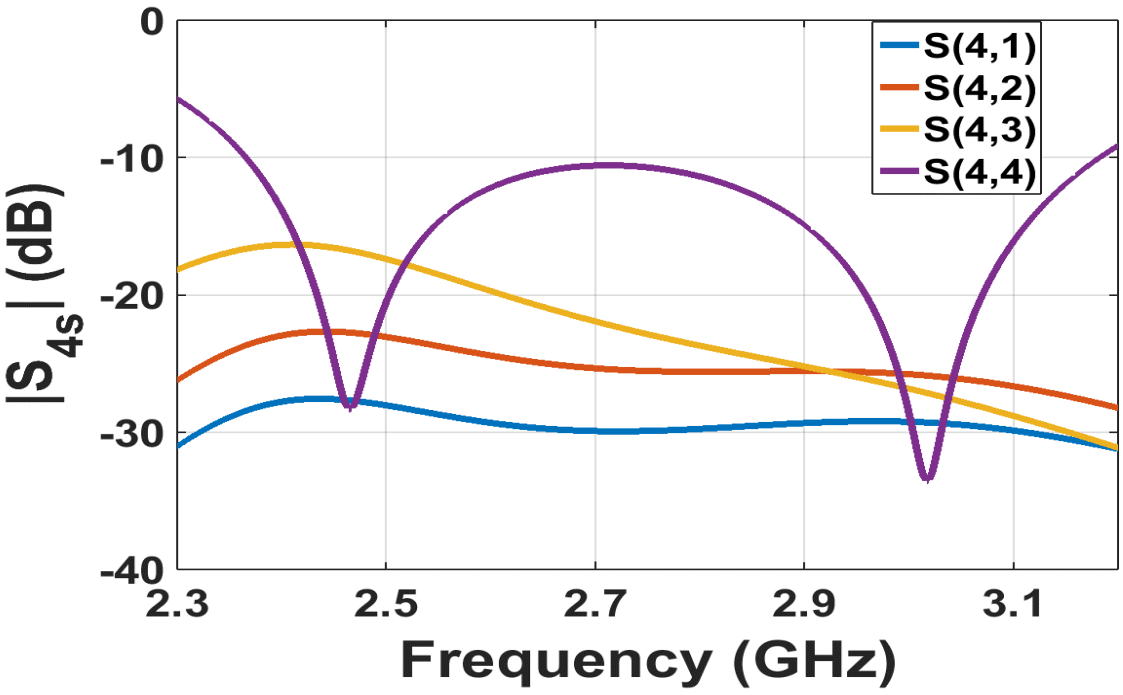

(d)

Figs. 3.2: (a) S_{11}, S_{12}, S_{13} and S_{14} (b) S_{21}, S_{22}, S_{23} and S_{24} (c) S_{31}, S_{32}, S_{33} and S_{34} (d) S_{41}, S_{42}, S_{43} and S_{44}.

Figs. 3.3 show the radiation pattern plot of the linear array at 2.45, 2.65, 2.85 and 3.05 GHz in the $\Phi=0^o$ and $\Phi=90^o$ planes. The coordinate axis has been defined in Fig. 3.1 (b). The maximum realized gain of the antenna varies from 13.2 to 14.7 dB within this operating range. The average sidelobe radiation observed varied from -0.36 to 2.4 dB. The sidelobe radiation along with the realized gain are seen to increase with frequency. The SLL is still around 13dB, which matches the expected theoretical value for the side lobe of a linear array of patch antennas which is 13.5dB [15]. The backlobe radiation is found to be significantly higher than the single element aperture coupled patch due to the presence of more slots. The F/B appear to be better at frequencies other than 2.45GHz, but this is due to the fact that backlobe radiation is defined as the lobe which is diametrically opposite to the mainlobe. But the radiation patterns seen for frequencies other than 2.45GHz have a higher level of back radiation at angles slightly displaced from 180^o. Another observation that can be made is that the radiation pattern is much more directive in the $\Phi=90^o$ plane as compared to the $\Phi=0^o$ plane. This is because the array is linear, hence the improvement in the radiation pattern can be seen only in one plane. By changing the orientation of the patches by 90^o we can obtain a similar pattern in the $\Phi=0^o$ plane too. So, if we desire highly directive radiation patterns in both the $\Phi=90^o$ and $\Phi=0^o$ plane we must construct a planar array antenna. The results for the maximum realized gain, Front to Back ratio (F/B), SLL and directivity have been summarized in Table 3.1.

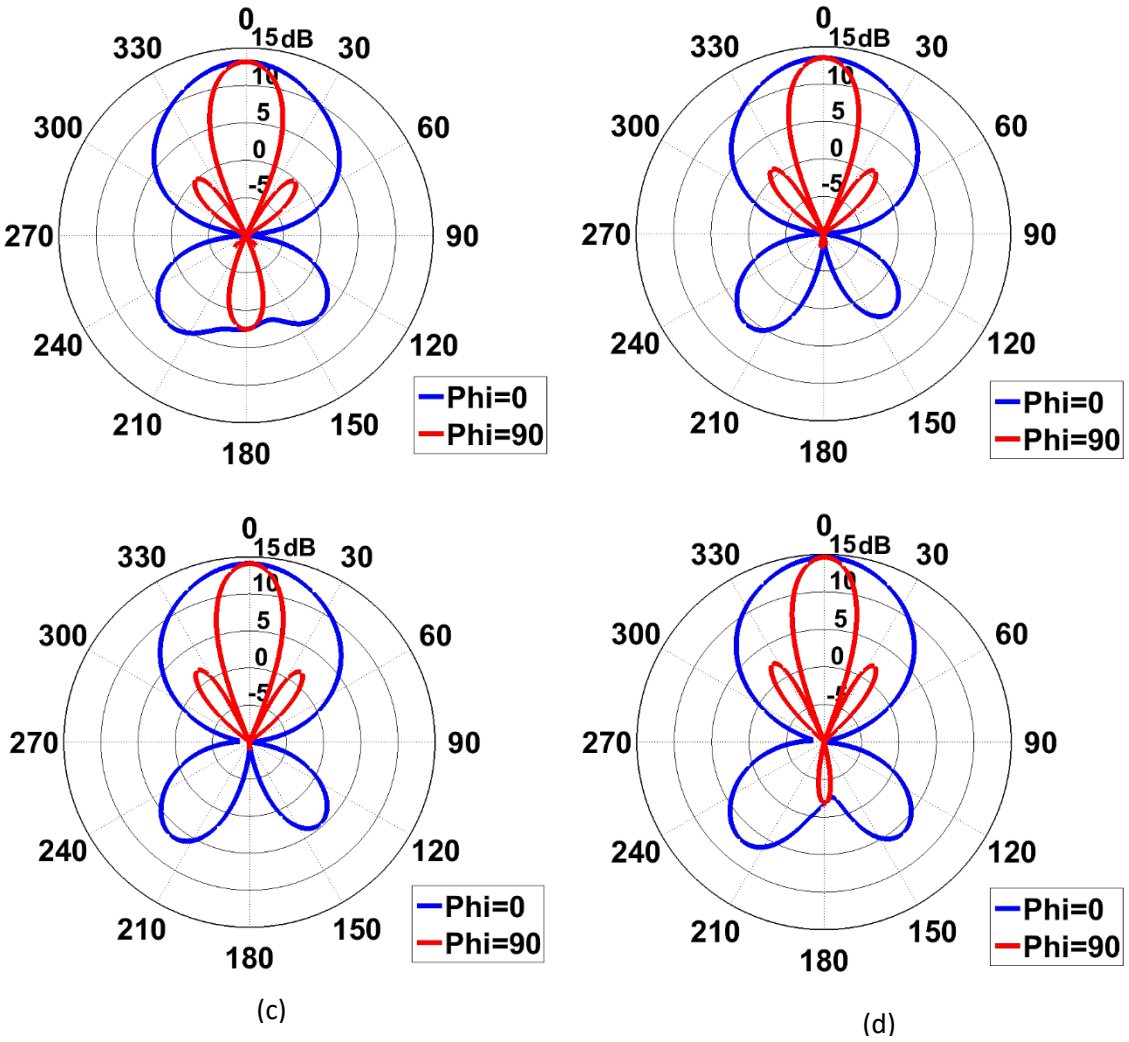

Figure 3.3: Radiation pattern of linear array.

Table 3.1: Summary of simulation results for linear array.

Frequency (GHz)	Realized Gain (dBi)	SLL (dB)	F/B (dB)	Directivity (dBi)
2.45	13.2	13.5	10.6	13.1
2.65	13.5	12.4	21.8	13.6
2.85	14.1	12.2	23	14.1
3.05	14.6	12.2	16.4	14.5

3.4 4X4 Planar Array Antenna

A 16-element, 4X4 rectangular array can be viewed as an array of 4, 4 element linear array antenna. The center to center inter-element separation between two elements in the antenna is still kept at d=62.5mm. The cross-sectional view and top view of this 4X4 planar array has been shown in Figs. 3.4.

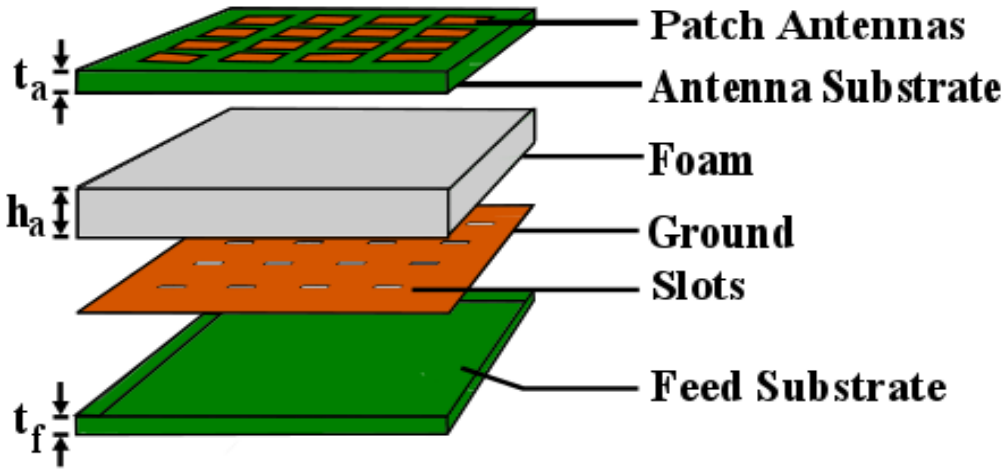

(a)

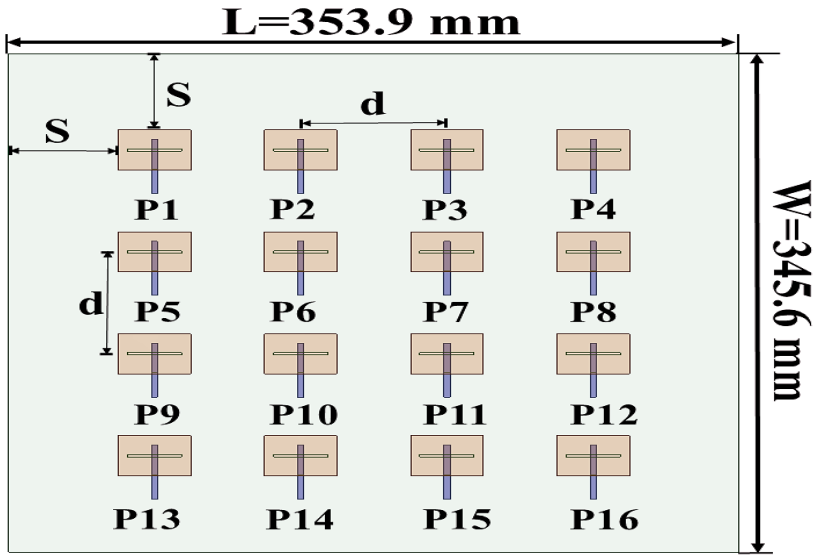

(b)

Figs 3.4: 4X4 array, (a) Cross-sectional view, (b) Top view.

The total dimensions of the antenna array is 353.9mm X 345.6mm X 12.52mm. Each element of the antenna is individually fed using separate feedlines. All 16 ports, P1 through P16 are labelled in Fig. 3.4 (b). The reflection coefficients at each port, *i.e.* the S_{nn} and the mutual coupling between the various ports, *i.e.* the S_{mn} are plotted below. Figs. 3.5 show the S_{nn} response observed in the simulation. The 16 reflection coefficients have been divided in two plots. Fig. 3.5(a) contains $S_{1,1}$ to $S_{8,8}$ while Fig. 3.5(b) depicts $S_{9,9}$ to $S_{16,16}$. All the S_{nn} plots show a very similar trend and put the operating frequency somewhere between 2.3 to 3.1 GHz, which is a minor reduction in bandwidth when compared to the 4 element linear array and can be attributed to the presence of more number of radiators packed closely together.

The mutual coupling between the various elements were evaluated and some of the poorly performing cases are plotted and presented in Figs. 3.6. Due to the array having 16 elements, there will be a total of 240 mutual coupling data sets that can be observed but the highest degree of coupling will occur between elements that are closer to each other. So Fig. 3.6 (a), (b), (c) and (d) present the S_{mn} plots observed between the elements lying on the diagonal of the array and its 4 closest neighbors. In this current configuration with an inter-element separation of d=62.5mm it is observed that the mutual coupling between antenna elements is lower than -15dB across the bandwidth.

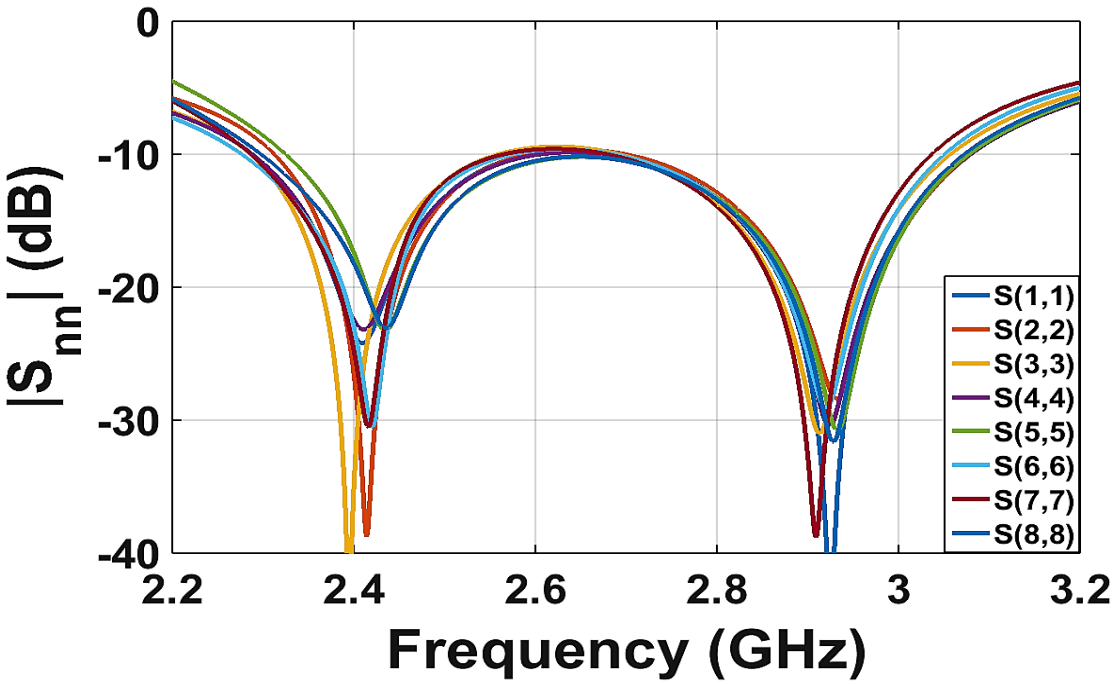

(a)

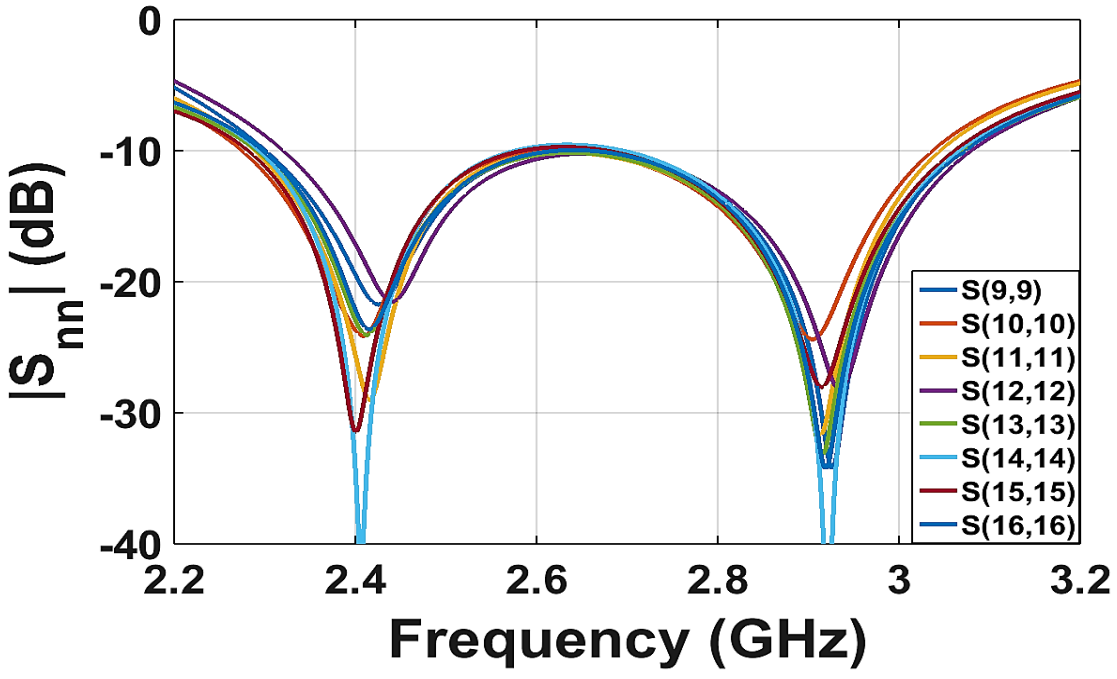

(b)

Fig. 3.5: (a) $S_{1,1}$ to $S_{8,8}$, (b) $S_{9,9}$ to $S_{16,16}$.

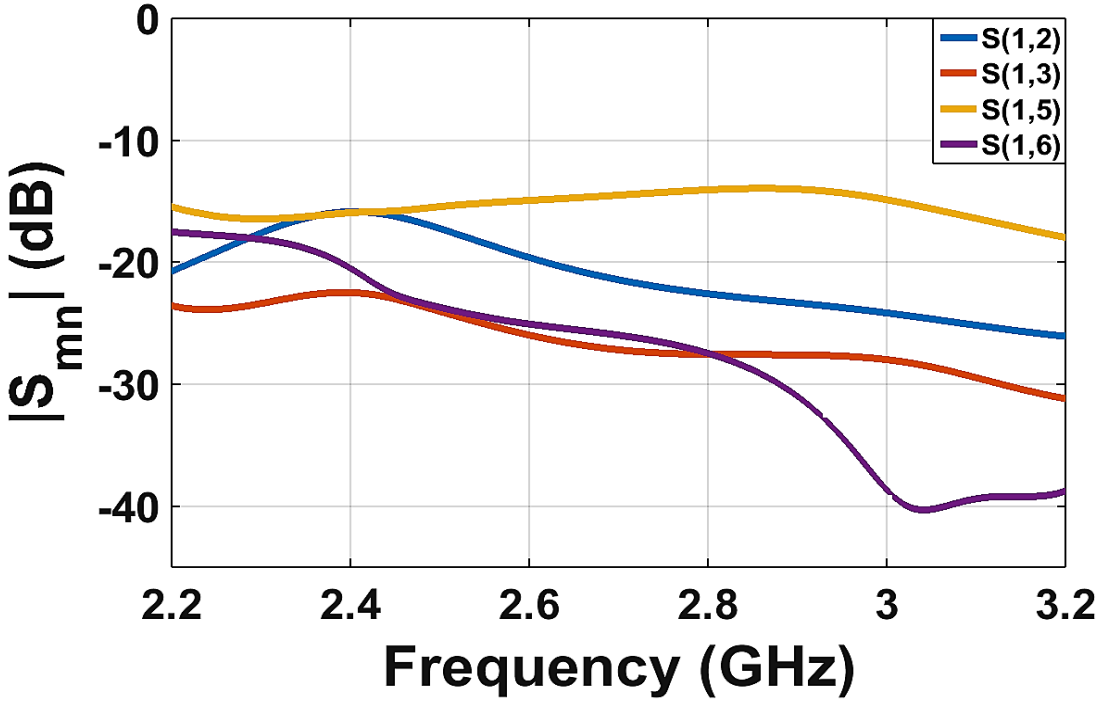

(a)

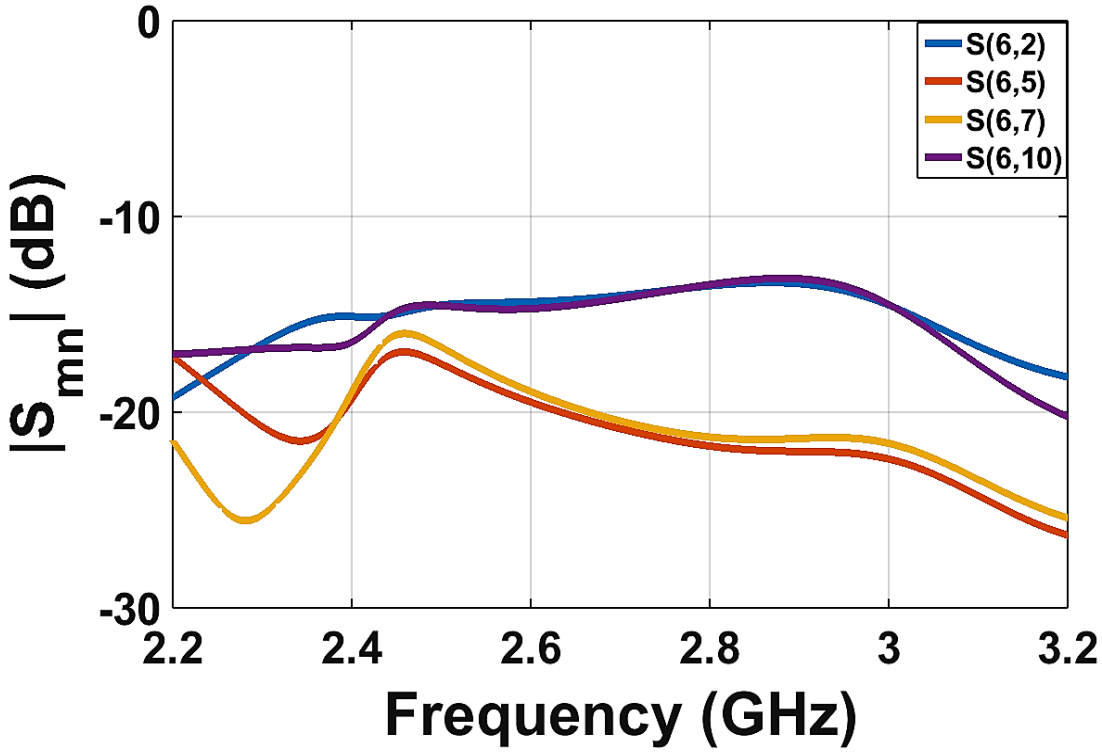

(b)

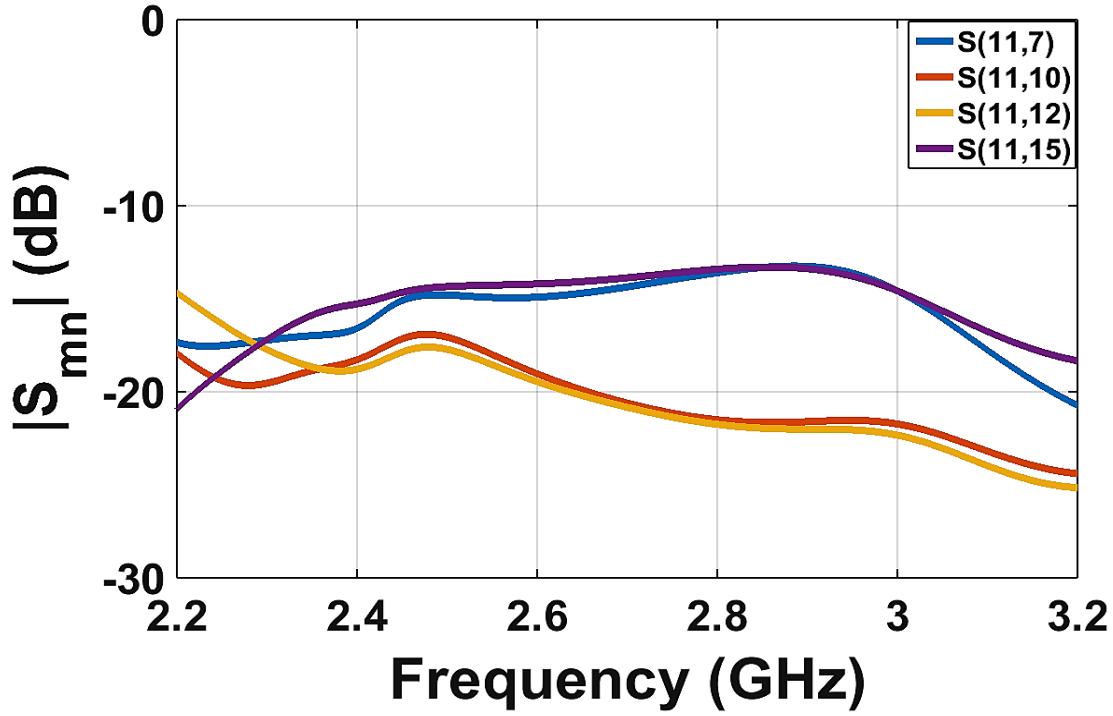

(c)

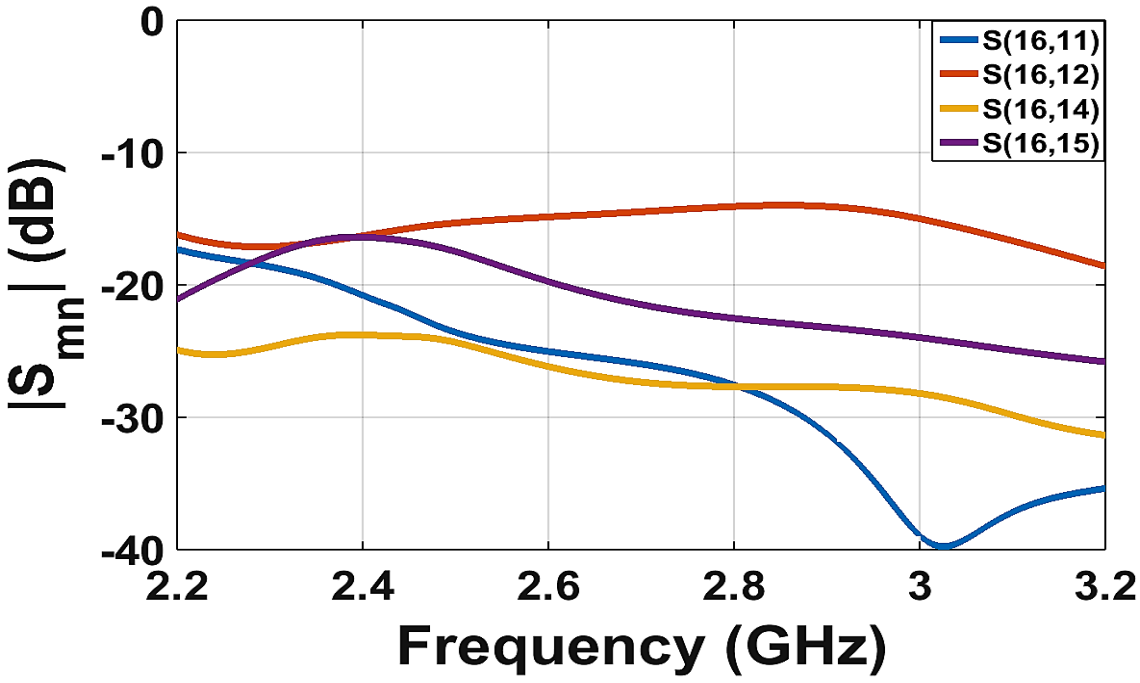

(d)

Fig 3.6: Mutual coupling (a) at Port 1,(b) at Port 6, (c) at Port 11, (d) at Port 16.

The radiation patterns for this planar array at the four frequency points are plotted in Fig. 3.7.

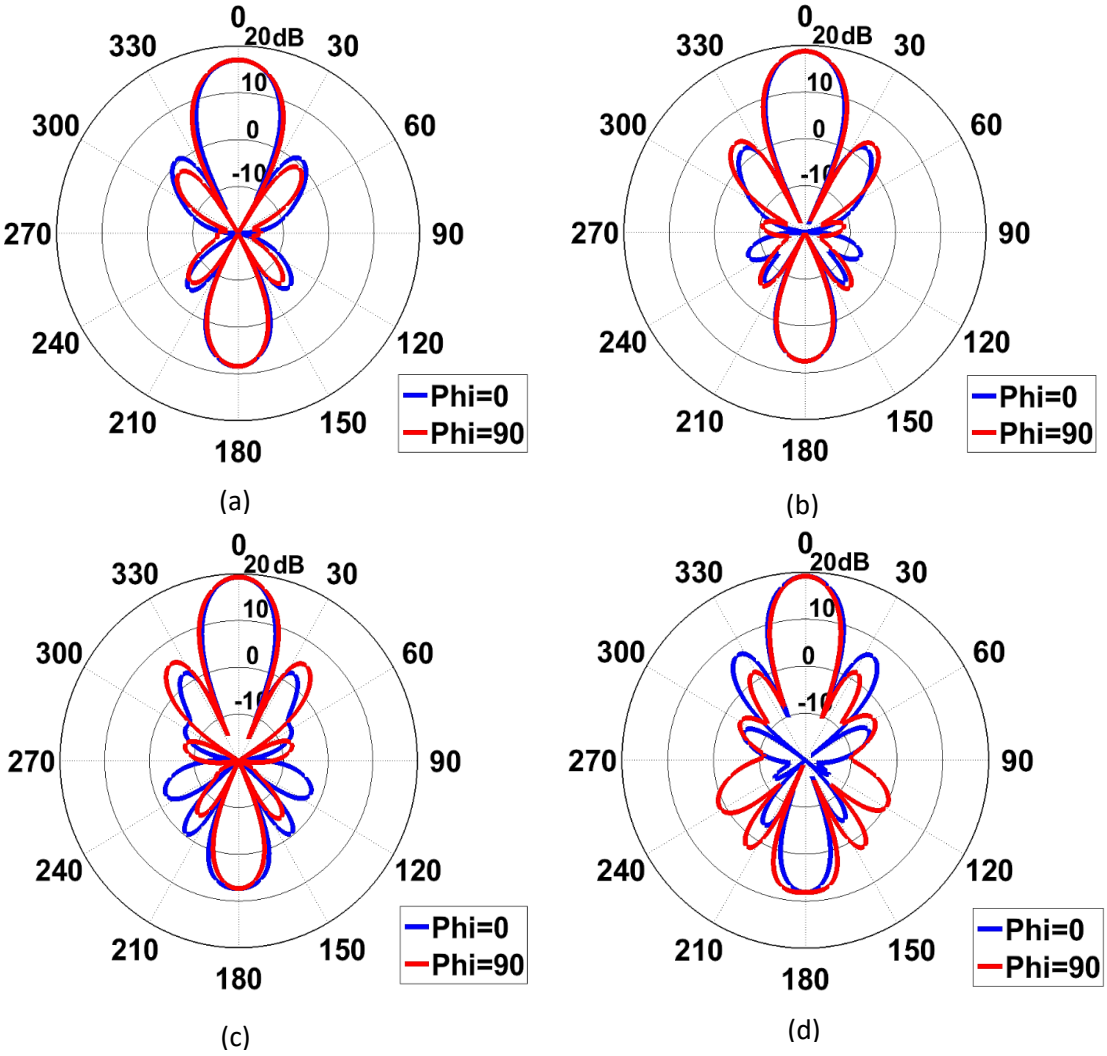

Fig. 3.7: Radiation patterns at (a) 2.45 GHz, (b) 2.65 GHz. (c) 2.85 GHz, (d) 3.05 GHz

The results observed from the radiation pattern plots have been summarized in Table 3.2.

Table 3.2: Summary of simulation results for individually fed planar array antenna.

Frequency (GHz)	**Realized Gain (dBi)**	**SLL (dB)**	**F/B (dB)**	**Directivity (dBi)**
2.45	17	16.3	8.6	17.4
2.65	18.7	14.3	11.2	18.4
2.85	19.3	14	12	19.1
3.05	19.2	12.6	11	19.4

From Table 3.2 and the radiation pattern plots above we can see that the planar array antenna has a realized gain which is 5dBi higher when compared to the linear array. The radiation pattern is also very symmetric in both the $\Phi=90^{o}$ and $\Phi=0^{o}$ plane, unlike the linear array which has a more directional pattern in the $\Phi=90^{o}$ plane. The SLL of this antenna array is slightly better than the linear array antenna even though the sidelobe radiation is still almost at the same level and this is because of the increase in the realized gain. But one big negative that is observed is the reduction of the F/B ratio which is due to the increased level of backlobe radiation caused due to the increase in the number of apertures. There are numerous techniques to deal with this backlobe radiation and will be discussed in later chapters.

Chapter 4: Antenna Array Feed Networks

4.1 Introduction

In the previous chapters the design and optimization of a wide band aperture coupled patch antenna array was presented. The reflection coefficient and mutual coupling between elements of the linear and a planar array was studied. The radiation pattern for all the above mentioned antennas were presented for four frequency points within the operating frequency range and their various characteristics like the maximum realized gain, F/B ratio, SLL and directivity were investigated. All the antennas discussed up until now were excited using separate feeds for each element and this is not a feasible approach to meet the needs of most practical applications. For example, a transmitting antenna would then require multiple sources and the amplitudes and phases of each source has to be individually regulated for the proper functioning of the antenna. To solve this problem corporate feed networks are used in antenna arrays. They help provide equal amplitude, in-phase excitation to each element of the antenna utilizing only one input or output source. The excitation amplitudes can be controlled using various tapering techniques. Phase variations can be also introduced to steer the mainlobe and create a phased array antenna. The phases can be controlled using phase shift lines which basically involve changing the path lengths of the signals. Alternatively MMIC phase shifters can also be utilized. This chapter presents the design of an equal amplitude and in-phase corporate feed network for a 4X4 planar antenna array.

4.2 The Corporate Feed Network

Corporate feed networks have been extensively used because of their simple geometry, compactness and ease of fabrication [17]. But the corporate feed will also introduce resistive loss which causes degradation in the input signal. Surface waves and radiation bleeding from the lines at high frequencies is also a matter of concern. In closely packed designs they also tend to cause mutual coupling between adjacent lines. All of these combined do put limitations on the practical design and have to be considered while design the feed network for an antenna array. Many of these effects have been studied and characterized in numerous studies [18-19] over the years. The design of the corporate feed network used for the 4X4 antenna array is shown below in Fig. 4.1. The coordinate axis used is been shown in the bottom right corner of Fig.4.1. In HFSS the input is modelled as a lumped port. The power is split equally at each junction so that every patch receives one sixteenth of the initial input power. The line lengths to each patch is also equal which is evident from Fig. 4.1, this ensures that each element receives an in-phase input signal with the same amplitude. Quarter wave transmission line sections are used to match the feed network. For quarter wave matching we need to match every junction where the impedance changes with a line with impedance [20],

$$Z_{\lambda/4} = \sqrt{Z_{in}.Z_0} \quad \ldots (4.1)$$

Here,

$$Z_{in} = 25\ \Omega \text{ and } Z_0 = 50\ \Omega$$

Therefore,

$$Z_{\lambda/4} = 35.36\ \Omega$$

The line widths that will give us these required impedances are found using [20], and they come out to be,

$$w_1 = 3.5\ mm\ (Z_0 = 50\ \Omega)$$

$$w_2 = 5.8\ mm\ (Z_{\lambda/4} = 35.36\ \Omega)$$

The length of the quarter wave transmission line section was found at f_c=2.45 GHz, for a RO4003c medium with thickness, t_f=1.52 mm. Again from [20] the guided wavelength in the medium is given by,

$$\lambda_g = \frac{c}{f_c \cdot \sqrt{\varepsilon_{eff}}} \quad \ldots (4.2)$$

$$\varepsilon_{eff} = \frac{\varepsilon_r + 1}{2} + \frac{\varepsilon_r - 1}{2} \frac{1}{\sqrt{1 + 12d/W}} \quad \ldots (4.3)$$

Where,

c= Speed of light in vacuum

ε_{eff}= Effective relative permittivity of the medium

d=t_f

W=w_2

If we evaluate the above expression, we find that the length of the required quarter wave transformer is,

$$\lambda_g/4 = 18.26\ mm$$

One other parameter that needed tuning was the length of the transmission line sections that feed the aperture, *i.e.* the section which is marked as l_f in Fig.4.1. This length l_f influences the vertical position (position along the x-axis) of the corporate feed with respect to the patches and the slots. We do not want this section to be very long as this will cause the corporate feed to get too close to the apertures in rows 2 and 4 and the line being too short will move the feed network closer to rows 1 and 4. Perfect symmetry is not possible in this case because of positioning and feeding constraints so a compromise must be sought to find the best possible configuration. A parametric sweep revealed the best performance for a length of l_f=19.25 mm.

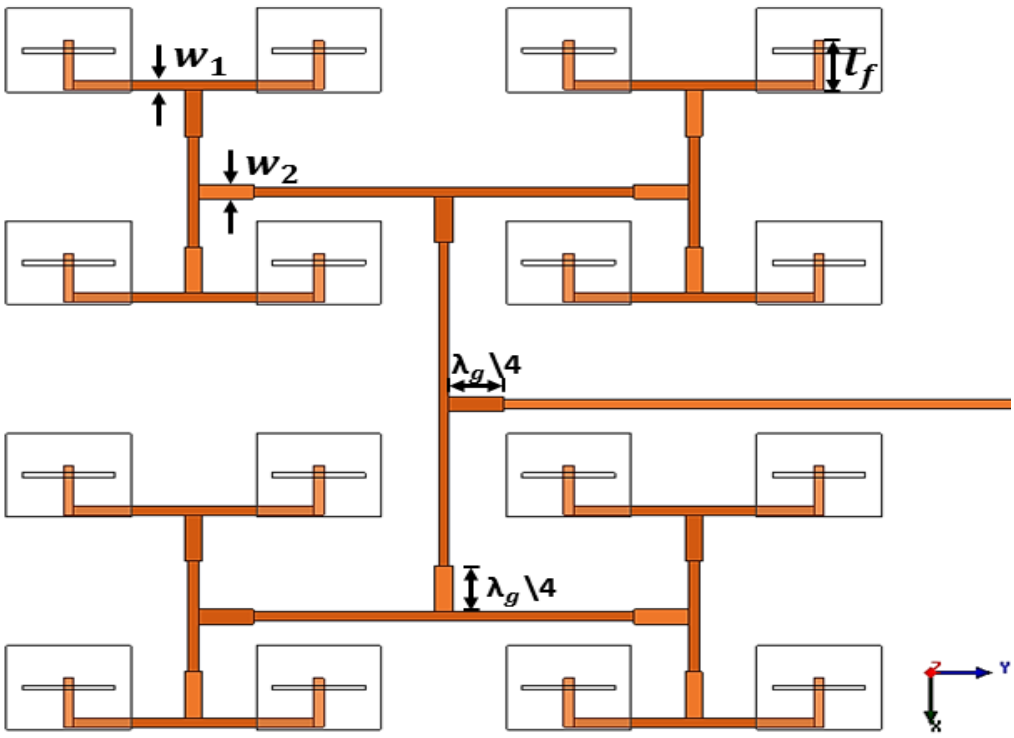

Fig. 4.1: Top view of array with corporate feed network.

The current inter-element spacing is d=62.5 mm, which is the same "d" we used in simulations in the previous chapter for the individually fed 4X4 linear array antenna. The simulated S_{11} data for the antenna shown in Fig. 4.1 has been plotted in Fig. 4.2. The S_{11} data obtained in this simulation does not match what is expected and the antenna has lost most of its bandwidth which it previously had. Previously the antenna displayed an operating frequency band of 2.3 to 3.1 GHz. But with the current corporate feed network the antenna has an operating band of 2.77 to 2.96 GHz. This new bandwidth is significantly narrower. The radiation pattern of this antenna has also been presented in Fig. 4.3. As expected, the realized gain is considerably lower than the individually fed array. The realized gain at 2.45 GHz is 15.6 dBi, with a SLL of 13.4 dB.

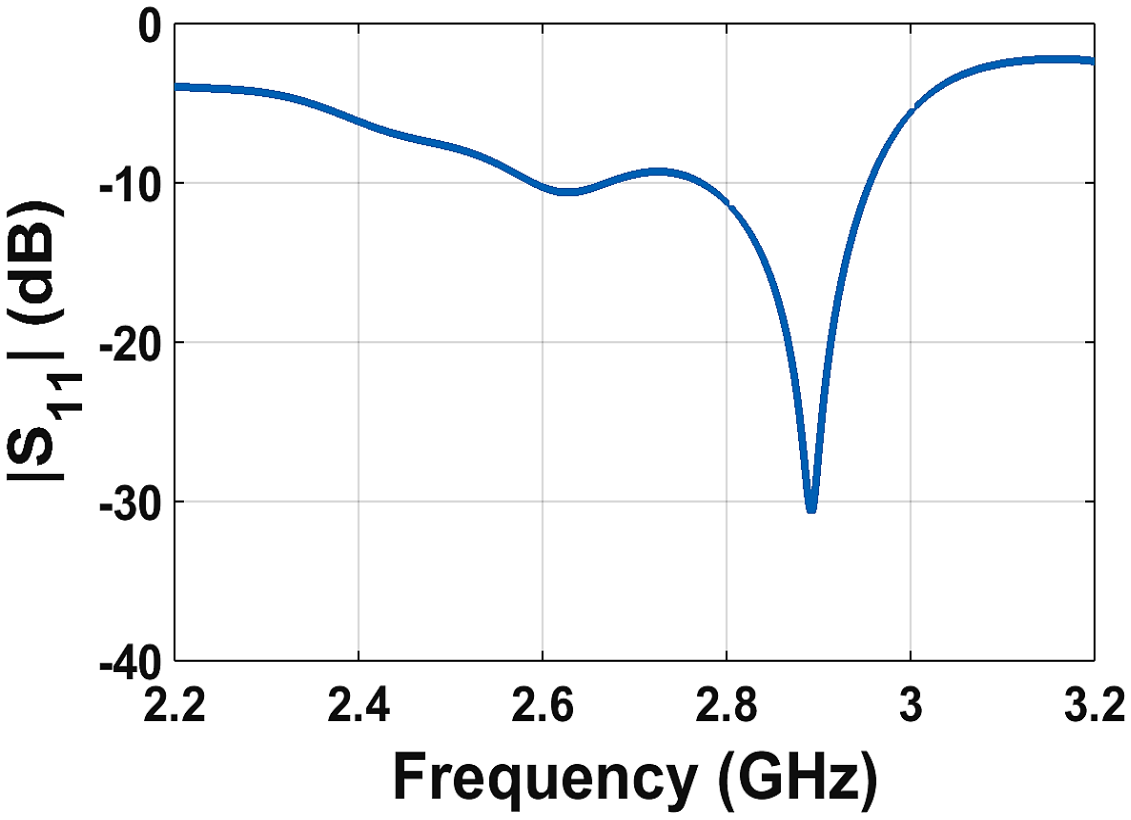

Fig. 4.2: S_{11} plot for planar array antenna with d=62.5 mm.

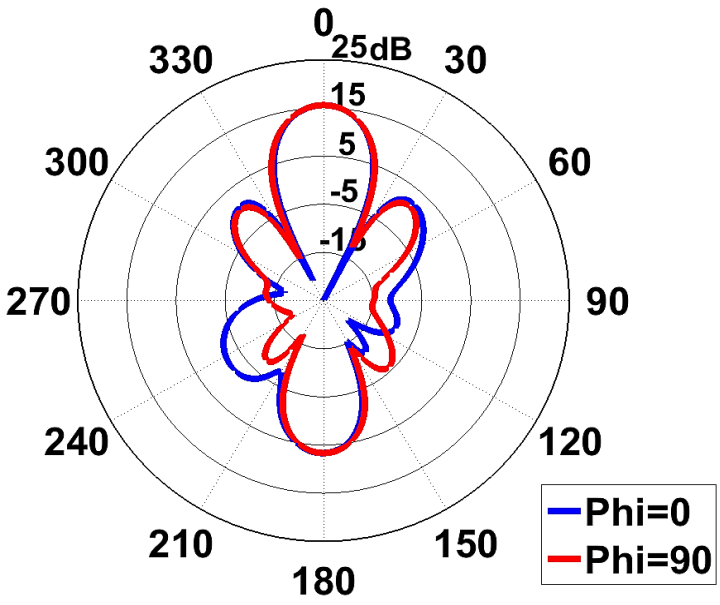

Fig. 4.3: Radiation pattern plot at 2.45 GHz.

It was found that the electric fields reaching the aperture was very low and through running simulations we were able to establish the cause of this decrease in bandwidth and the consequential deterioration of bandwidth to coupling between the feedlines which are relatively closely spaced to each other. Fig. 4.4 shows the E-field magnitude profile for the ground plane and the corporate feed network.

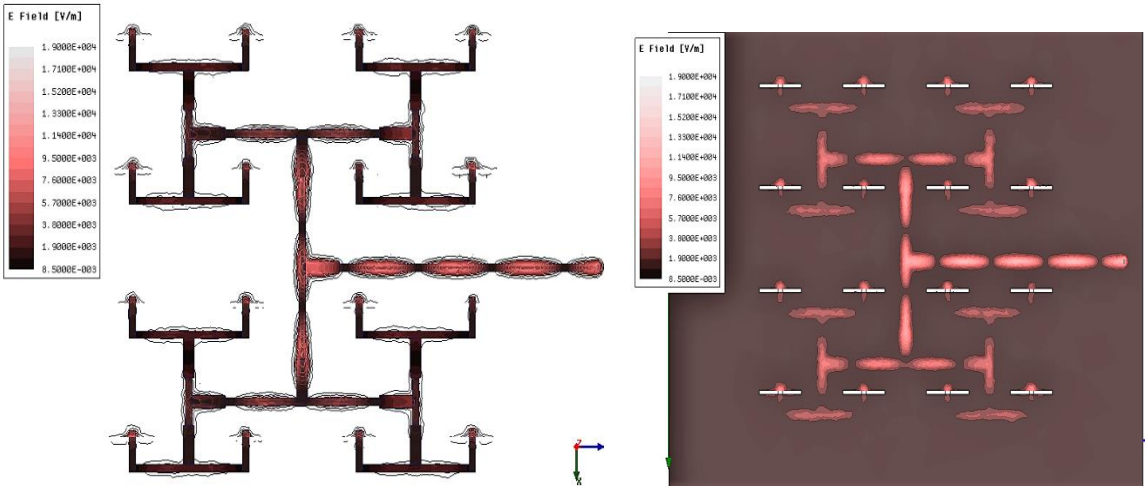

(a) (b)

Fig. 4.4: (a) Magnitude of E-field on feedline (b) Magnitude of E-field on ground plane.

To solve this problem, we increased the inter-element separation, "d" to 83.3mm (2λ/3) while keeping everything else the same. The only structural difference that was caused due to increasing the inter-element separation was that it increased the overall size of the antenna array and the new size of the array is, 416.3mm X 407.6mm X 12.52mm. For this new configuration, the E-field magnitude seen on the corporate feedline and on the ground plane are shown below in Fig. 4.5.

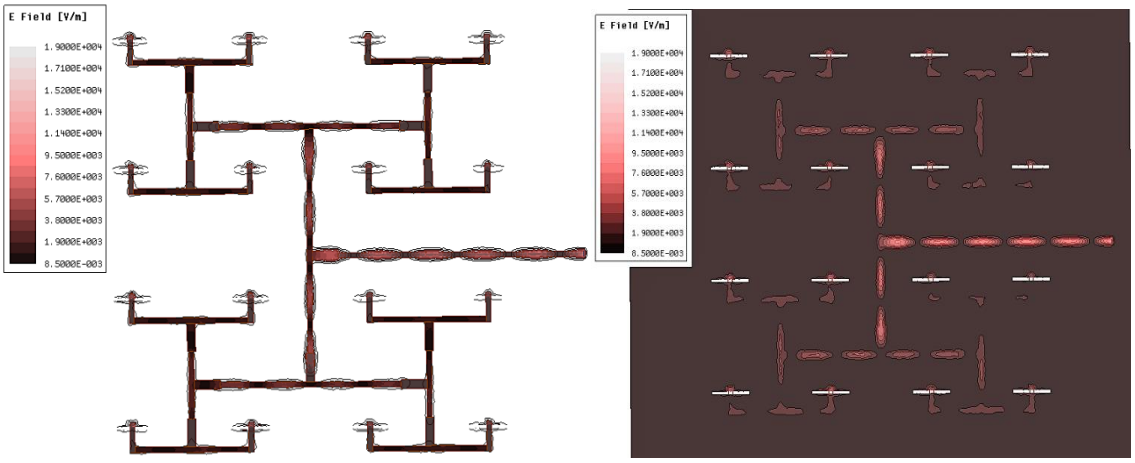

(a) (b)

Fig. 4.5: (a) Magnitude of E-field on feedline (b) Magnitude of E-field on ground plane.

It is evident from Fig. 4.5 that the E-fields are uniformly distributed across the feedline and aperture when the inter-element separation is increased to, d=83.3mm. The performance of an individually excited 4X4 antenna array with an inter-element separation of 83.3mm are presented before showing the performance of the corporate feed network with this new, increased separation. Figs. 4.6 shows the S_{nn} performance of the antenna. The S_{nn}s have been divided into two plots, the first plot Fig. 4.6(a) depicts the performance of antennas from port 1 to port 8, whereas Fig. 4.6(b) shows the reflection coefficient performances seen at ports 9 through 16. The same port labelling

convention has been used as described in Fig. 3.4(b). The reflection coefficient performances seen for this configuration with an increased inter-element separation is better than our previous design across each port. The operating frequency range is still almost the same, lying between 2.3 to 3.1 GHz, but the S_{nn} levels are lower near our design frequency. In the previous design, the S_{nn}s had a region between 2.6GHz to 2.7GHz where they briefly touched or even went past -10dB. This problem has also been resolved by increasing the inter-element separation.

The mutual coupling between the elements lying on the diagonal of the array and their four nearest neighbors have been plotted in Fig. 4.7. These four plots basically represent the worst mutual coupling performances seen among the worse elements in the antenna. Even so, the S_{mn} performance lies below -20dB for most of the region across the impedance bandwidth and the overall mutual coupling performance is much better than the previous design, which is mainly due to the increased separation between the elements.

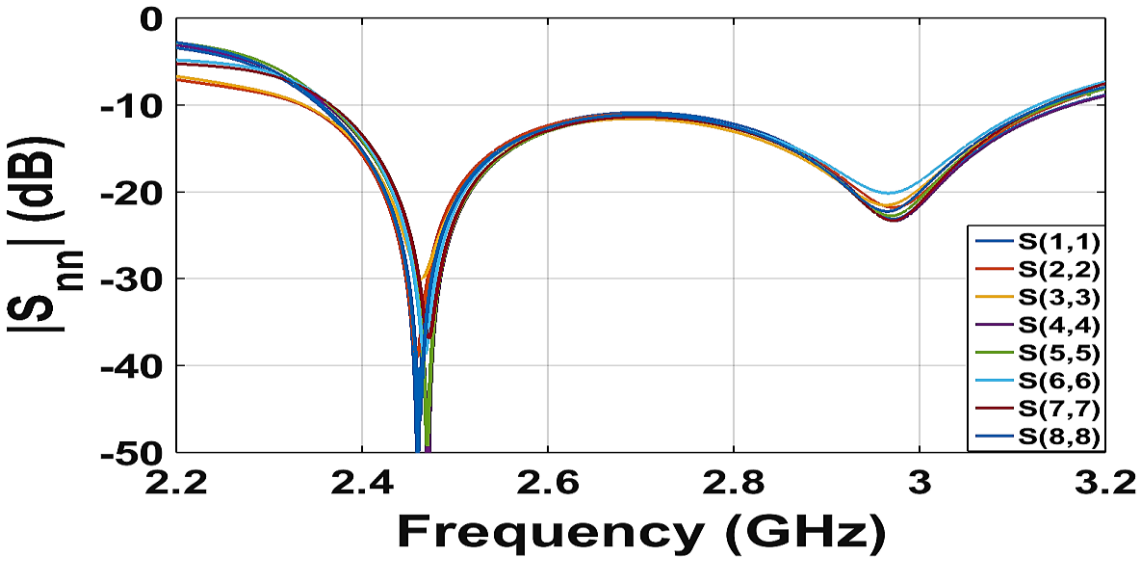

(a)

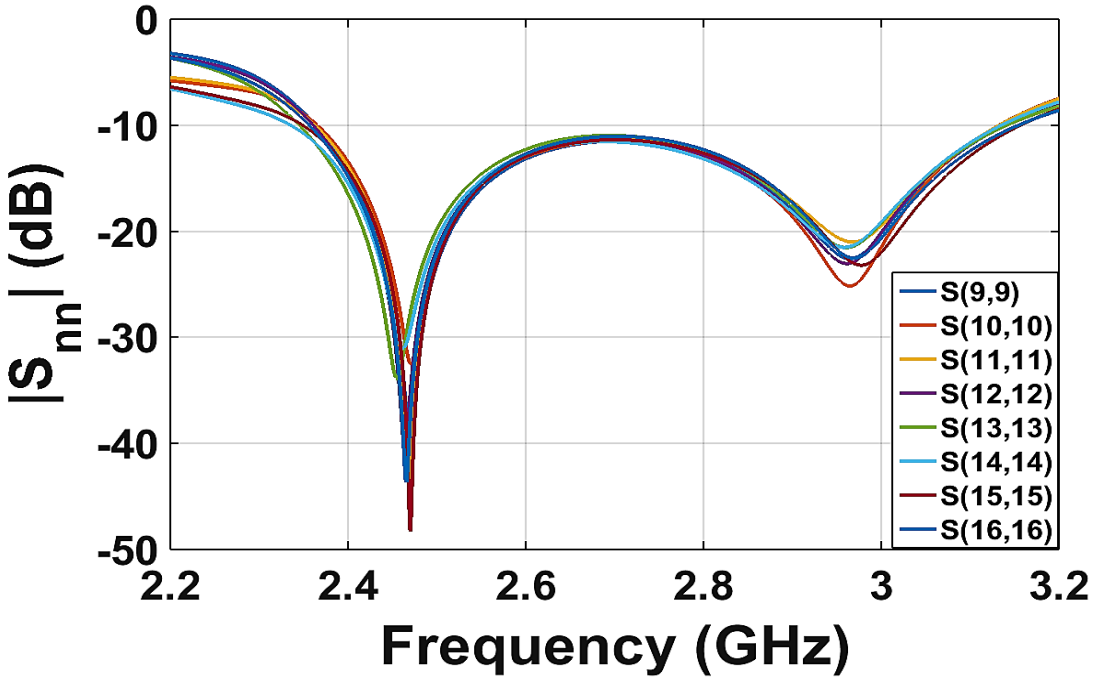

(b)

Fig 4.6: (a) $S_{1,1}$ to $S_{8,8}$, (b) $S_{9,9}$ to $S_{16,16}$.

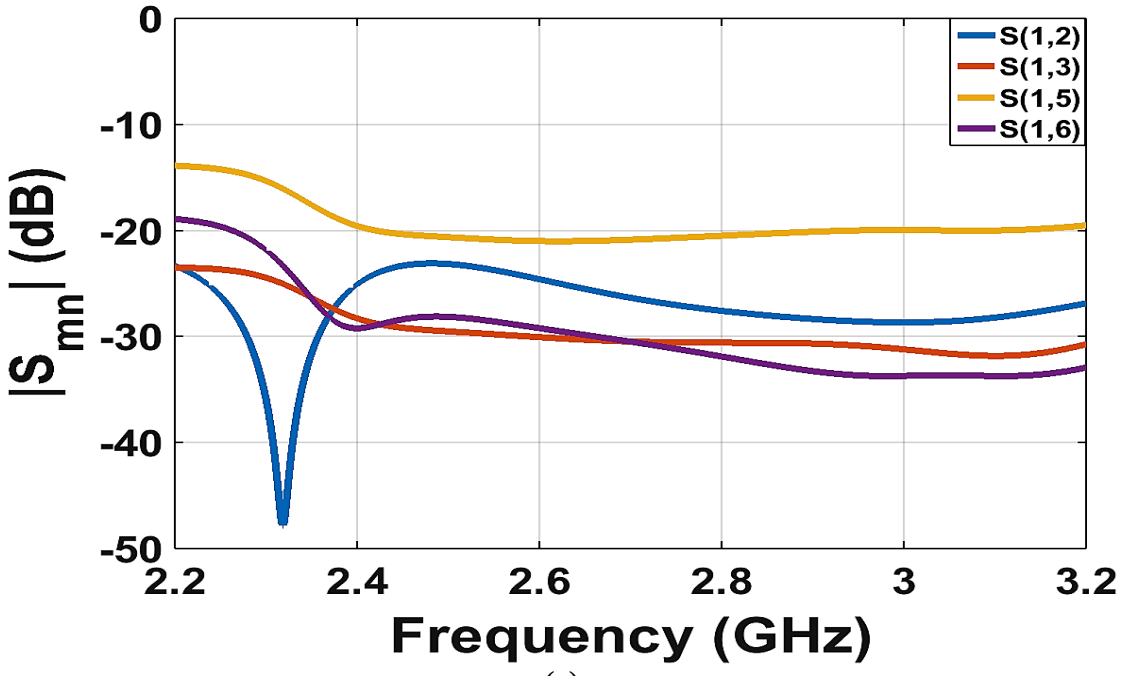

(a)

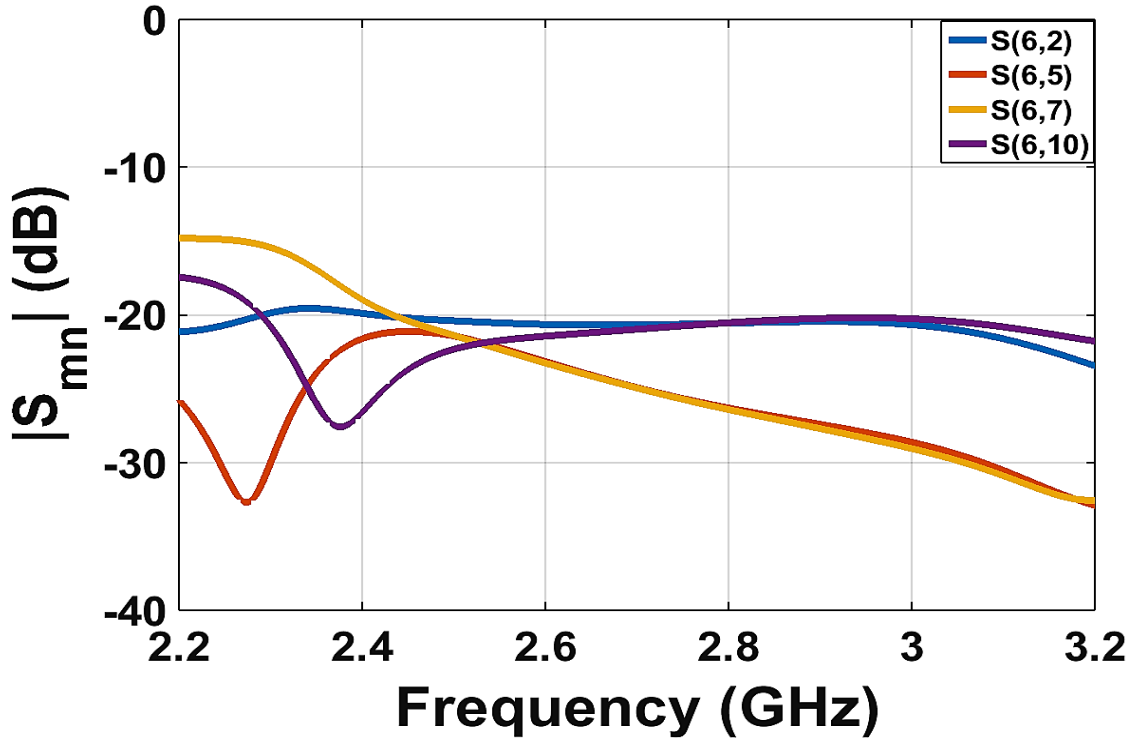

(b)

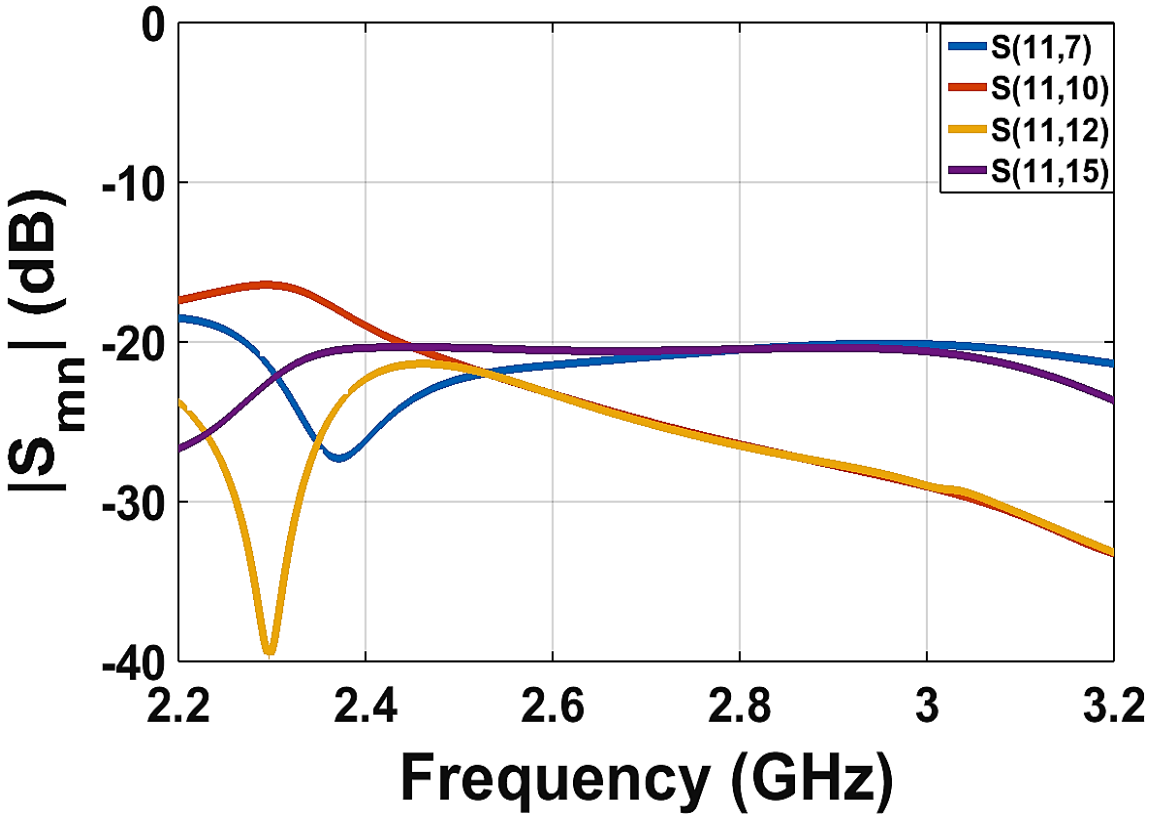

(c)

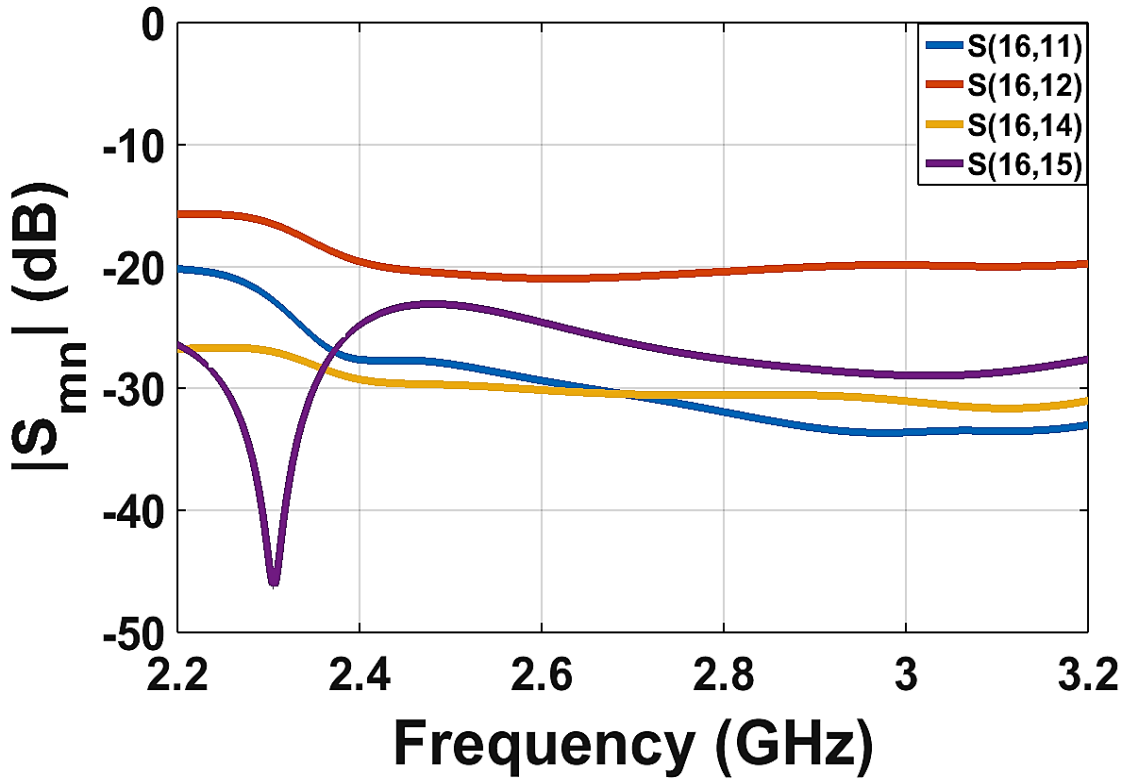

(d)

Fig 4.7: Mutual Coupling (a) at Port 1,(b) at Port 6, (c) at Port 11, (d) at Port 16.

The radiation patterns for this new array are plotted below in Figs. 4.8 and the results are summarized in Table 4.1.

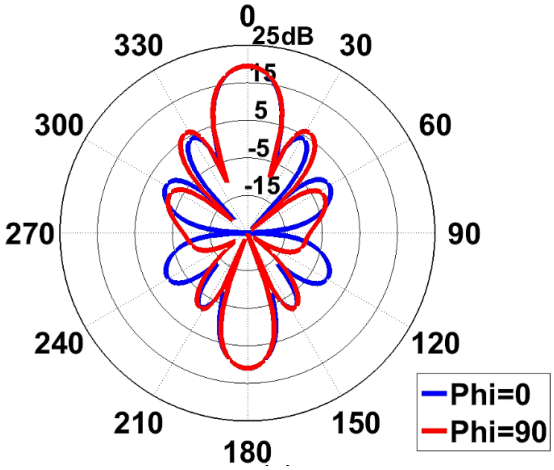

(a)

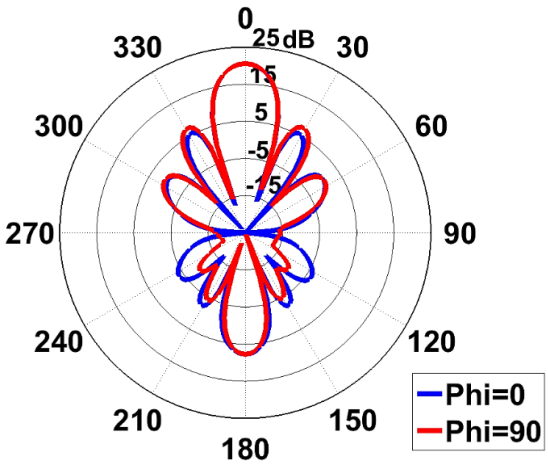

(b)

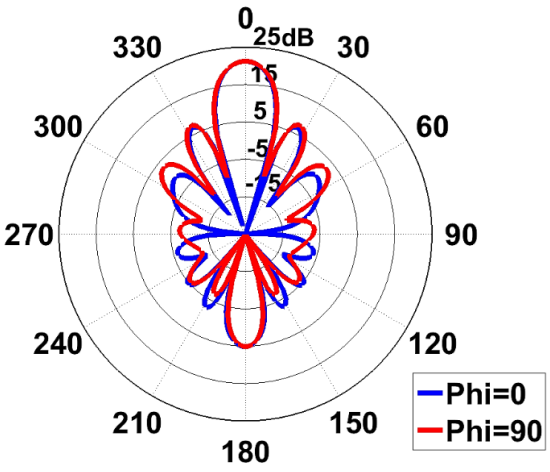

(c)

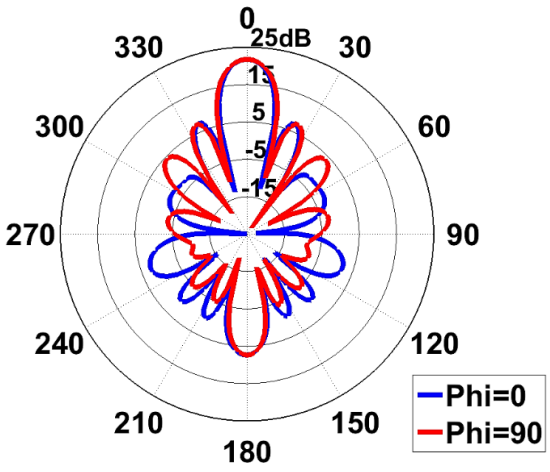

(d)

Fig. 4.8: Radiation patterns at (a) 2.45 GHz, (b) 2.65 GHz, (c) 2.85 GHz, and (d) 3.05 GHz.

Table 4.1: Summary of simulation results for individually fed planar array antenna with increased separation.

Frequency (GHz)	Realized Gain (dBi)	SLL (dB)	F/B (dB)	Directivity (dBi)
2.45	19.4	13	18.4	19.5
2.65	20.6	13.3	12.8	20.5
2.85	21.3	13.7	16.2	21.3
3.05	21.8	14.5	14.4	21.9

We see a 2dB or more improvement in the realized gain of the antenna across the operating spectrum when the inter-element separation is increased. Another positive effect seen is the decrease in the backlobe, which along with the increased gain has caused a very significant increase in the F/B ratio. At 2.45GHz the F/B ratio has improved by as much as 10dB. There is also a slight improvement in the total measured directivity. The only characteristic of the radation pattern that has suffered is the SLL

which has not only incresed in intensity, we now see 4 minor lobes in the front region of the antenna as opposed to the previous two. The SLL has risen by a dB to as much as 3 dB at some frequencies and it seems to have moved closer to the mainlobe

4.3 4X4 Array with Increased Separation and Corporate Feed Network

So, after determining that the bandwidth performance problem and the radiation pattern of the antenna indeed improves by increasing the inter-element separation, we design the corporate feed network for the antenna, which looks exactly the same and has all the same parameters as shown in Fig. 4.1, but is just placed on a larger substrate now. The S_{11} plot for this corporate fed antenna array is shown below in Fig. 4.9.

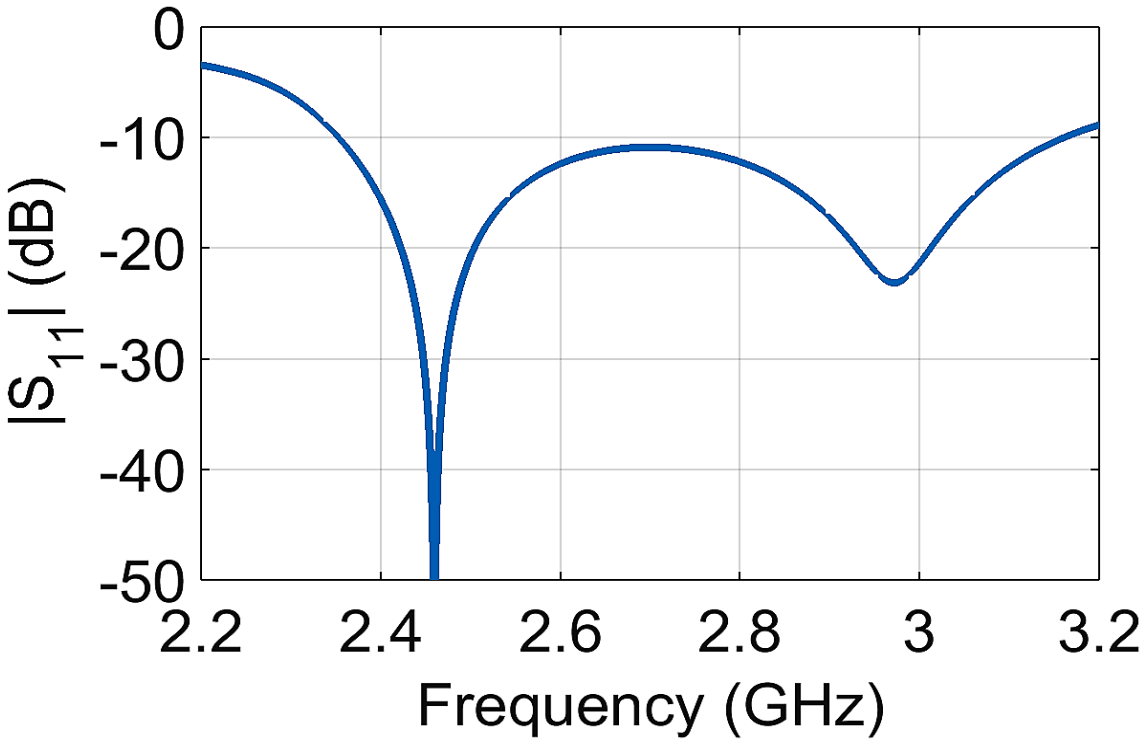

Fig. 4.9: S_{11} plot for planar array antenna with d=83.3mm.

The 4X4 planar array has a bandwidth of 0.85 GHz. The array has an operating frequency which spans 2.3 to 3.15 GHz. The radiation patterns for the four frequencies, 2.45, 2.65, 2.85 and 3.05 GHz are plotted below. If we compare the radiation patterns obtained from the simulations for the corporate feed array and the individually fed antenna array, the radiation patterns and results are a very close match. The realized gain is slightly lower because of the losses caused due to the transmission lines and the mismatch at the multiple junctions. Even though we have used quarter wave sections to match the circuit, we have designed our quarter wave transformer at 2.45 GHz and the reflections are bound to increase with an increase in frequency. The SLLs are almost same or a little lower at some frequencies which is exactly the case with the total directivity too. There is an increase in backlobe radiation though, which is due to the added sections of transmission lines in the bottom of the substrate which would inadvertently lead to an increase in spurious radiations in the backward direction. This increased backlobe radiation and decreased gain result in a lower F/B ratio compared to the individually fed antenna array. All of these radiation pattern characteristics have been summarized in Table 4.2.

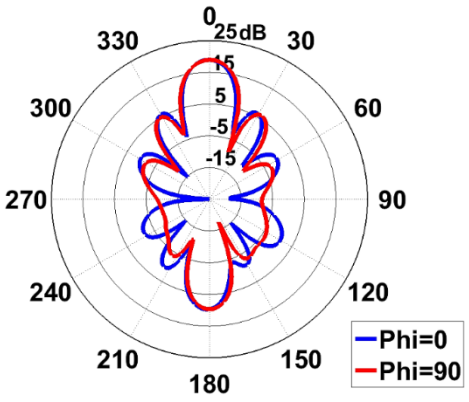

(a)

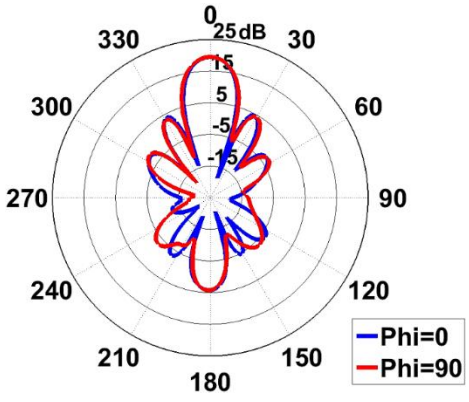

(b)

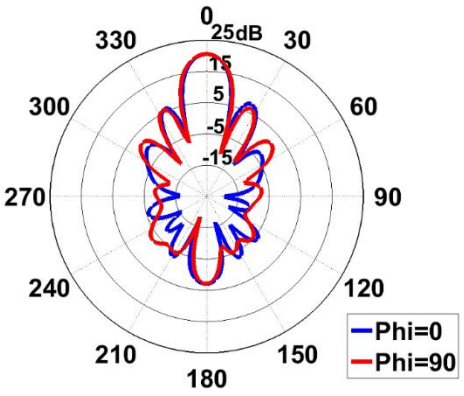

(c)

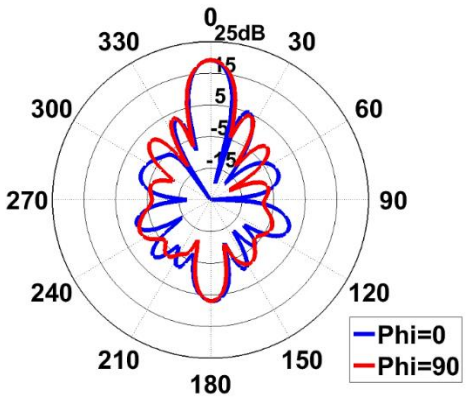

(d)

Fig. 4.10: Radiation patterns at (a) 2.45 GHz, (b) 2.65 GHz, (c) 2.85 GHz, and (d) 3.05 GHz.

Table 4.2: Summary of simulation results for planar array antenna fed using a corporate feed.

Frequency (GHz)	**Realized Gain (dBi)**	**SLL (dB)**	**F/B (dB)**	**Directivity (dBi)**
2.45	19	12.9	9.3	19.4
2.65	19.5	15.1	15.3	20.3
2.85	20.6	12.7	17.6	21.1
3.05	19.2	15	12.3	21.3

Chapter 5: Reducing Sidelobe and Backlobe Levels in Planar Arrays

5.1 Introduction

Amplitude tapering is the most commonly used method for controlling the sidelobe radiation produced by an antenna array. The central elements usually receive the maximum illumination and this excitation amplitude tapers off as we go farther away from the central element or elements. There are numerous ways of determining the taper profile of an antenna. It mainly depends on our requirements like the maximum tolerable SLL, minimum directivity, gain and Half Power Beamwidth required, the maximum to minimum illumination that would be practically realizable, etc. and each technique comes with its pros and cons. There is usually a trade-off between all the aforementioned parameters and we must choose the best case scenario that fits our design requirements. In this chapter we will first look at the performance of some of these commonly used amplitude taper profiles, namely the binomial array, Dolph-Chebyshev array and a custom designed taper coefficient profile which will be discussed later in the text. We shall look at the taper coefficient profiles and their resulting radiation pattern characteristics using an individually fed antenna array and after we determine the best performing antenna array, we will see how to generate a corporate feed network so as obtain our required illumination ratios.

Just like the SLL the F/B ratio is an important characteristic of any antenna. It tells us how much radiation is being emitted in the backlobe as compared to the main

beam. We can improve this ratio by increasing the main beam directivity and/or decreasing the backlobe radiation. But in the case of our aperture coupled patch antenna, the gain is increased by adding more radiating elements but that also means more number of apertures and these apertures are mainly responsible for the high level of backlobe radiation seen in aperture fed antennas. Many techniques have been explored for controlling the backlobe radiation, some of them include altering the shape of the aperture, many different aperture patterns like E, H, U and dumbbell shaped apertures have been shown to successfully reduce the back radiation [21-22]. Another way around this problem is by using reflectors placed behind the antenna array at an appropriate distance. The reflectors can be a dielectric, an EBG or a simple metal reflector plate [23] which will act as a shield that blocks out the E-fields. For this array a metal reflector plate has been used to suppress the backlobe radiation because of its effectiveness and simplicity of design.

5.2 Binomial Antenna Arrays

Binomial arrays are one of the simpler amplitude tapered arrays. It was first proposed by J. S. Stone as a technique to achieve antennas with no side lobes [24-25]. The taper coefficients follow a binomial series expansion which for an N element linear array can be expressed as [26],

$$A_n = \frac{(N-1)!}{(N-n)!\,(n-1)!} \quad \ldots (5.1)$$

And the corresponding array factor is given by,

$$AF(\theta) = (1 + e^{j\psi})^{N-1} = \sum_{n=0}^{N-1} \left[\frac{N-1}{n}\right] e^{j\psi n} \quad \ldots (5.2)$$

So, for a four element linear binomial array the coefficients will be, [1 3 3 1] which when normalized is approximately [0.3 1 1 0.3]. As defined earlier in Chapter 3, the array factor of a planar array is basically the product of array factors of two linear arrays lying orthogonal to each other, therefore,

$$AF = AF_{xM}.AF_{yN} \quad \ldots (5.3)$$

And,

$$AF_{xM} = \sum_{m=1}^{M} w_{m1} e^{j(m-1)\psi_x} \quad \ldots (5.4)$$

$$AF_{yN} = \sum_{n=1}^{N} w_{1n} e^{j(n-1)\psi_y} \quad \ldots (5.5)$$

Thus from the two equations above we can conclude that the amplitude coefficient for a planar array antenna would be given as,

$$w_{mn} = w_m.w_n \quad \ldots (5.6)$$

Using this result, the excitation profile for a 4X4 planar binomial array antenna is calculated and the taper coefficients are as shown below in Fig. 5.1.

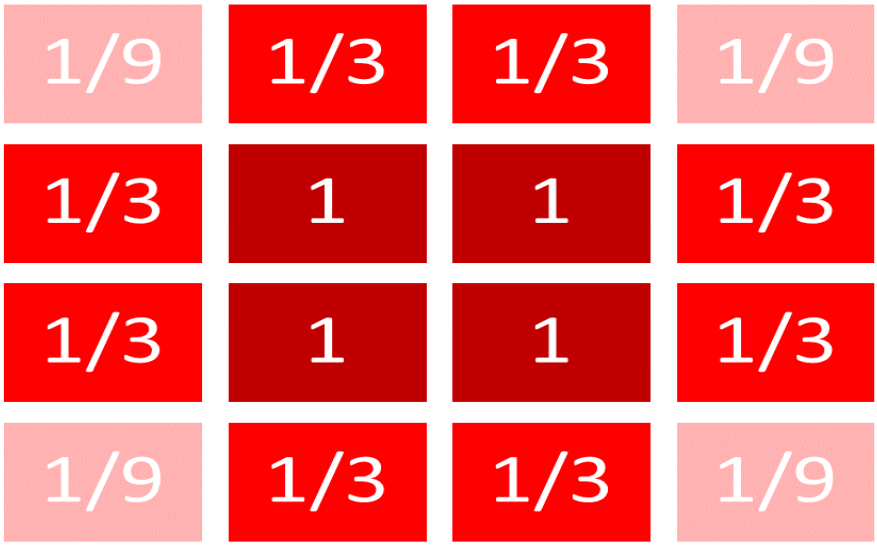

Fig. 5.1: Binomial taper excitation coefficient.

The radiation patterns observed for a binomial planar array are shown below in Fig. 5.2. The SLLs seen for the binomial array are much lower than the uniformly excited array but we see that the directivity of the binomial array is also lower than the uniformly fed array. The mainlobe also becomes broader due to the binomial tapering. The realized gain and directivity are lower by 0.5 to 0.8 dB. The F/B at 2.45GHz is seen to be much lower than that of the uniformly excited array but the response at other frequencies is in line with the loss in gain. The main improvement can be seen in the SLL. The SLL for the binomial array lies between 23 to 25 dB as compared to the 13.5 dB SLL maximum for the uniformly fed antenna array which is a major performance boost. The radiation pattern parameters for the binomial array are summarized in Table 5.1.

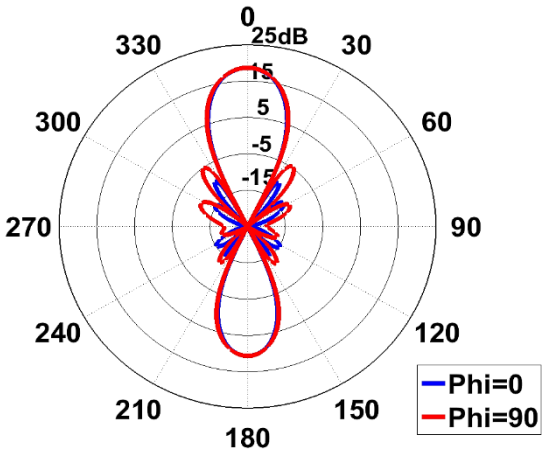

(a)

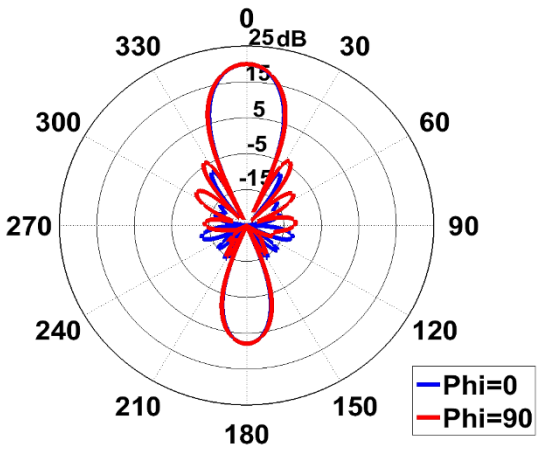

(b)

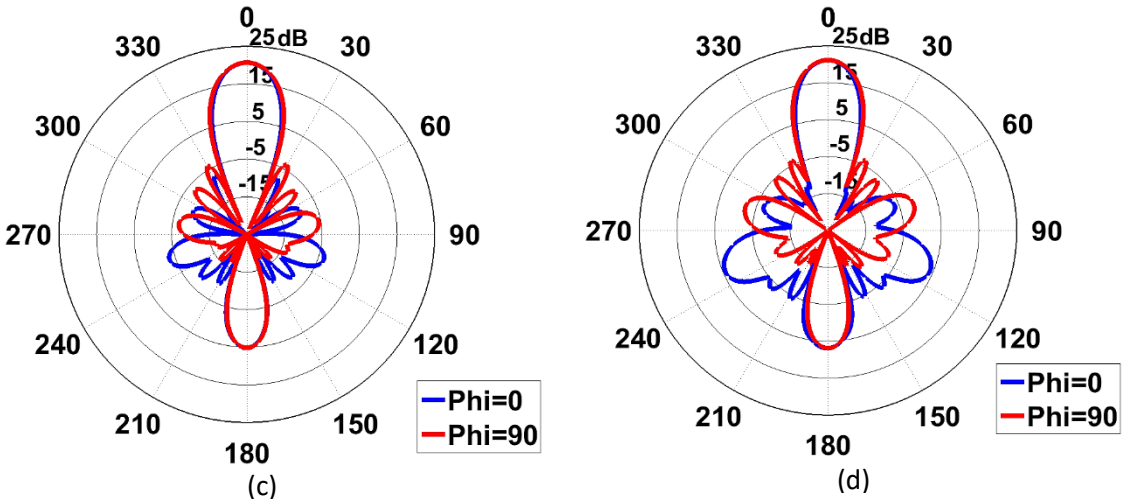

Fig. 5.2: Simulated radiation patterns of binomial array at (a) 2.45 GHz, (b) 2.65 GHz. (c) 2.85 GHz, (d) 3.05 GHz.

Table 5.1: Summary of radiation pattern data for binomial array.

Frequency (GHz)	Realized Gain (dBi)	SLL (dB)	F/B (dB)	Directivity (dBi)
2.45	18.7	23.4	8.1	21.2
2.65	20	23.8	12.1	20
2.85	20.7	24.9	15.6	20.8
3.05	21.2	24.9	14.3	21.2

5.3 Dolph-Chebyshev Antenna Arrays

Designing amplitude taper coefficients for an antenna array is similar to selecting filter design coefficients while designing a filter [27]. In 1946 Dolph proposed a method for obtaining weights for a uniformly spaced linear array directed towards the broadside. This approach allowed the user to specify the SLL, gives sidelobes having equal magnitudes and also has minimum null to null beamwidth. This technique works by using

the Chebyshev polynomials which are defined using a recursive relation shown below [27],

$$T_0(z) = 1$$

$$T_1(z) = 1$$

$$T_m(z) = 2zT_{m-1}(z) - T_{m-2}(z)$$

For m= 2, 3, 4…

This polynomial when plotted shows an equal-ripple response which ensures the SLLs are uniform throughout the E-plane and H-plane. Now, for a Dolph-Chebyshev array the array factor is given as [26-27],

$$AF = \sum_{n=1}^{M} w_n \mathrm{Cos}[(2n-1)u], \text{ (even array)}$$

$$AF = \sum_{n=1}^{M} w_n \mathrm{Cos}[2nu], \text{ (odd array)}$$

$$u = kd\cos(\frac{\theta}{2})$$

We can find the taper weights by using this substitution on the trigonometric expansion of the above expression [27],

$$\mathrm{Cos}(u)t_0 = t$$

$$t_0 = \mathrm{Cosh}\left[\frac{\mathrm{Cosh}^{-1}(S)}{N-1}\right]$$

Here S represents the SLL in linear units. Using the above equation to determine the taper coefficients for a 4 element linear array with a SLL of 25 dB we find the normalized weights comes out to be [0.42 1 1 0.42]. Converting these coefficients from a

1D space to 2D space results in a taper profile as shown in Fig. 5.3. This is then followed by radiation patterns observed for the Dolph-Chebyshev array. The realized gain and directivity for the Dolph-Chebyshev array lies somewhere between the uniformly excited array and the binomial array. Same can be said for the beamwidths, SLLs and the F/B. The min to max illumination seen here is also better compared to the binomial array, which means the line widths required to realize the corporate feed for this array will not have large variations, which in turn means a better match. The radiation pattern characteristics for the Dolph-Chebyshev array are summarized in Table 5.2.

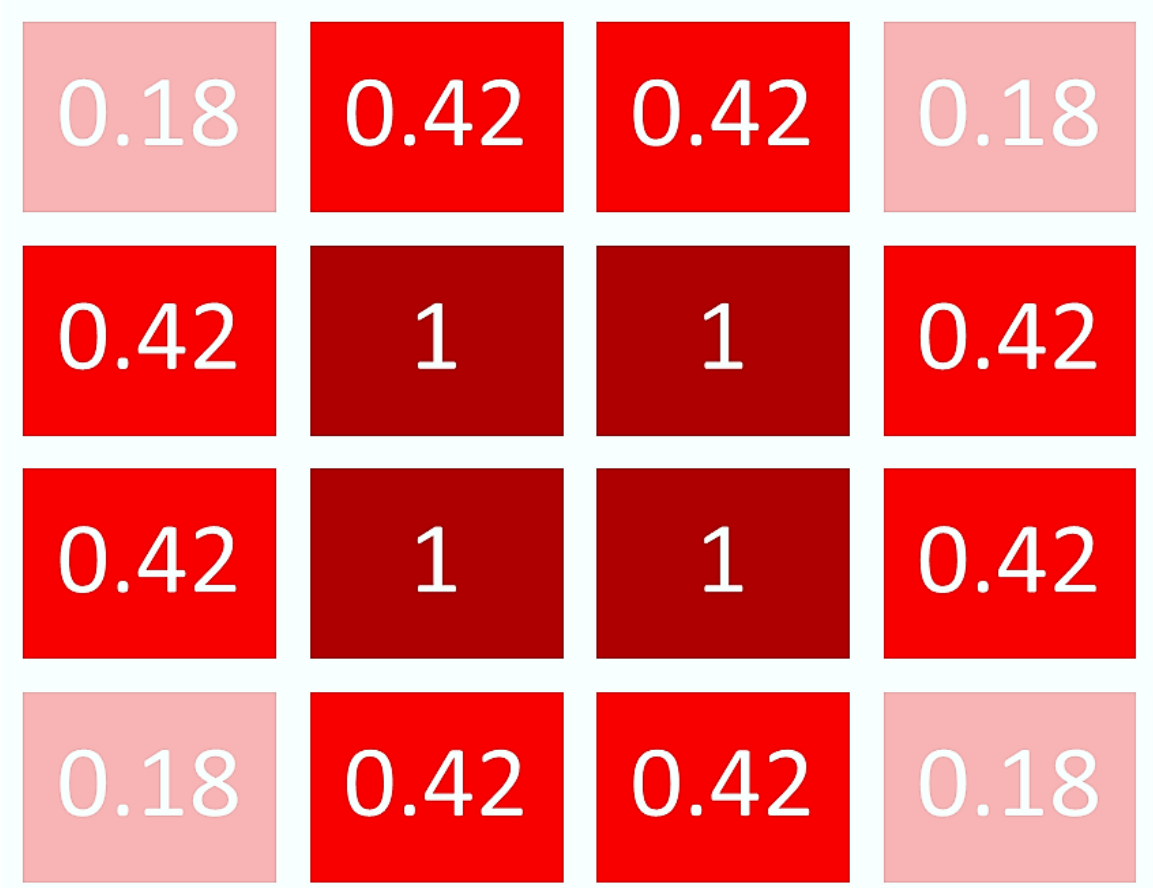

Fig. 5.3: Dolph-Chebyshev taper excitation coefficient.

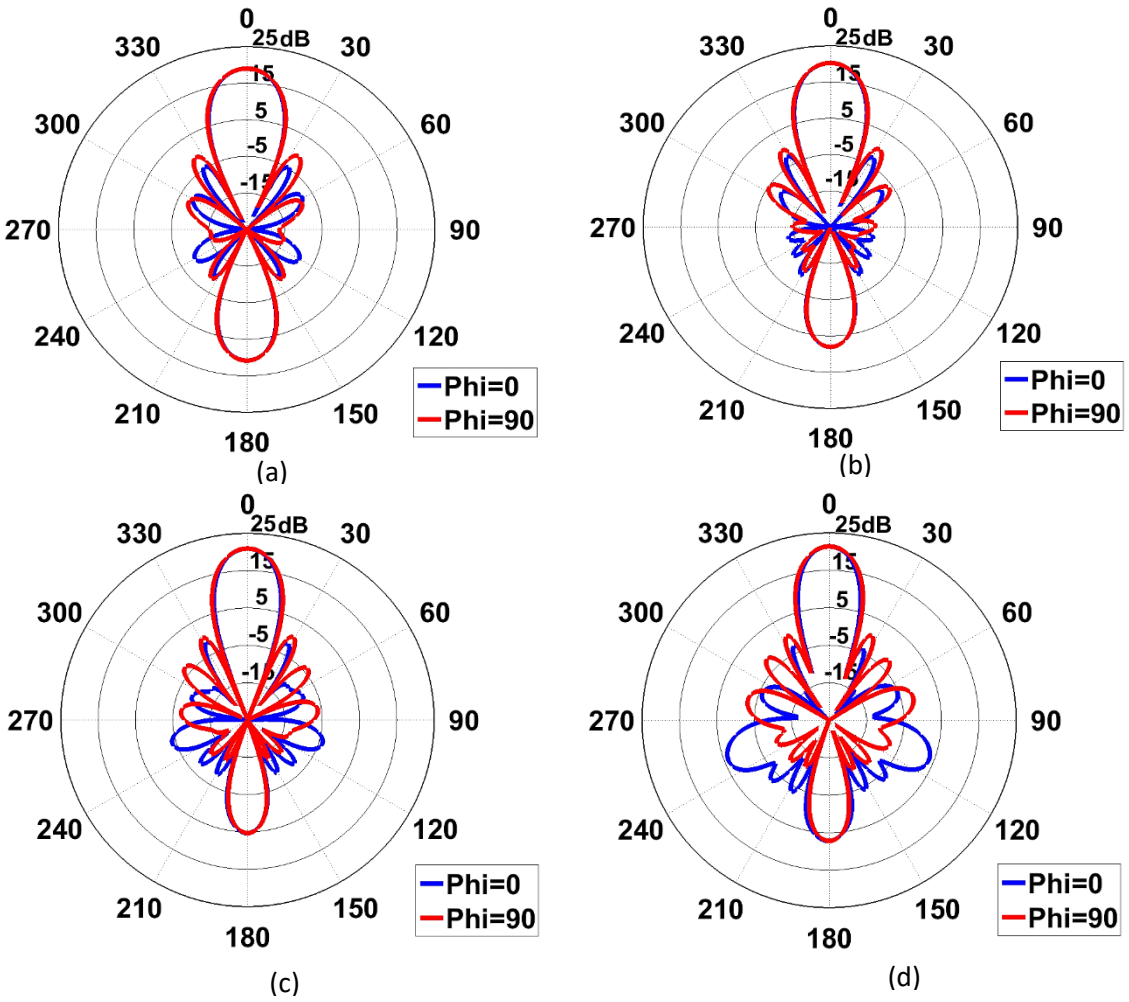

Fig. 5.4: Simulated radiation patterns of Dolph-Chebyshev array at (a) 2.45 GHz, (b) 2.65 GHz. (c) 2.85 GHz, (d) 3.05 GHz.

Table 5.2: Summary of radiation pattern data for Dolph-Chebyshev array.

Frequency (GHz)	**Realized Gain (dBi)**	**SLL (dB)**	**F/B (dB)**	**Directivity (dBi)**
2.45	19	19.7	8.2	19.2
2.65	20.3	20.16	12.3	20.2
2.85	20.9	20.6	15.7	21
3.05	21.4	21.1	14.2	21.5

5.4 Synthesizing Array Factors to Meet User Requirements

Our design goal is to design an antenna array with a SLL of at least 25 dB at 2.45 GHz. A great deal of research has been done on how to do this [28-31] by engineers from various fields including microwave engineers to computer science experts. There are multiple algorithms developed using Fourier, Inverse Fourier transform techniques, genetic search algorithms [28] and other advanced mathematical techniques which help us determine an array factor that would perfectly fit our design constraints if they are achievable and physically realizable. A method developed by Dr. W. Keizer [32-33], which involves taking successive inverse Fourier transforms of the array factor and using curve fitting to find the required array factor has been utilized hear to find the taper weights for a linear array. This is an iterative technique which updates the array factor till it fits all the design parameters that need to be met. The design parameters at our disposal are, the frequency of operation, number of elements, minimum required SLL and maximum allowable max to min illumination ratio. The frequency was chosen to be 2.45 GHz, the number of elements is 4, the SLL is 25 dB and the max to min illumination ratio was chosen so that the minimum required line widths should not fall below 0.3 mm, as it would be difficult for us to fabricate printed circuit boards with traces thinner than 0.3 mm with a high degree of precision and reliability. The normalized taper profile, [0.23 1 1 0.23] satisfies all of the above mentioned requirements. Converting the obtained linear taper profile for a planar array would lead to an amplitude distribution as shown in Fig. 5.5.

Fig. 5.5: Synthesized taper excitation coefficient for SLL of 25 dB.

The main drawback of the taper profile shown above is the huge difference in power being delivered to the four elements in the center versus the power being delivered to the patches in the four corners, the max to min illumination for this antenna is 18.5:1. Even though the gradient is very steep, this antenna array is still physically realizable. Fig. 5.6 represents the simulated radiation pattern data for an amplitude tapered individually fed planar antenna array. The realized gain and directivity of this array is slightly lower than the two arrays previously discussed, the beamwidths are almost the same and the backlobe radiation levels are also comparable. The most redeeming quality

of this antenna though is its superior SLL performance. The SLL at 2.45 GHz is 28.3 dB, which exceeds expectations by more than 3 dB. The SLL is seen to decrease as the frequency increases but the antenna has a SLL of 20 dB or higher throughout the operating frequency band. At higher frequencies more sidelobes start appearing, these lobes also have a higher amplitude and this phenomenon is seen more pronounced in the $\Phi=0^{o}$ plane rather than the $\Phi=90^{o}$plane. The results for the radiation pattern of this antenna have been tabulated in Table 5.3.

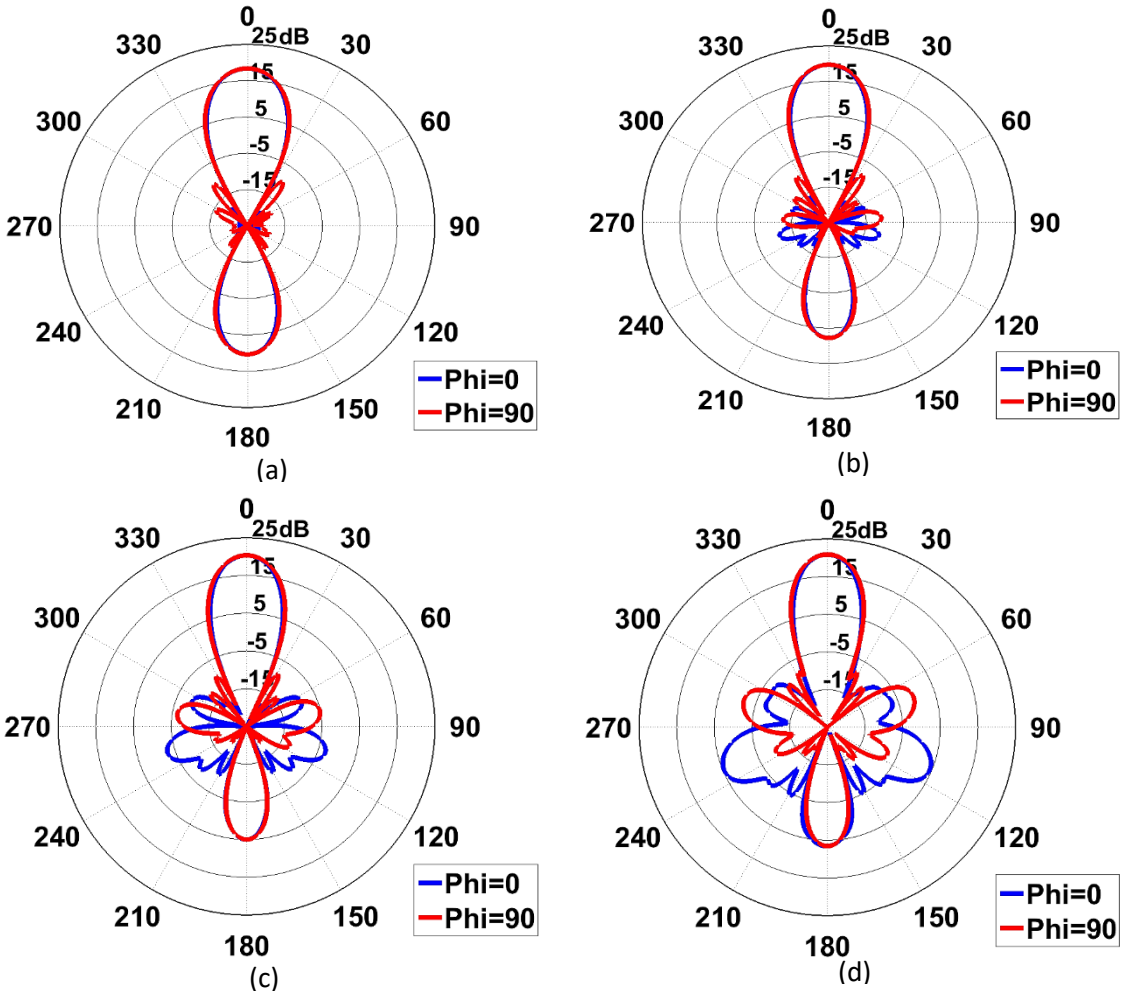

Fig. 5.6: Radiation patterns of array at (a) 2.45 GHz, (b) 2.65 GHz. (c) 2.85 GHz, (d) 3.05 GHz.

Table 5.3: Summary of radiation pattern data for synthesized array.

Frequency (GHz)	Realized Gain (dBi)	SLL (dB)	F/B (dB)	Directivity (dBi)
2.45	18.4	28.3	8	18.6
2.65	19.7	28.6	11.9	19.7
2.85	20.3	25.2	15.3	20.5
3.05	20.9	21.6	14.4	20.9

5.5 Amplitude Tapered Corporate Feed

To obtain the radiation patterns shown in Fig. 5.6 we need the taper coefficients to be as shown in Fig. 5.5. This means we need to develop a corporate feed network which splits the input power in the ratio shown in Fig. 5.5. There are many ways to achieve this, we can use MMIC attenuators and control them so as to attenuate the signal at each input arm such that it matches our taper profile. Another simpler approach would be to use power division networks as part of the corporate feed network. Many different power division networks have been successfully used to do this including but not limited to Wilkinson power dividers, rat race hybrids and T-junctions. For our design we utilize a series of cascaded T-junction power dividers so as to obtain the desired unequal power split. The T-junction was chosen for its simplicity of design, implementation and ease of matching. The rest of the corporate feed network is matched using quarter-wave transformer sections exactly like that described in Section 4.2. Fig. 5.7 below shows the design of the amplitude tapered corporate feed section used to feed the array.

Even with the tapering, the feed network still maintains its symmetry. How the various line widths required for the power division and match are obtained is discussed in this

section. The line with width w_1=3.5 mm has a characteristic impedance of 50 Ω and the line with width w_2=5.8 mm has an impedance of 35.36 Ω as mentioned in the previous chapter. Now, let us say P_{IN} is the power entering the node lying between the arms labelled w_3 and w_4. If P_3 and P_4 are the powers flowing in the respective arms, then we can say that,

$$P_{IN} = P_3 + P_4 \quad \ldots (5.7)$$

Therefore for an unequal power distribution [15],

$$P_3 = kP_{IN} \quad \ldots (5.8)$$

$$P_4 = (1-k)P_{IN} \quad \ldots (5.9)$$

So to obtain a match at the terminal the impedances have to be as follows,

$$Z_3 = \frac{Z_1}{k} \quad \ldots (5.10)$$

$$Z_4 = \frac{Z_1}{(1-k)} \quad \ldots (5.11)$$

So basically Z_3 and Z_4 are the required equivalent impedances seen looking in from arms 3 and 4 respectively to obtain a matched network with the desired power division ratio. Therefore, the impedance of the quarter wave transformer sections needed to match the network will be given by [20],

$$Z_{w3} = \sqrt{Z_3 Z_1}$$

$$Z_{w4} = \sqrt{Z_4 Z_1}$$

Solving the above equations we find,

$$Z_{w3} = 54.76\ \Omega$$

$$Z_{w4} = 113.8\ \Omega$$

So to obtain the above mentioned required impedances, we will need lines with widths [20],

$$w_3 = 2.94 \text{ mm}$$

$$w_4 = 0.6 \text{ mm}$$

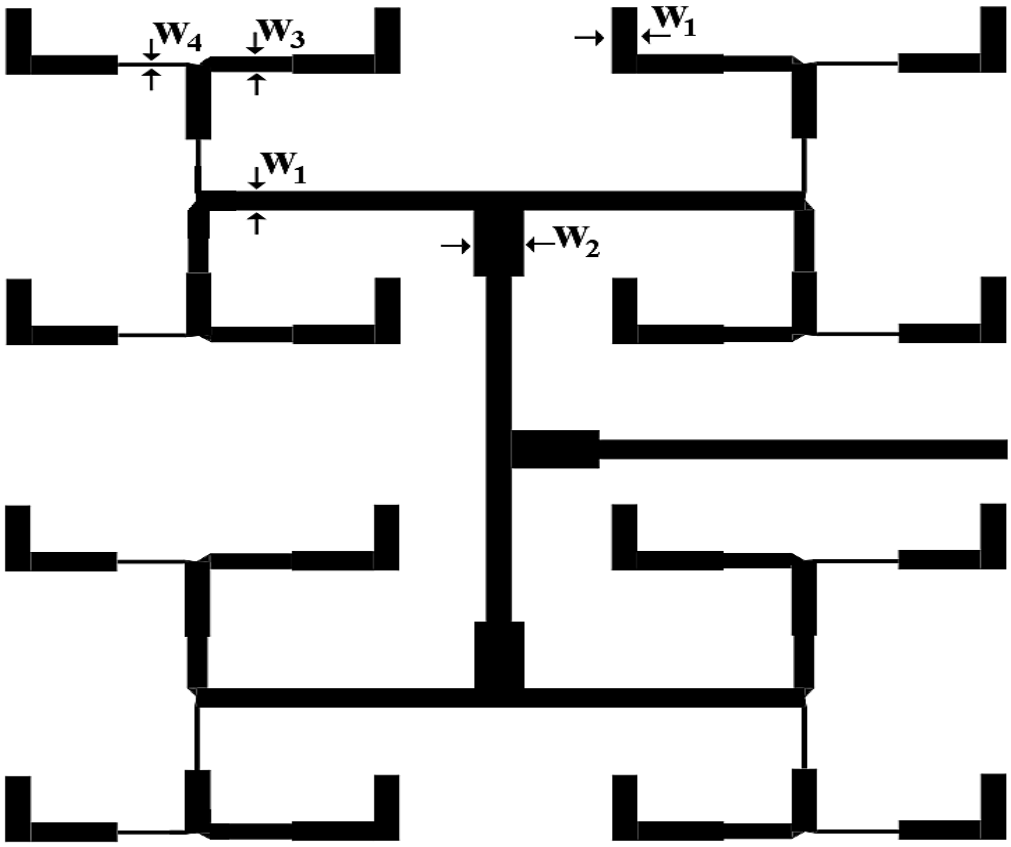

Fig. 5.7: Tapered corporate feed network.

To maximize the bandwidth of the array, further parametric simulations were run after designing the tapered corporate feed network. It was observed that a wider bandwidth was achievable by decreasing the thickness of the antenna substrate. Fig. 5.8 shows the S_{11} response of the antenna array as the antenna substrate thickness is varied from 0.2 mm to 1.2 mm in steps of 0.2 mm. Maximum bandwidth is obtained when the antenna substrate is 0.2 mm. The S_{11} plot for the antenna array consisting of the tapered corporate feed network with the new antenna substrate thickness is shown in Fig. 5.9 below. From this plot we can see that the antenna has an operating bandwidth of 2.32 to 3.2 GHz barring a very small region between 3 GHz to 3.12 GHz where the S_{11} briefly increases to about -8.7 dB.

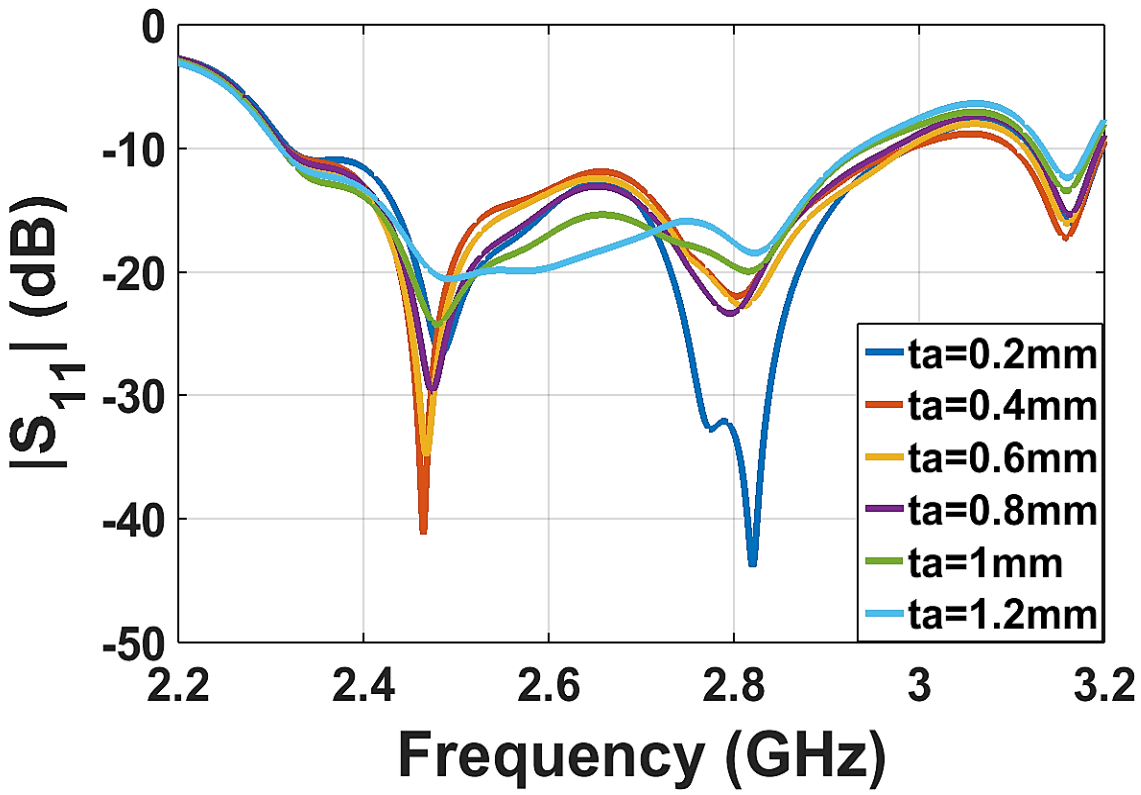

Fig. 5.8: S_{11} plot for 4X4 array with tapered corporate feed network when the antenna substrate thickness is varied.

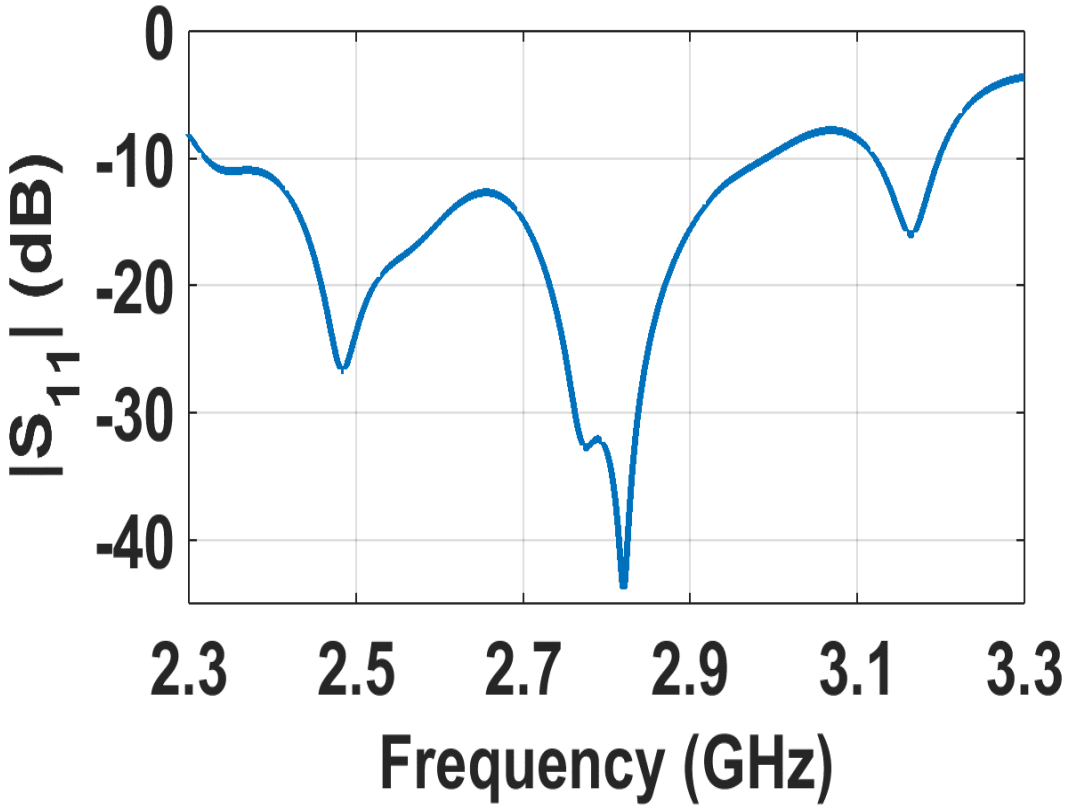

Fig. 5.9: S_{11} plot for 4X4 array with tapered corporate feed network.

The radiation pattern plots have been presented in the Figs. 5.10 below. One small change that has been made while presenting the radiation pattern plots for this array and all subsequent radiation pattern plots is that plots have been presented for the frequencies, 2.45 GHz, 2.65 GHz, 3 GHz and 3.1 GHz. The last two frequency reference points were moved from 2.85 GHz and 3.05 GHz to 3 GHz and 3.1 GHz respectively because the practical measurements of the radiation patterns were made at these frequencies thus having simulation data at the same frequencies help us compare the results better. The reason why the antennas were measured at these frequencies will be discussed in the next Chapter. The Half Power Beamwidth (HPBW) of the array has also been mentioned while evaluating the radiation characteristics of this array. The HPBW of an array is

basically the angle formed by the two points where the mainlobe radiation falls by 3dB or half its original value with the center of the plot [9]. This allows us to determine how spatially selective an antenna is *i.e.*, how narrow the mainlobe is. Depending on the application the HPBW can be a very important determining factor. Phased array antennas having a very narrow HPBW allows the antenna to very precisely transmit and receive power in a given direction and gives the antenna a much higher resolution in applications such as radar antennas and in modern day mobile systems narrow beamwidths are very desirable as they help minimize co-channel interference [34]. The HPBW for our antenna varies from 22^o to 17^o depending on the frequency of observation. All the results obtained in this radiation pattern plot simulations have been summarized in Table 5.4.

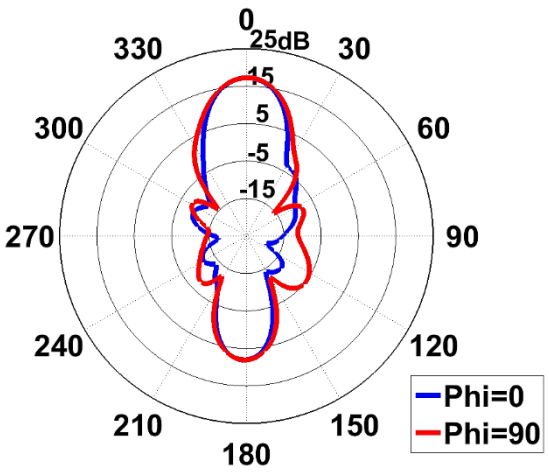

(a)

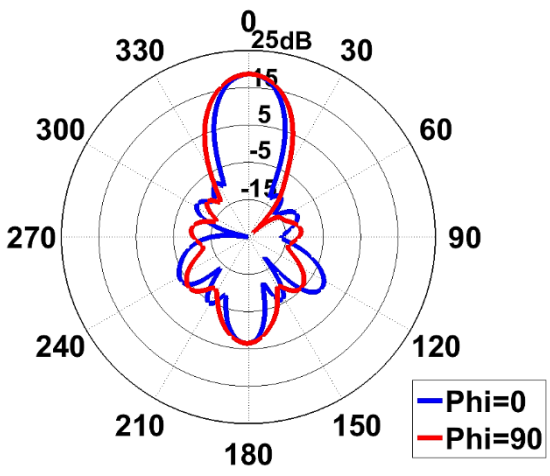

(b)

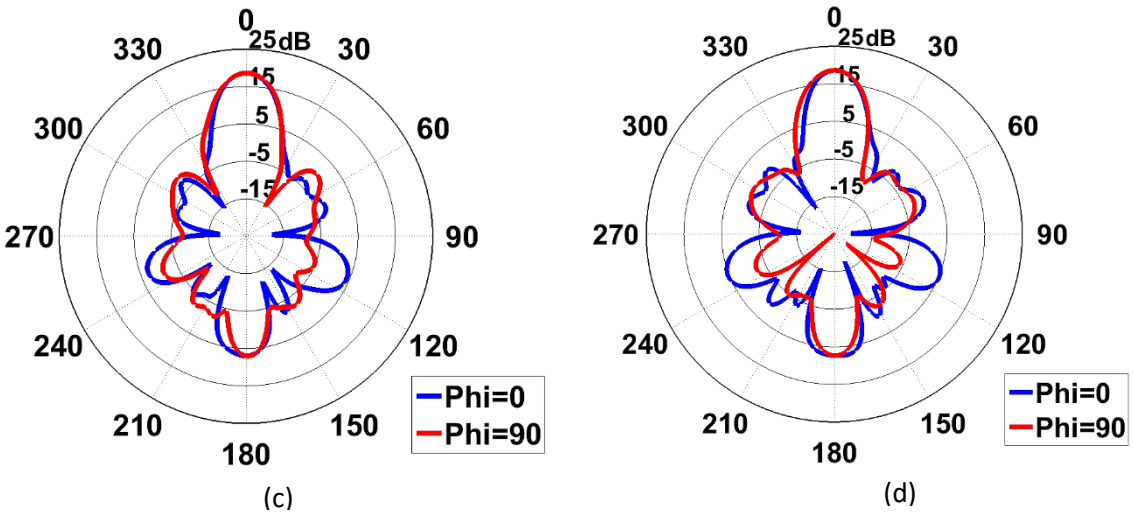

Fig. 5.10: Radiation patterns of tapered corporate-fed array at (a) 2.45 GHz, (b) 2.65 GHz. (c) 3 GHz, (d) 3.1 GHz.

Table 5.4: Summary of radiation pattern data for array with tapered corporate feed.

Frequency (GHz)	Realized Gain (dBi)	SLL (dB)	F/B (dB)	Directivity (dBi)	HPBW (Degrees)
2.45	17.2	25.5	9.3	17.7	22.2
2.65	18.6	27.2	15.2	19.3	20
3	18.6	18.5	11.7	19.7	17
3.1	18.6	18.6	11.3	20	17.5

5.6 Reducing Backlobe Radiation

Backlobe radiation is a significant point of concern while designing most antenna systems. Apart from the waste of radiated energy and reduced antenna efficiency most commercial, defense and space research antennas have limits on the tolerable backlobe radiation levels. In commercial applications such as mobile devices there is a maximum allowable Specific Absorption Rate (SAR) which must be met by an antenna system for it

to be considered safe for human use [35]. Similarly for space antennas and radar antennas that are placed close to the surface of the earth a high level of backlobe radiation causes the radiation to get reflected off the ground and interfere with the incoming signal which deteriorates performance.

For this array, a metal reflector has been used to block the backlobe radiation. This metal reflector acts as a secondary ground plane. The feed substrate is separated from the reflector by a layer of ROHACELL 71HF foam with thickness h_r. The reflector being used is made of aluminum and overshoots the array by an inch at each edge. The cross-sectional view of the antenna with the reflector can be seen in Fig. 5.11.

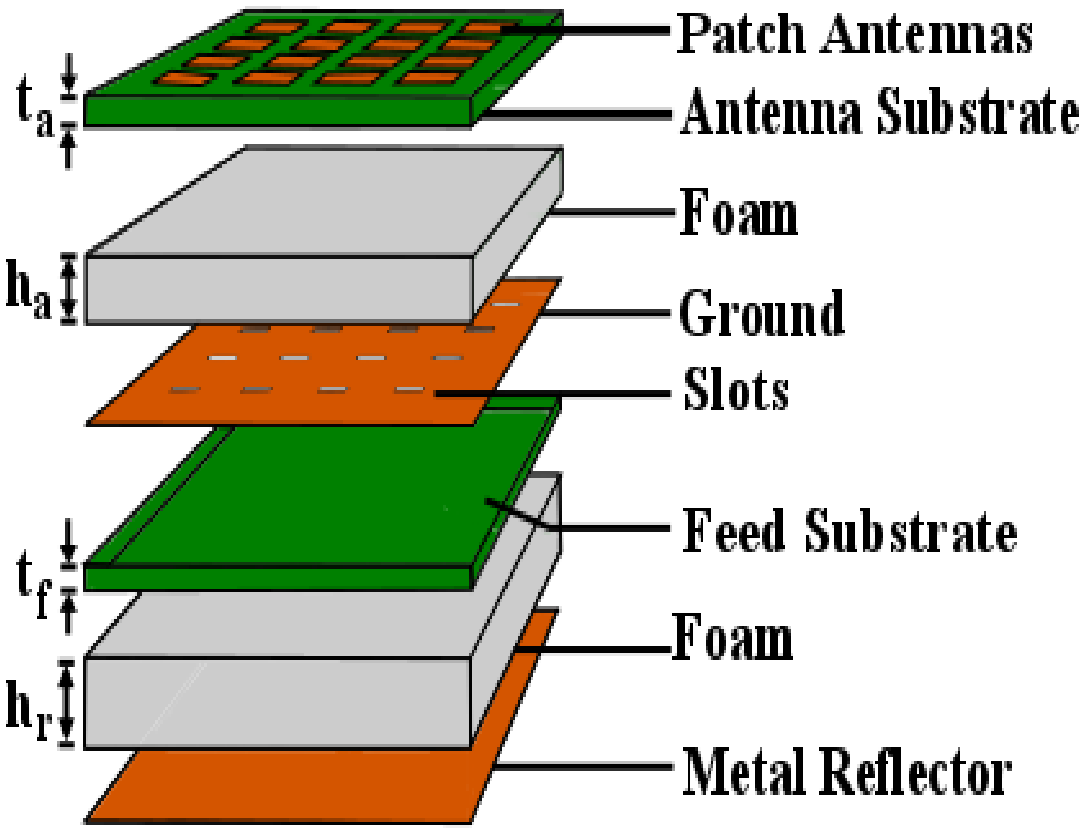

Fig. 5.11: Cross-sectional view of array with the reflector.

A parametric simulation was run to determine the optimum distance at which the metal plate must be placed so as to obtain maximum backlobe suppression while minimizing any deleterious effect on the desired front lobe radiation pattern. The results of the parametric sweep have been shown in Fig. 5.12. From the S_{11} plot below it can be clearly seen that the best bandwidth performance is seen when the reflector is placed at a distance of h_r=25 mm from the corporate feed network at the bottom. The radiation pattern plots seen when the reflector distance is varied is shown in Figs. 5.13 - 5.16. It was also observed that the closer the reflector was placed to the array higher the impact it had on the main lobe radiation. When the reflector was placed too close to the antenna the main lobe was seen to get wider with higher levels of SLLs. The impedance bandwidth obtained when h_r=25 mm is 0.86 GHz, it spans from 2.35 GHz to 3.21 GHz. The S_{11} at 2.45 GHz is seen to be -23.86 dB which is very favorable.

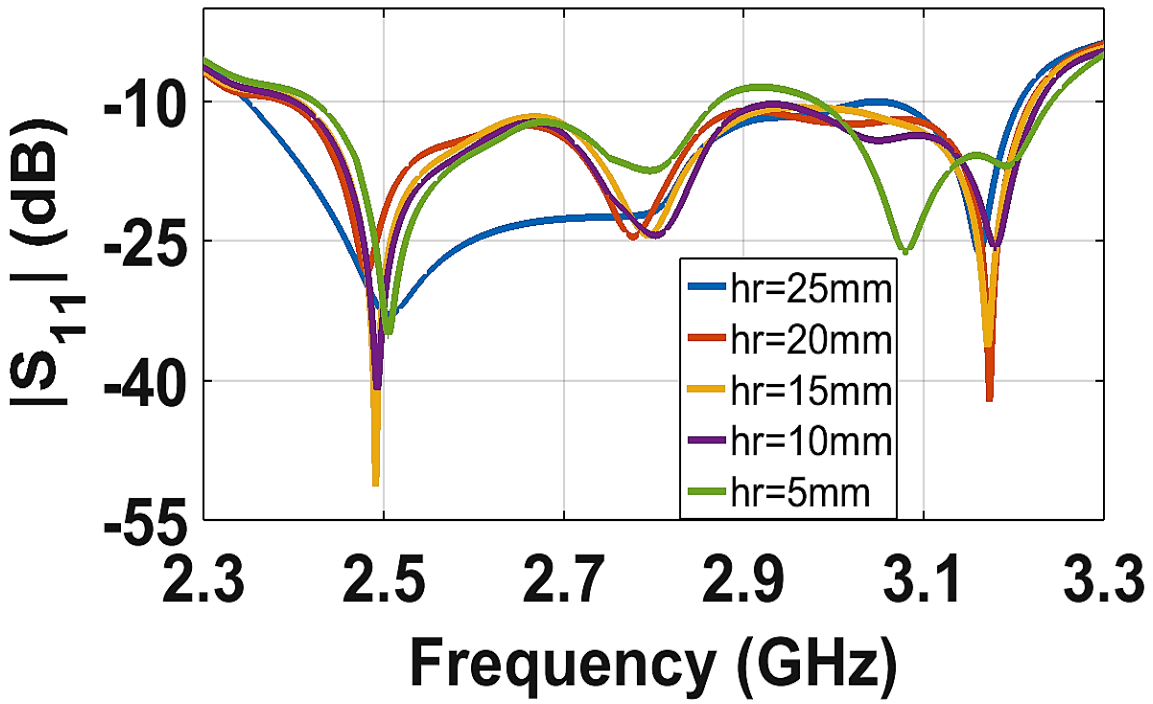

Fig. 5.12: S_{11} response when position of reflector is changed.

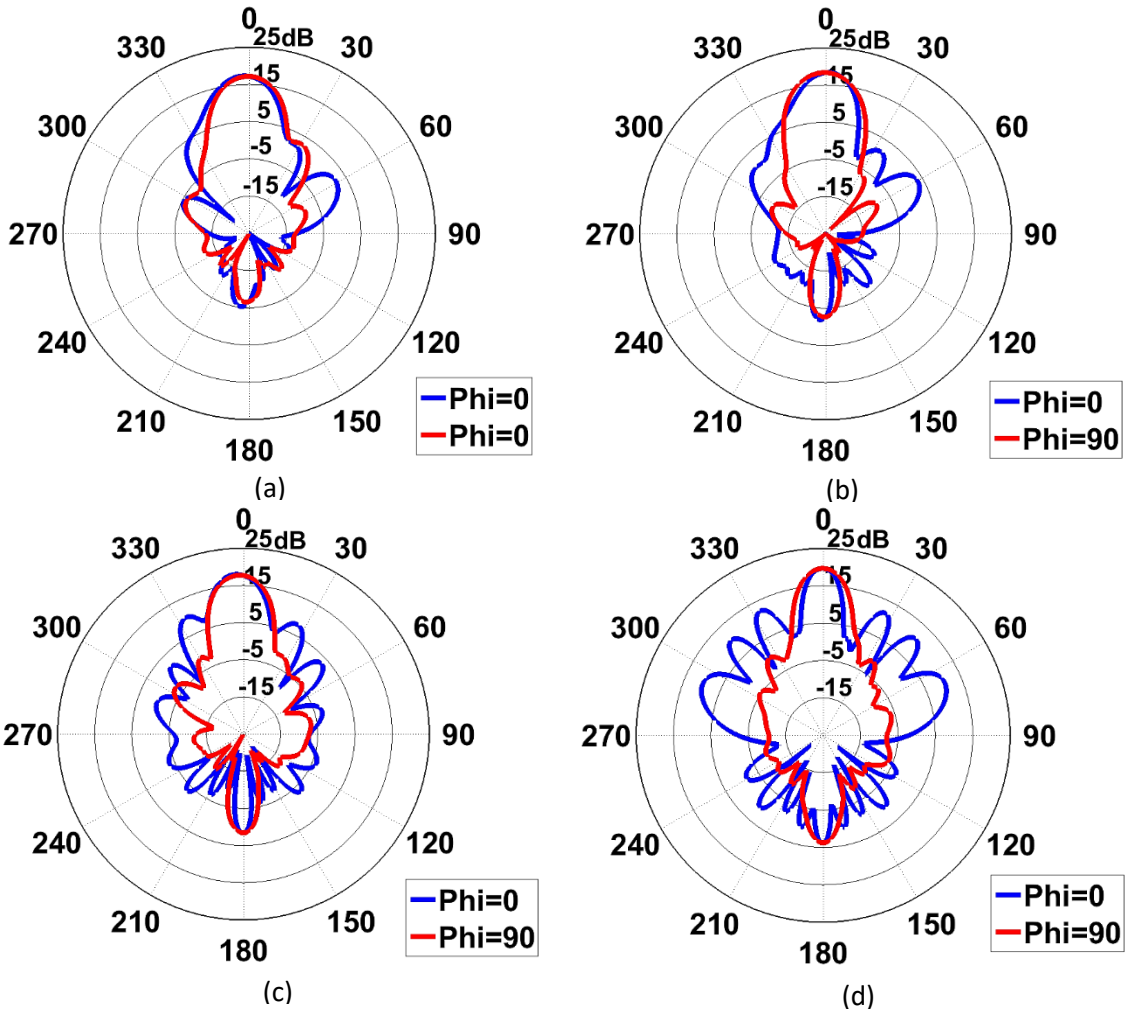

Fig. 5.13: Radiation pattern plots when h_r=10 mm at (a) 2.45 GHz, (b) 2.65 GHz. (c) 2.85 GHz, (d) 3.05 GHz.

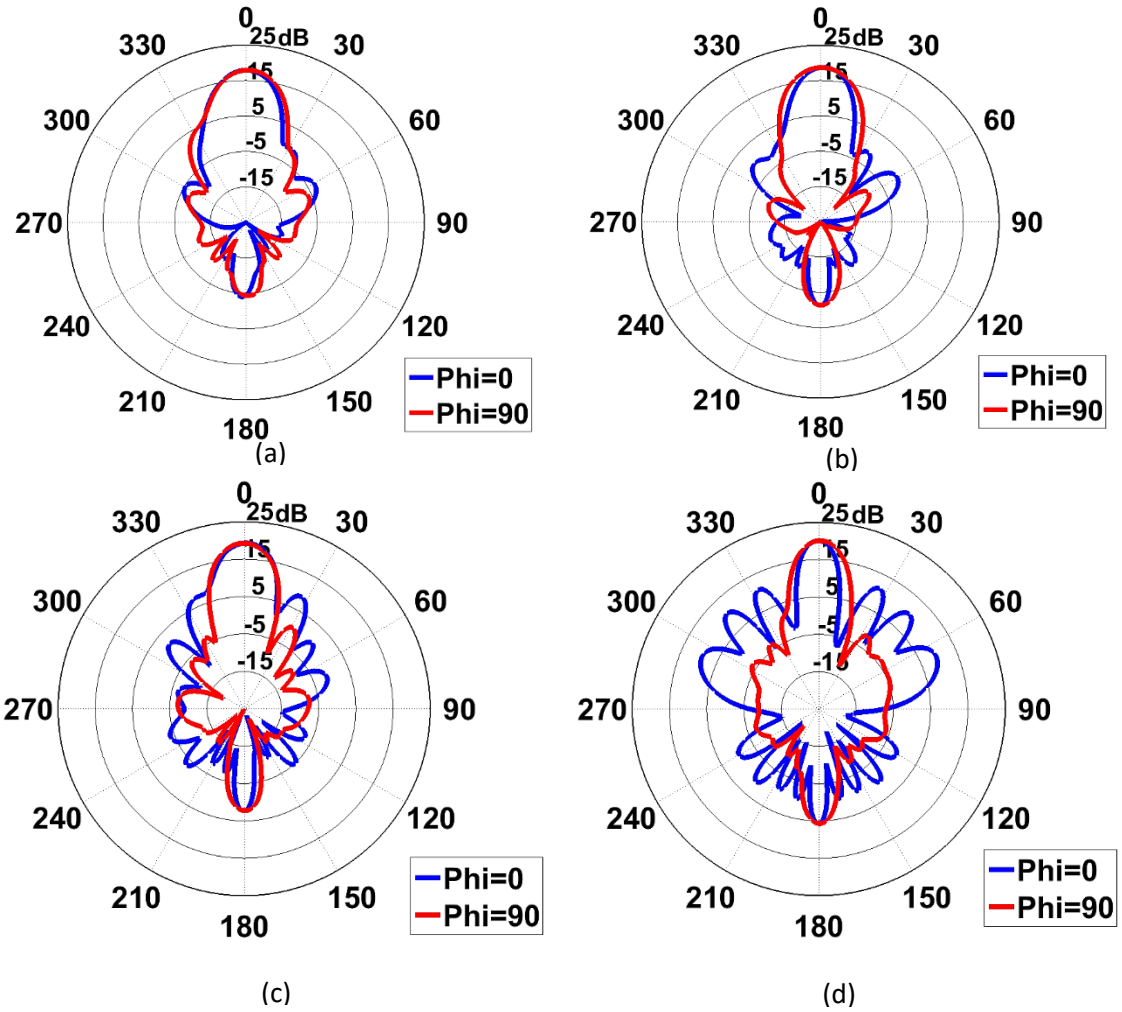

Fig. 5.14: Radiation pattern plots when h_r=15 mm at (a) 2.45 GHz, (b) 2.65 GHz. (c) 2.85 GHz, (d) 3.05 GHz.

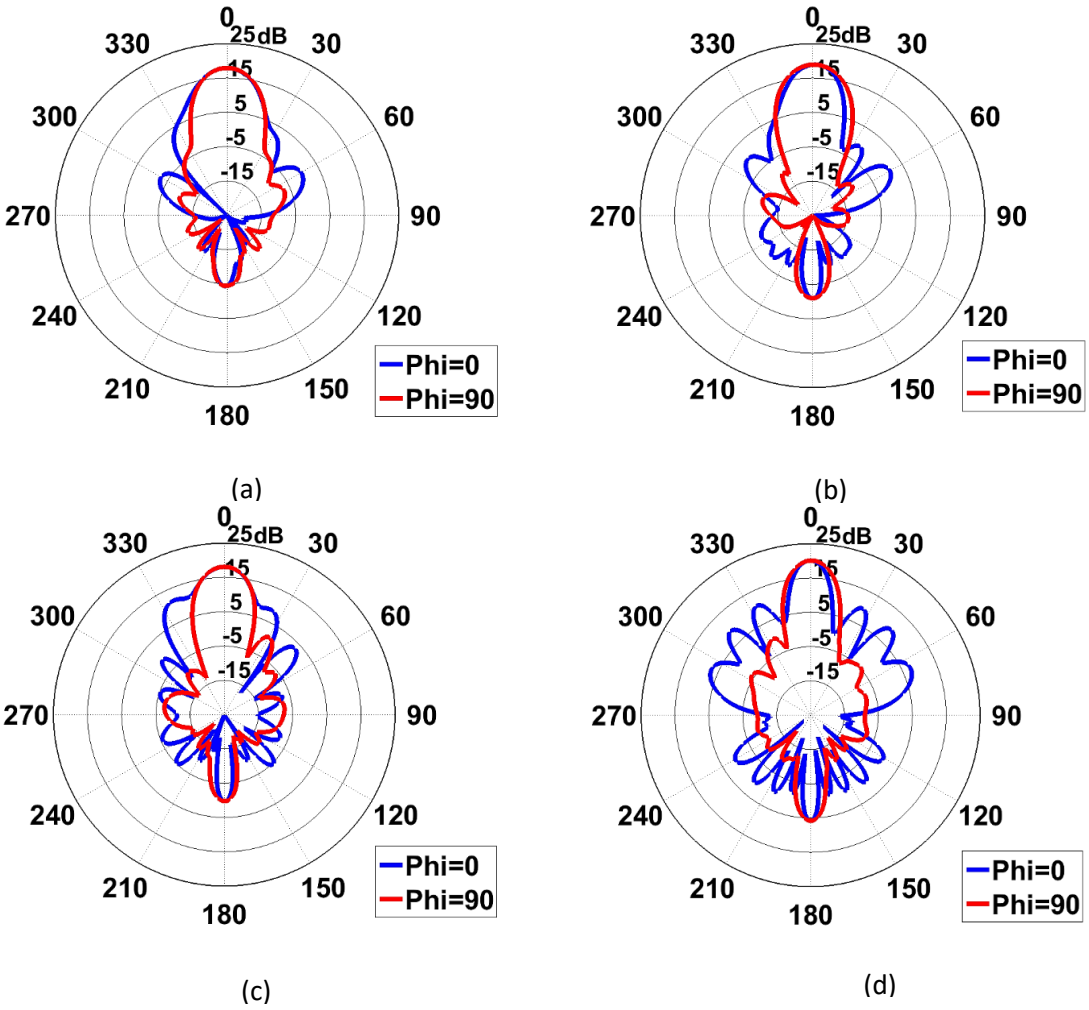

Fig. 5.15: Radiation pattern plots when h_r=20 mm at (a) 2.45 GHz, (b) 2.65 GHz. (c) 2.85 GHz, (d) 3.05 GHz.

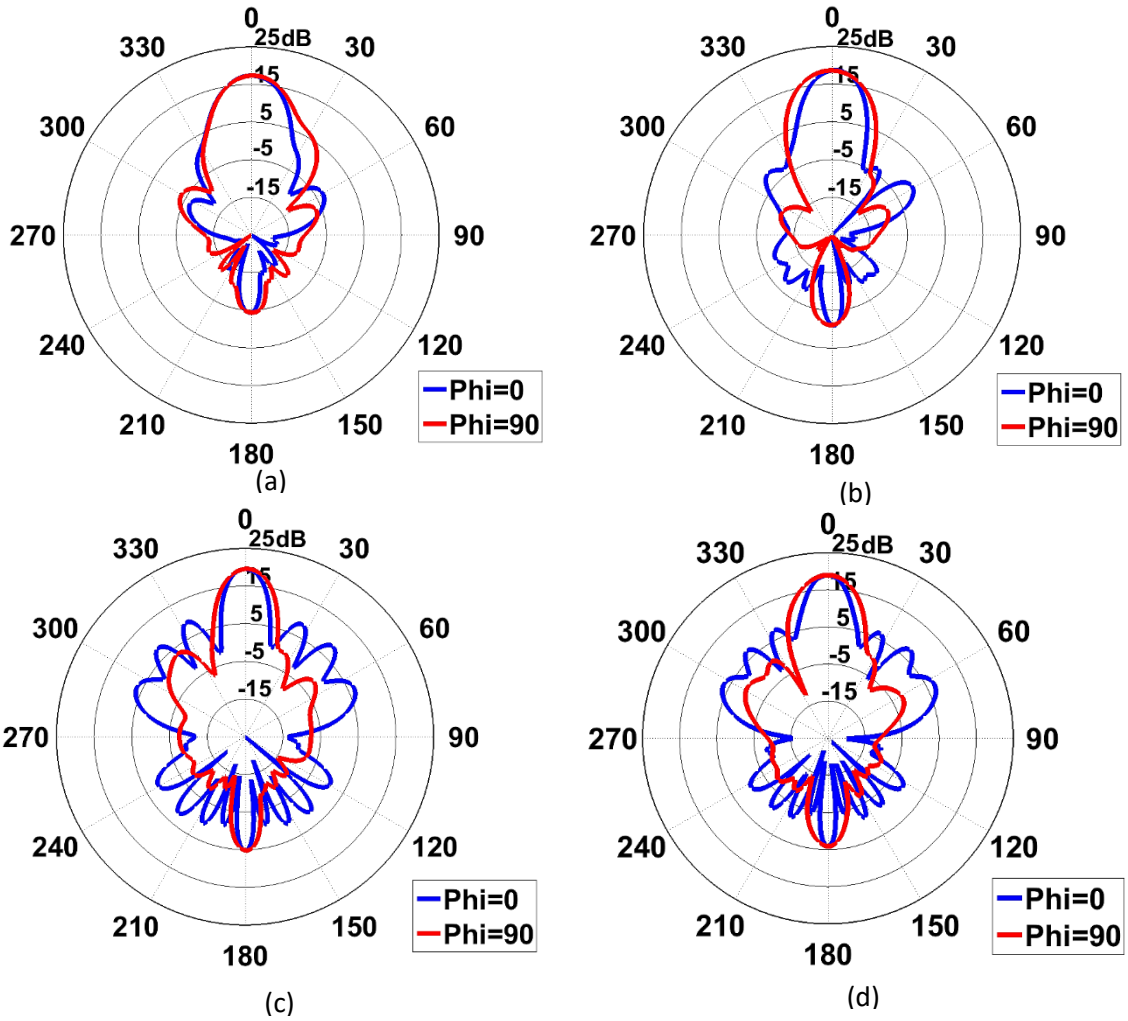

Fig. 5.16: Radiation pattern plots when h_r=25 mm at (a) 2.45 GHz, (b) 2.65 GHz. (c) 3 GHz, (d) 3.1 GHz.

The radiation pattern plots at the four frequencies of interest are plotted in Fig. 5.16 above. In the final design the reflector was placed 25 mm below the feed substrate because of its better performance around the 2.45 GHz range. The other shown reflector heights can be chosen as well as they too exhibit very acceptable performance parameters. In fact, for applications which require a more compact design one of the closer reflector spacing might be more preferable. The reflector is seen to marginally boost the realized gain of the antenna throughout the operating frequency band. But the

biggest drawback which can be seen is the increased SLLs. The addition of the reflector plate increases the SLL by about 5 to 6 dB across the frequency band. This increased SLL and increased number of sidelobes is greater at higher frequencies as the taper was designed with a central frequency of 2.45 GHz. There is a very minor drop-off in the directivity which can be attributed to the increased radiation in the sidelobes. The HPBW is almost the same or even better at some frequencies. The HPBWs mentioned are the average of the HPBWs in the $\Phi=0^o$ and $\Phi=90^o$ planes. As we can see from Fig. 5.16, the main beam radiation has a narrower lobe in the $\Phi=0^o$ plane when compared to the $\Phi=90^o$ plane, but we also observe a greater number of sidelobes and higher overall level of SLL in this $\Phi=0^o$ plane. The reflector however helps decrease the backlobe radiation by as much as 12.3dB, which is very significant improvement. The F/B ratio thus obtained after utilizing the reflector is seen to be much higher. The values obtained via simulation for the realized gain, SLL, F/B, directivity and HPBW of the antenna with the reflector are summarized in Table 5.5.

Table 5.5. Simulation data for the 4X4 array with metal reflector.

Frequency (GHz)	**Realized Gain (dBi)**	**SLL (dB)**	**F/B (dB)**	**Directivity (dBi)**	**HPBW (Degrees)**
2.45	17.4	20.4	21.8	17.4	22
2.65	18.7	18.9	19.8	18.7	20
3	19.6	12.9	14.4	19.6	14
3.1	18.9	12.3	14.8	18.9	15

Chapter 6: Fabrication and Measurements of Array

6.1 Introduction

This chapter goes over the step by step fabrication of the array, the constraints faced during developing the printed circuit boards and the compromises that had to be made in order to circumvent these obstacles. This is then followed by the test setup and measurement data obtained for the various antenna configurations already discussed in the previous chapters. Measurements were made for the 4X4 antenna array without the reflector, the 4X4 array with the reflector and two more additional cases were also measured where the performance of the antenna with and without the reflector were measured when a superstrate was placed on top of the antenna. The superstrate used was a FR4 (ε_r=4.4, tanδ=0.018) sheet the size of the array with a thickness of 1.6 mm. The main purpose behind using the superstrate was to tune the designed antenna array so as to obtain a better S_{11} response and the effects of doing so have been discussed in this chapter. So, a total of four cases have been implemented and their performance measured. The S_{11} performance of each of these arrays were measured in our lab using a Vector Network Analyzer (Agilent E5071C) and the radiation pattern measurements were done in a Satimo SG-64 Anechoic Chamber located at the Wireless Research Center in North Carolina. The radiation patterns were measured at 2.45, 2.65, 3 and 3.1 GHz so as to assess the radiation performance of the antenna throughout its operating bandwidth. All

of this data has been plotted, summarized and compared with the simulation data presented in the former chapters.

6.2 Fabrication

Chemical photo-etching was used to build the feed substrate and the antenna substrate. Both these substrates were first coated with a negative photo-resistive coating and then exposed to light in a UV box after the appropriate masks were placed on top of them. The negative photo-resist bonds with the substrate when it is exposed to ultra violet light, which is achieved in the UV box. Once this is done we treat the boards with a diluted solution of a negative photo-developer which is usually a strong base so as to remove the photo-resist coating from regions which are of no interest to us *i.e.*, the regions which were kept in the dark, thus exposing the copper coating below and leaving a layer of photo-resist in the pattern of the required trace. The board is then placed in an etching tank which consists of a temperature controlled tank filled with ammonium persulfate. The ammonium persulfate reacts with the exposed copper on the board stripping it off and leaving only the substrate behind which in our case is RO4003c. The trace is protected because it is still covered with a layer of photo-resistive coating. When all the unnecessary copper has been stripped from the board we remove the substrate from the tank and then treat it with a very strong solution of the previously used developer in order to remove the photo-resist coating thus obtaining the required trace. To obtain a well etched board many factors need to be taken into consideration. Some of the important factors are the exposure time in the UV box, the strength of the developer solution being used and the temperature and time that the boards are allowed to sit in the etching tank have to be monitored closely or else the boards might get over etched. If the

board is exposed to light for too long then the regions that are supposed to be in the dark under the mask also get exposed and may not properly wash off when treated with the developing solution and similarly when the exposure time is too little the photo-resist might not bond strongly enough to the board which will cause it to come off when placed in the developer solution or the etching tank. Through multiple trial and error attempts it was found that an exposure time of 150 seconds gave the best results. The developer solution was diluted in the ratio of 1:12 for the pre-etching stage and a raw solution was used post etching to remove the photo-resist. The ammonium persulfate solution used was created by dissolving a kilogram of persulfate per 4 liters of water and the temperature was controlled as per the progress of the etching.

The major problem that was encountered while trying to etch the boards was the large size of the array. The array has a length of approximately 354 mm and a width of 345.6 mm but the size of the UV box is only 25 mm X 40 mm and the etching tank is also not large enough to fit the entire array. So because of this, the array was divided into four rectangular sub-arrays with 4 elements each. Each sub-array, *i.e.*, the four patches and its respective feed boards and corresponding ground planes with the apertures were etched separately. The sub-arrays are not all the same size because if divided symmetrically the feedline running through the center of the array would get cut along its width and aligning it would not be easy and it would not be very accurate. Fig. 6.1 shows the top layer or the patch layer of the antenna array.

Fig. 6.1: Top view of array.

The four sub sections of the array can be clearly seen from the above figure. These four separate sections were joined together using scotch tape. Some of the patches developed small holes in them due to over etching, these holes were filled using solder. The top layer was placed on top of the foam and was taped together with the bottom layer to hold them in place. The bottom layer, which is the feedline substrate was also etched in four parts as mentioned earlier. Figs. 6.2 shows the four different sections separately.

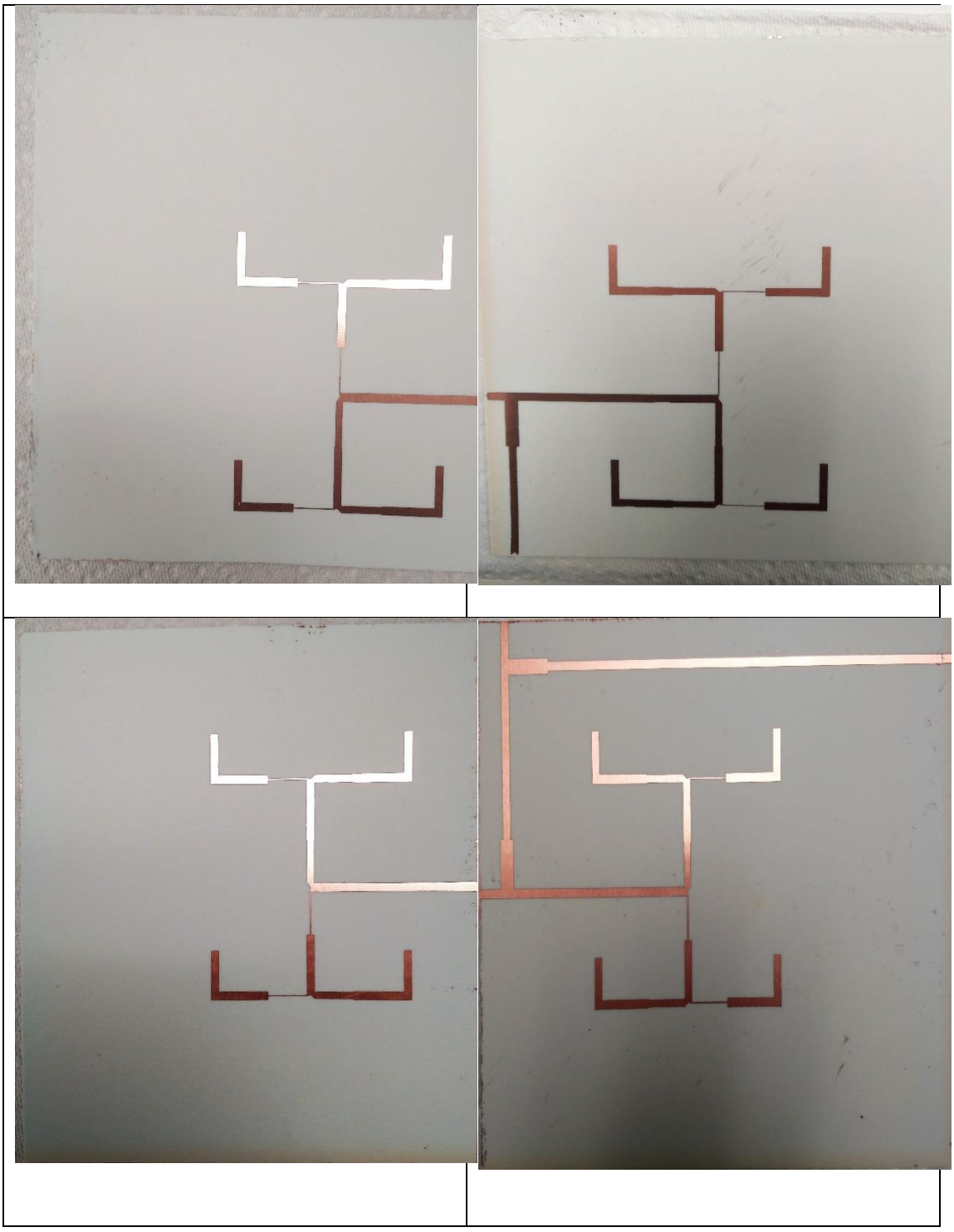

Fig. 6.2: Feedline sections.

These four sections were put together and aligned properly. Small sections of copper tapes with widths of 3.5 mm were used to bridge the feedlines running across the

sub-parts and these copper tapes were soldered on both ends. The other face of these boards contain the ground plane and the apertures. The same procedure was followed here too, copper tape was used to establish connectivity and then it was soldered. Some scotch tape was applied on both sides to make sure it was sturdy. Fig. 6.3 shows the completed corporate feedline. The feed sections on the second and fourth quadrant of the feedline substrate did not align exactly due to minor displacements while placing the masks, but were then corrected keeping the displacement as low as possible. Fig. 6.4 shows the ground plane with the apertures.

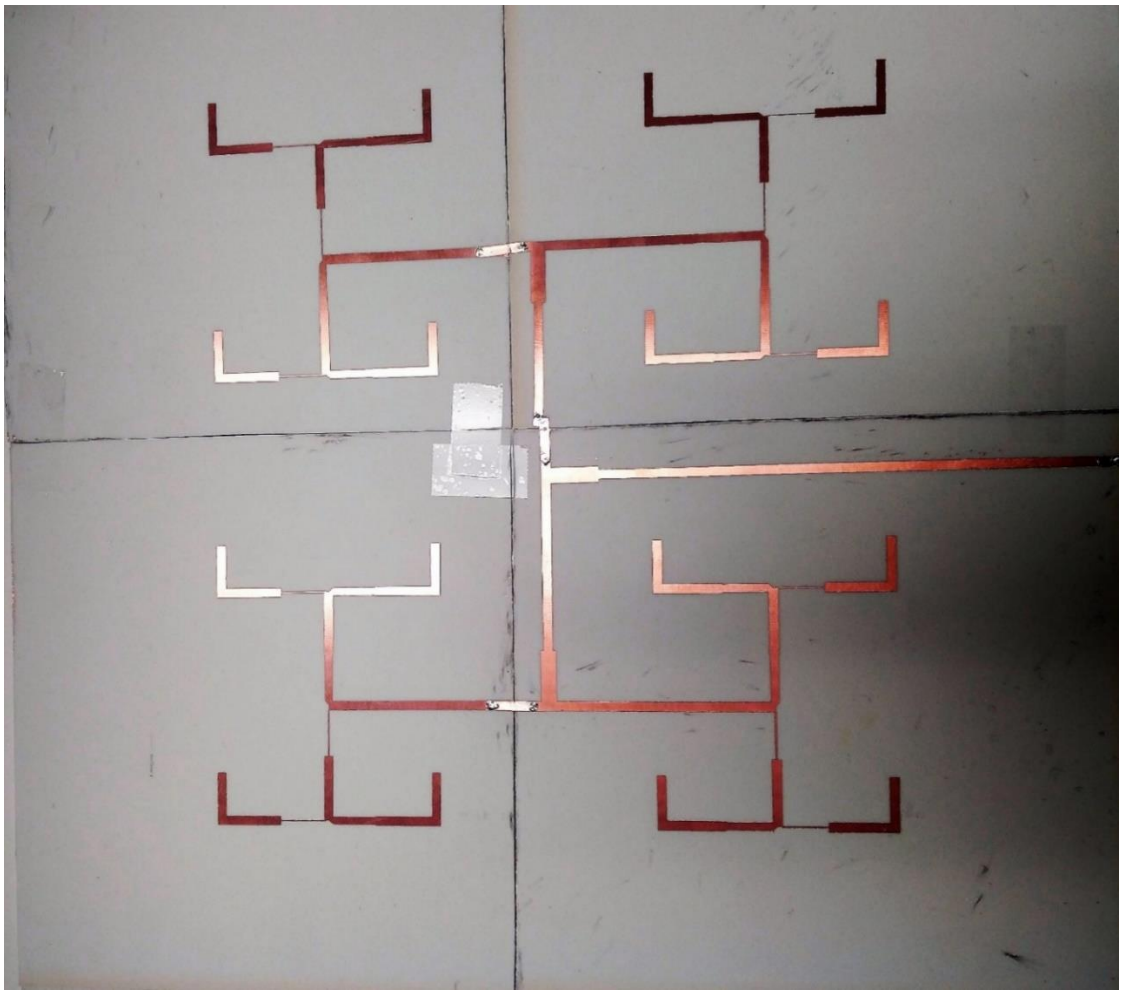

Fig. 6.3: Corporate feed network.

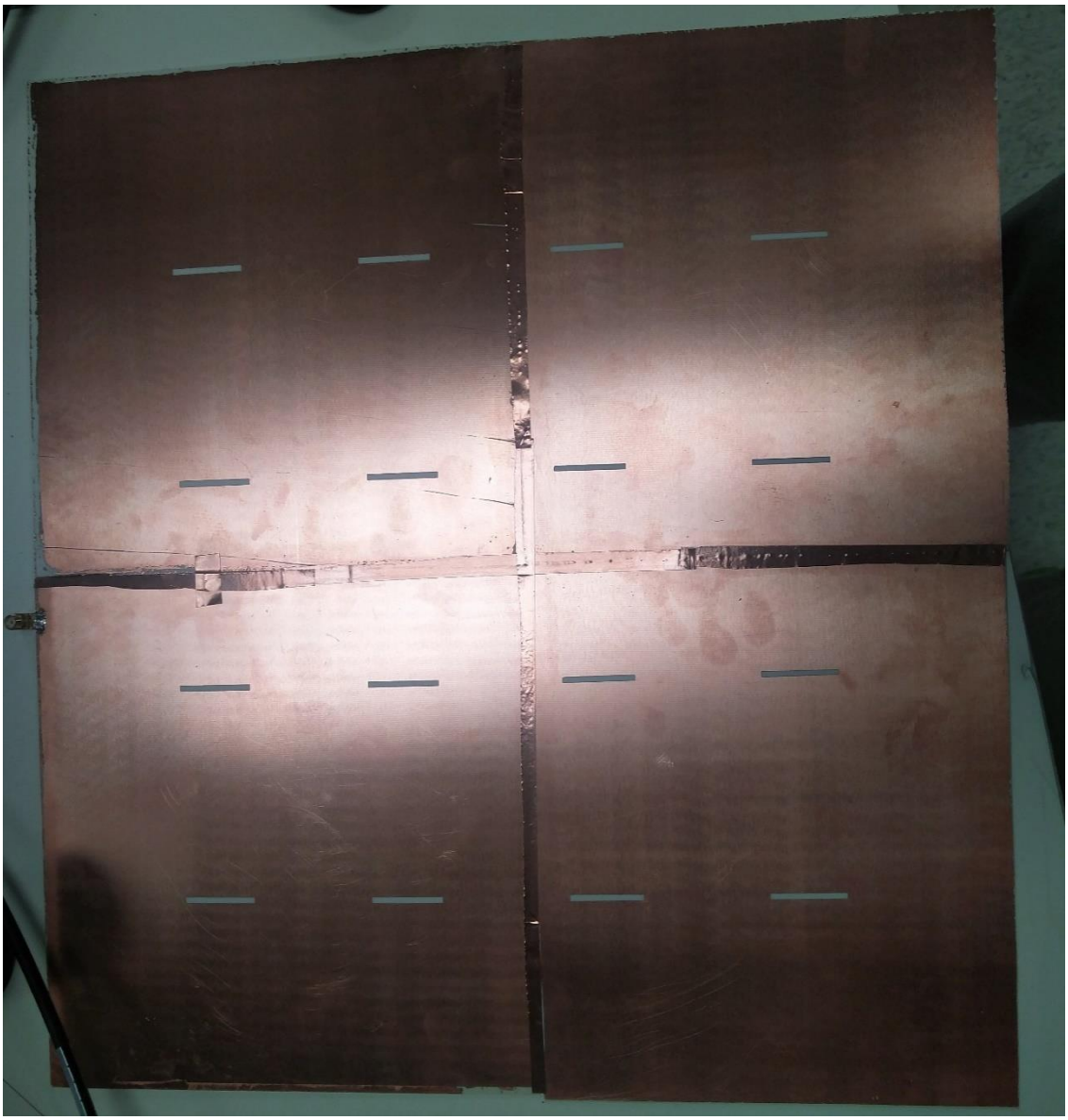

Fig. 6.4: Ground plane with apertures.

6.3 Measurement Results for 4X4 Array

The feedline substrate lies at the bottom of the array with the ground plane facing upward. This is then followed by a layer of foam which is placed on top of it. The substrate containing the patch array is placed on top of the foam. All layers are aligned as precisely as possible and they have been taped together at all four ends. The side view of

this 4X4 array has been shown in Fig. 6.5. The bottom substrate sits on top of a 25 mm thick foam pedestal, which acts as the foam spacer used at the bottom to position the reflector below the array. Measurements were made with and without the foam legs placed under the array and no difference was observed. The array is fed using a SMA soldered to its edge.

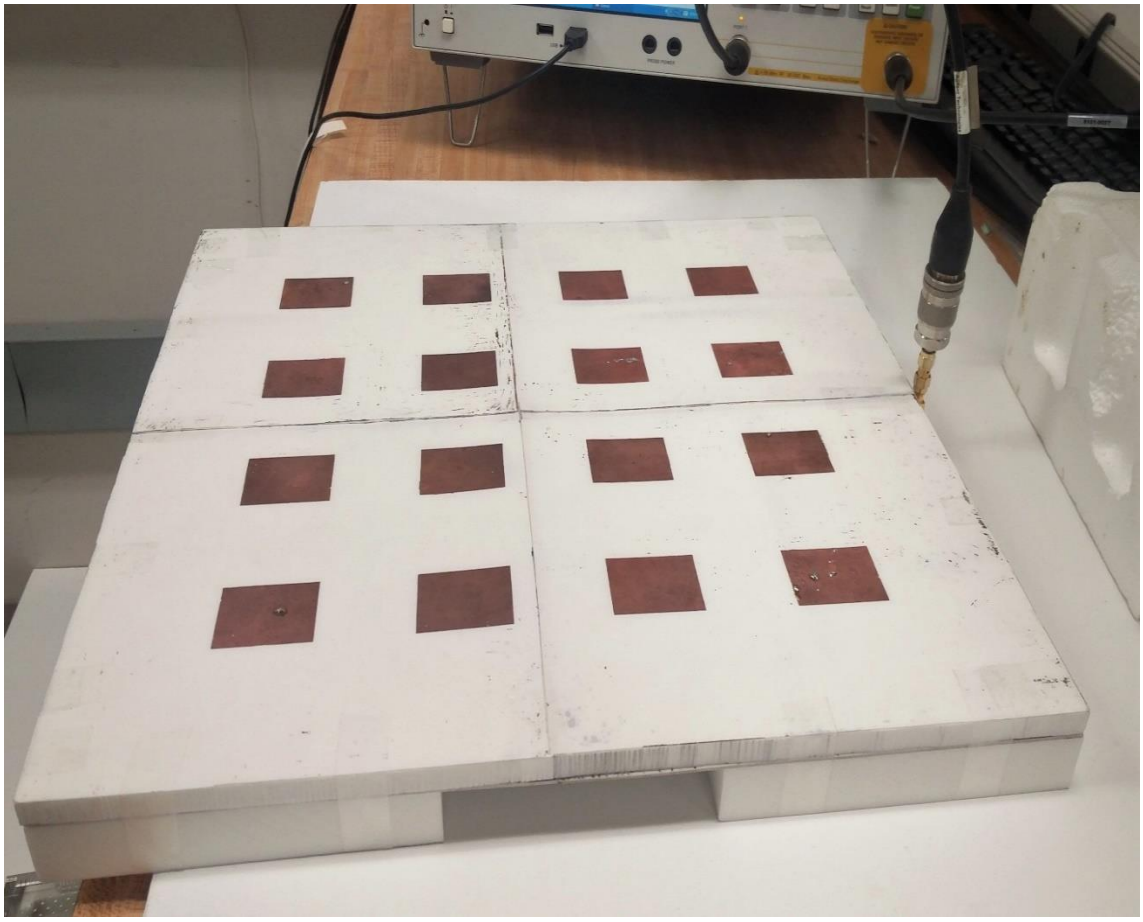

Fig. 6.5: Side view of 4X4 array.

The measured reflection coefficient for this 4X4 array has been plotted in Fig. 6.6 below. It can be seen from the measured S_{11} plot that the antenna has a reflection coefficient greater than -10 dB for a small frequency band between 2.82 to 2.96 GHz. The S_{11}

deteriorates to as much as -8 dB somewhere around 2.9 GHz. This can be mainly attributed to the minor differences in the widths of the line, w_4=0.6 mm and the alignment challenges faced because of the antenna being made from 4 separate boards. It was observed that there were small sections of w_4 which were over-etched to as much as 0.5 mm in some places. This can be attributed to uneven exposure to UV light due to inconsistencies in the UV mask and possibly uneven exposure to the photo-developer. These minor changes in line widths are responsible for the aberrations seen in the S_{11} performance as that would cause a change in impedance which will cause the feed network to be mismatched at the various T-junctions. Even so, the radiation patterns measured are quite consistent with the simulation data. The antenna setup inside the anechoic chamber can be seen in Fig. 6.7.

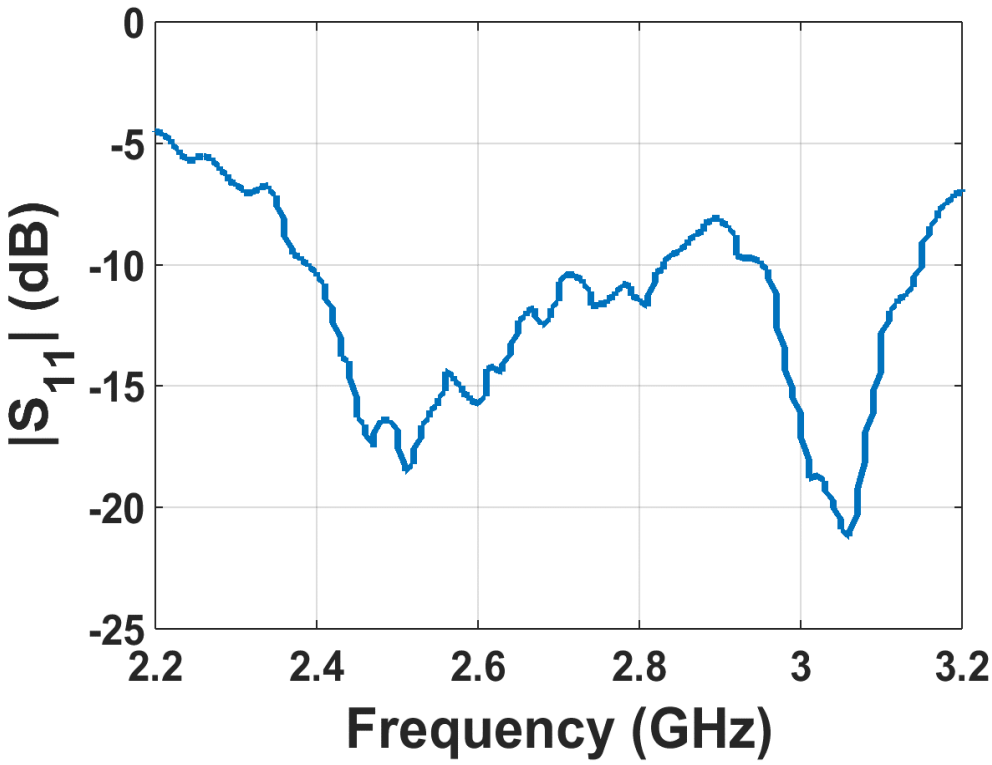

Fig. 6.6: Measured S_{11} data.

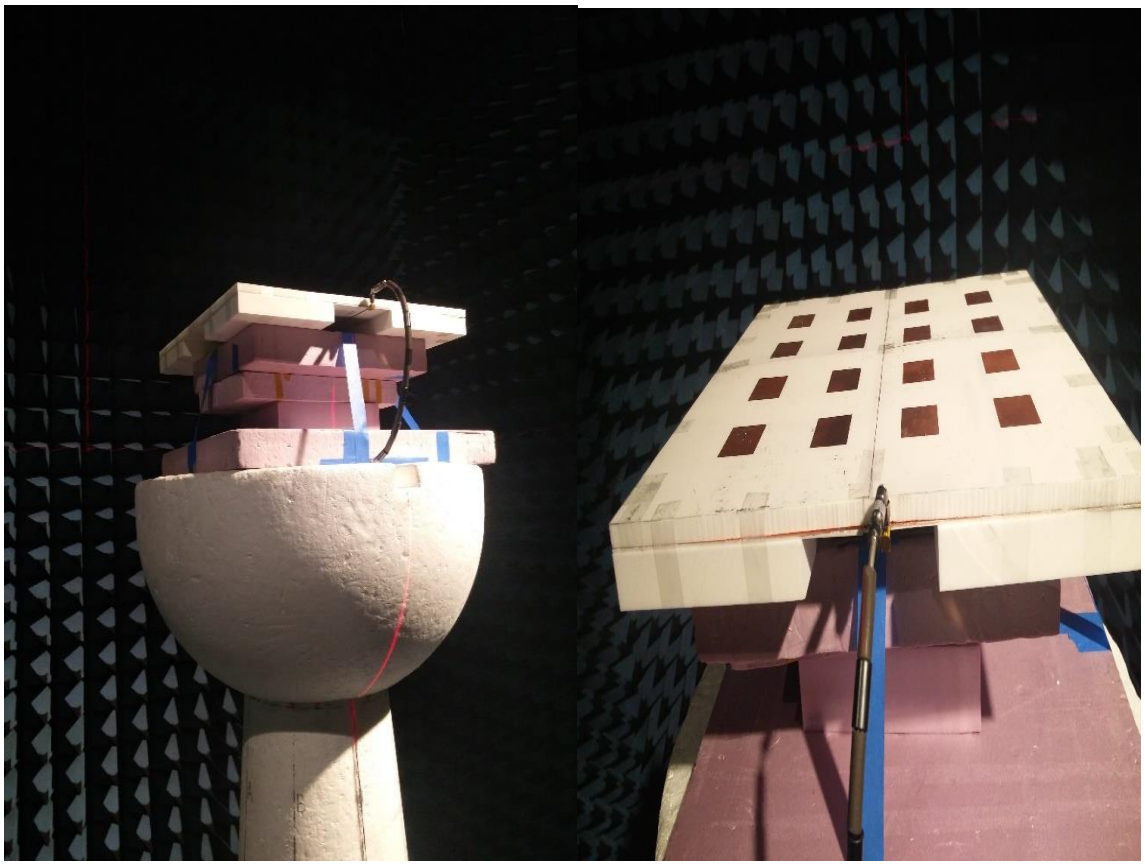

Fig. 6.7: Antenna setup inside the anechoic chamber.

The measured radiation patterns have been plotted in Fig. 6.8 and the Realized Gain, SLL, F/B, Directivity and HPBW data is summarized in Table 6.1.

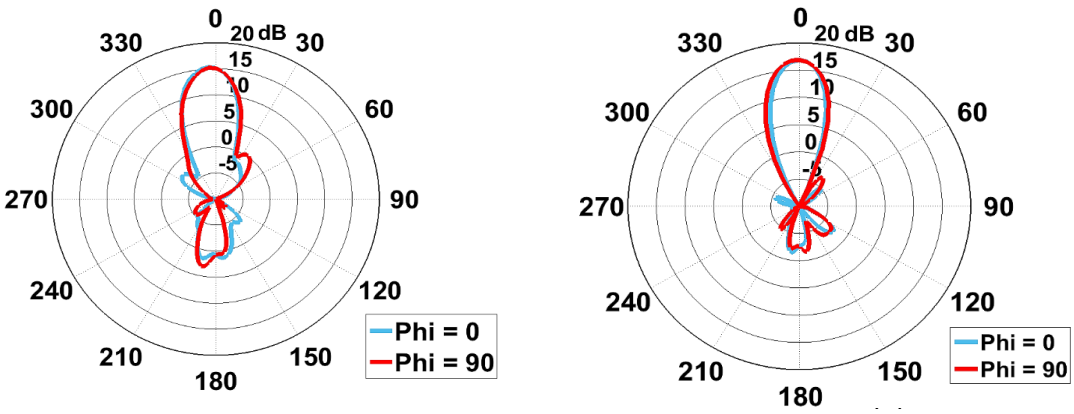

(a) (b)

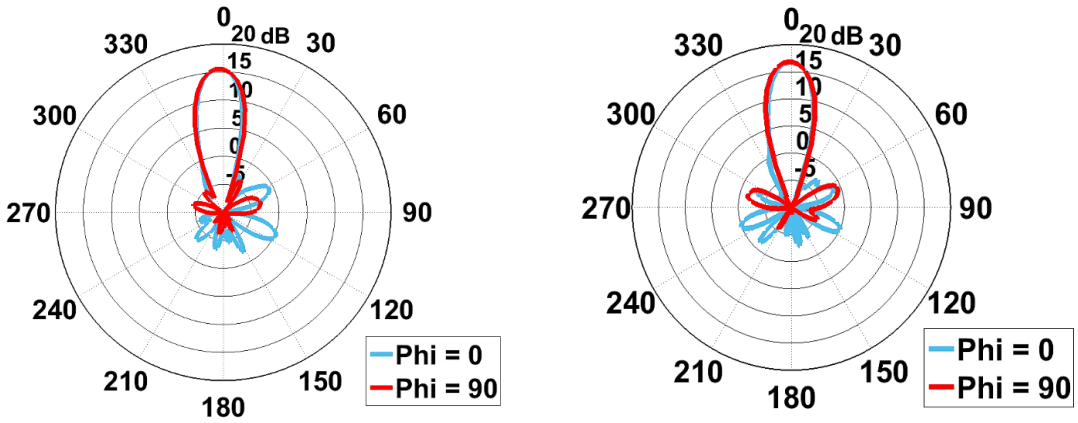

(c) (d)

Fig. 6.8: Radiation patterns measured at (a) 2.45 GHz, (b) 2.65 GHz, (c) 3 GHz, (d) 3.1 GHz.

Table 6.1: Measured data for 4X4 array.

Frequency (GHz)	Realized Gain (dBi)	SLL (dB)	F/B (dB)	Directivity (dBi)	HPBW (Degrees)
2.45	15.4	15.3	14.7	17.4	< 21
2.65	16.9	20.7	19.5	19	< 24
3	15.7	16.5	22.9	18.9	< 21
3.1	16.8	17.6	25.4	19.6	< 21

The maximum realized gain observed in the measured data is seen to be about 1.7 to 2.8 dB lower than what the simulations suggest, whereas the measured directivity matches the simulation results very closely. Surprisingly though, the F/B ratio realized is much better than expected due to significantly lower levels of back-lobe radiation. The measured back-lobe radiation was lower than the expected results by about 7 to 16 dB and this effect was more pronounced at the higher end of the operating band. The measurement setup in the anechoic chamber is such that the region right under the

pedestal cannot be measured. To be precise a total angle of 23.6^o lies in this blind spot. The software uses a predictive algorithm to estimate the radiation pattern in this region based on various factors like the magnitude of the radiation pattern right before the blind spot, the rate of change, etc. and extrapolates on the basis of this data. This could also be a possible source of discrepancies seen in the backlobe radiation. The measured maximum SLLs seem to be lower than what the simulations suggest. But this is due to the presence of very narrow singular lobes being generated at and around $\theta=60^o$ and $\theta=300^o$. The changes in the line width also contribute to increasing the SLLs. The measured HPBWs are in very close agreement with the simulation data putting the average beamwidth of the antenna close to 21^o. The beamwidths could not be very precisely calculated as the measurement setup had a resolution of 3^o, hence the actual beamwidth of the antenna could be lower by as much as 6^o.

6.4 Measurement Results for 4X4 Array with Reflector

An aluminum plate which is an inch larger than the array is placed below the antenna. The legs help position the array accurately over the reflector. S_{11} and radiation pattern measurements were made as described in the previous sections. The measurement setup for the 4X4 array with the metal reflector can be seen in Fig. 6.9 and the S_{11} plot is presented in Fig. 6.10 below. The S_{11} response seen on the Vector Network Analyzer shows that the reflection coefficient of the antenna briefly increases from -10 dB to a maximum of -8.2 dB between 2.7 to 2.98 GHz. This again can be attributed to the minor inconsistencies in the line widths of the various elements in the corporate feed which tend to cause the antenna not be matched as well as desired. The radiation patterns measured are depicted below in Fig. 6.11.

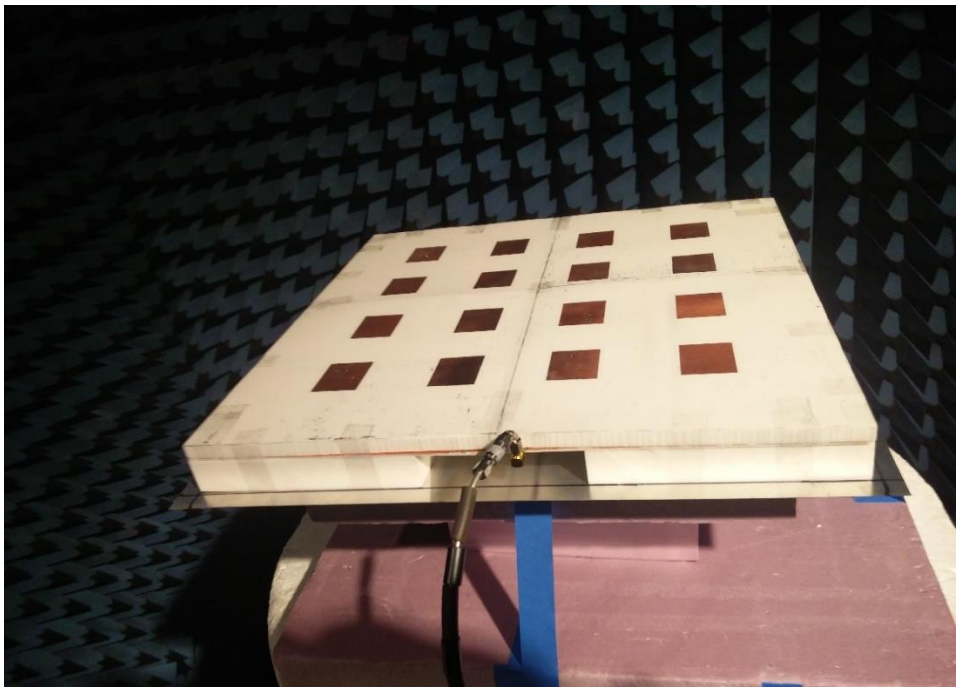

Fig. 6.9: Radiation pattern measurement setup for array with reflector.

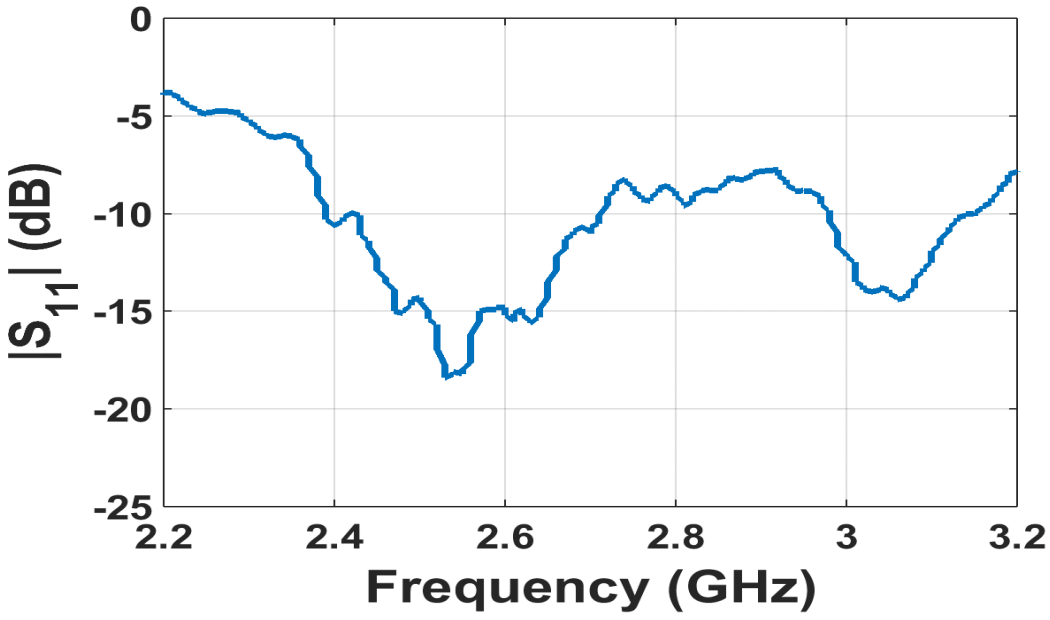

Fig. 6.10: Measured S_{11} performance of 4X4 array with reflector.

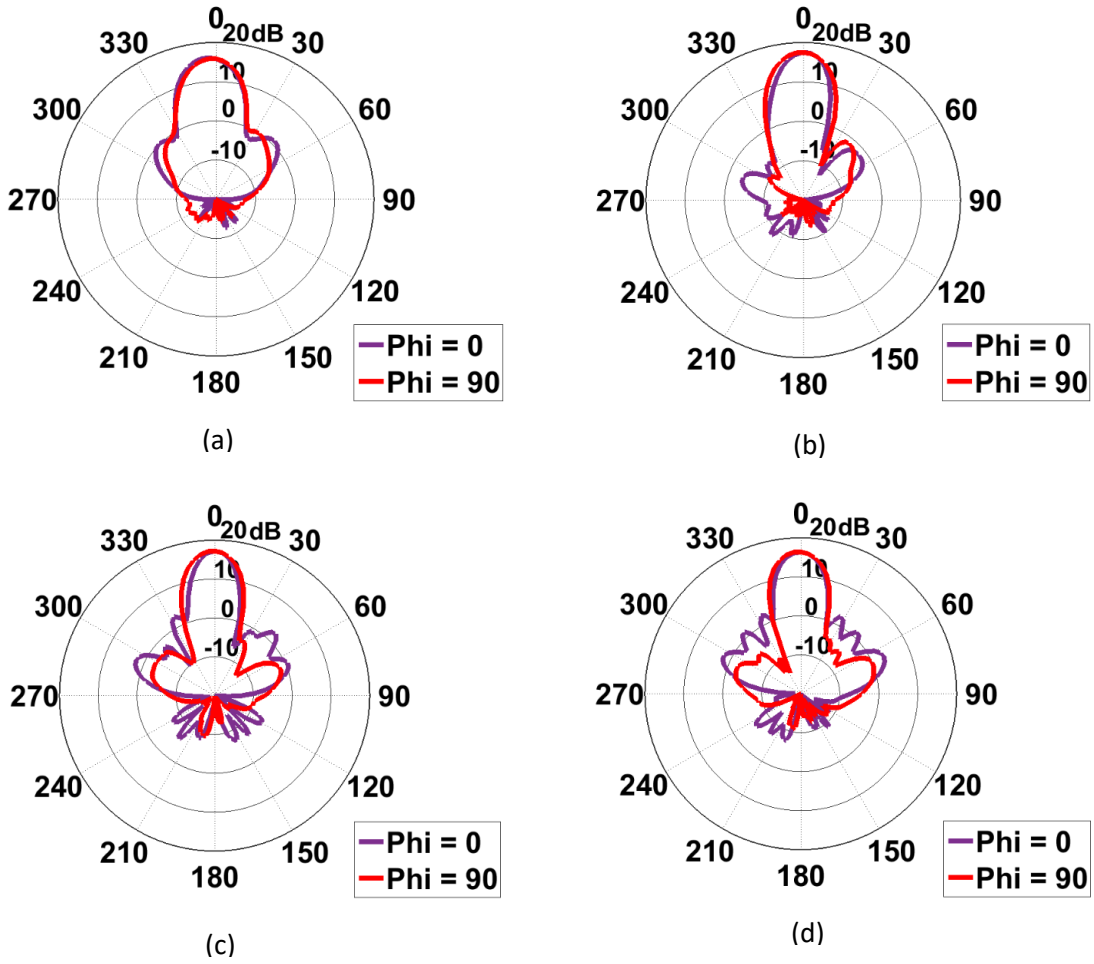

Fig. 6.11: Measured radiation pattern plots for array with reflector at (a) 2.45 GHz, (b) 2.65 GHz, (c) 3 GHz, (d) 3.1 GHz.

Table 6.2: Measured data for 4X4 array with reflector.

Frequency (GHz)	**Realized Gain (dBi)**	**SLL (dB)**	**F/B (dB)**	**Directivity (dBi)**	**HPBW (Degrees)**
2.45	16.2	15.2	37.1	17.9	< 21
2.65	17.5	19.2	43.3	19.4	< 18
3	17.2	15.3	38.7	20	< 18
3.1	16.4	13.4	37.2	19.3	< 18

6.5 Measurement Results for 4X4 Array with Superstrate

Dielectric superstrates have been used to improve the directivity and reflection coefficient response of antennas and arrays from decades now. It was initially studied by Trentini and Sasser [36-37], and they attributed this performance boost to the multiple reflections occurring at the air-superstrate and superstrate-air interfaces causing images of the source being generated. So, if the permittivity and separation are controlled it is possible to enhance the array performance at certain frequencies. A great deal of research has been dedicated to quantify and establish the effects of various parameters like permittivity, separation, superstrate size, etc. [38-39] and the gain enhancement has been attributed to "leaky waves" [40-41]. The antenna array with the superstrate has been shown in Fig. 6.12. The superstrate used was FR4 with a thickness of 1.6 mm and the reason for using it was its ease of availability. The superstrate is lightly placed on top of the array, which means there is extremely thin air film between the superstrate and the antenna. The S_{11} response has been plotted in Fig. 6.13. There is a very noticeable improvement in the S_{11} response of the antenna. The antenna is now perfectly tuned in the frequency range of 2.35 GHz to 3.18 GHz. The minor region around 2.9 GHz where the S_{11} response jumped above -10 dB has been eliminated and overall the reflection coefficient is much lower compared to the array without the superstrate.

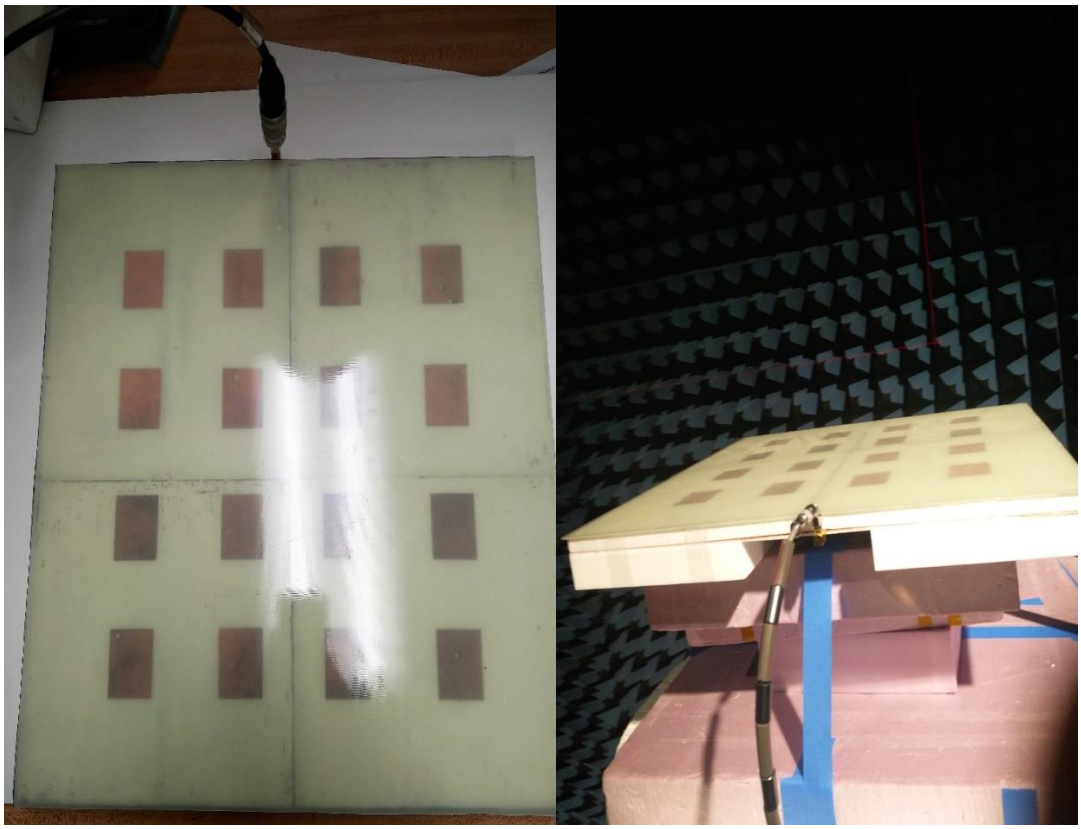

Fig. 6.12: S_{11} and radiation pattern measurement setup for array with superstrate.

The radiation patterns for the 4X4 array with the superstrate at the four frequencies has been plotted in Fig. 6.14. The realized gain and the directivity are higher as would be expected but the improvement is in the range of half a dB which is lower than what should be expected after seeing the improvement in the S_{11}. The high dielectric loss tangent of FR4 is responsible for reducing the gain. The F/B ratio is better due to improved gain and lower backlobe radiation. The HPBW of the array is also slightly improved at certain frequencies. But the main advantage of using the superstrate can be seen looking at the SLL performance. The SLLs at the lower end of the band is significantly improved (as much as 5 dB) but this enhancement in SLL seems to vanish at

the higher frequencies in the operating band. All the measured data has been summarized in Table 6.3.

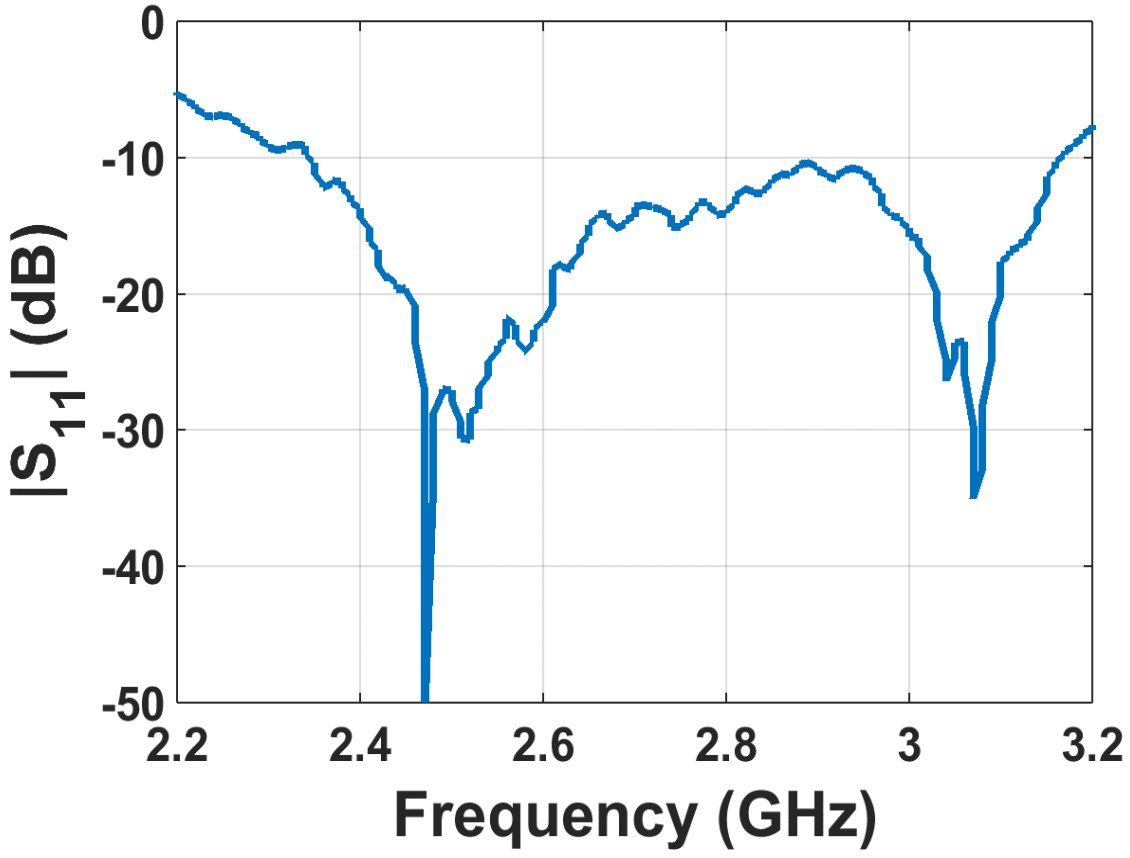

Fig. 6.13: Measured S_{11} performance of 4X4 array with superstrate.

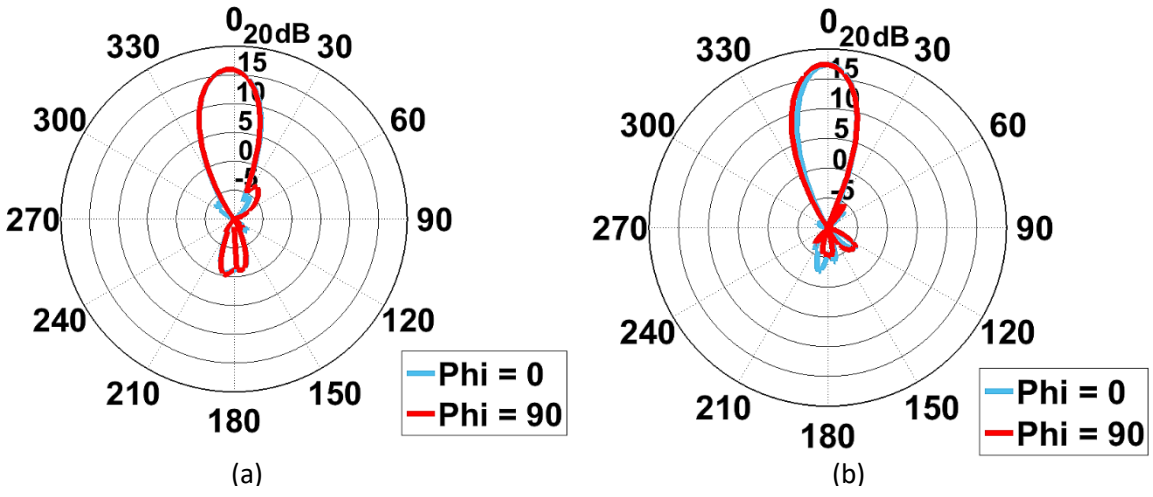

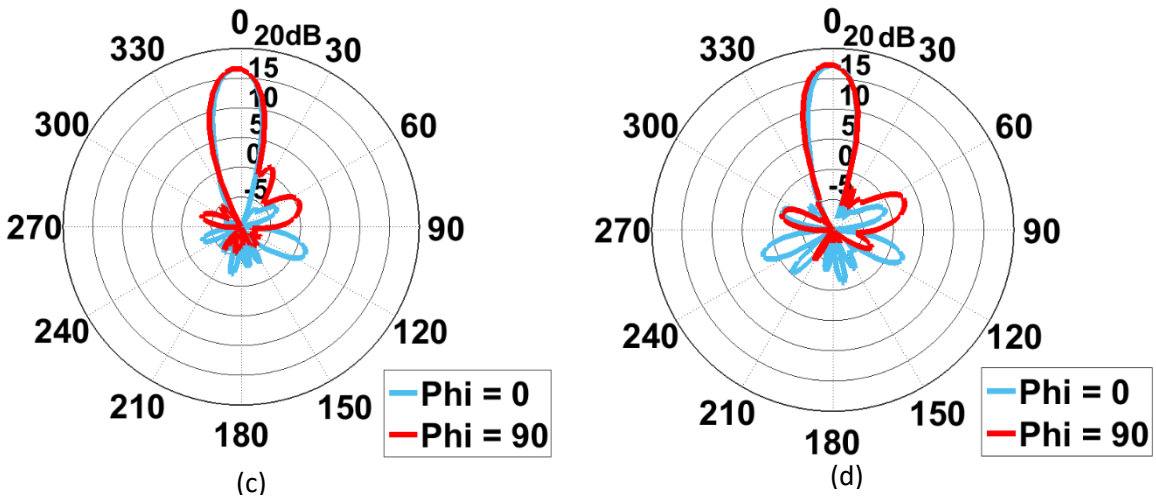

Fig. 6.14: Measured radiation pattern plots for array with superstrate at (a) 2.45 GHz, (b) 2.65 GHz, (c) 3 GHz, (d) 3.1 GHz.

Table 6.3: Measured data for 4X4 array with superstrate.

Frequency (GHz)	Realized Gain (dBi)	SLL (dB)	F/B (dB)	Directivity (dBi)	HPBW (Degrees)
2.45	16.1	21.4	17.2	17.8	< 21
2.65	17.4	23.9	22.9	19.3	< 21
3	16.7	16.1	23.6	19.4	< 21
3.1	17.3	14.5	25.1	19.7	< 18

6.6 Measurement Results for 4X4 Array with Reflector and Superstrate

Just like the previous case, the effect of the superstrate on the antenna array with the reflector was studied. The S_{11} measurement and radiation pattern measurement setup for this array is shown in Fig. 6.15. The S_{11} response for this antenna is represented in Fig. 6.16. The superstrate significantly improves the S_{11} response of the array with the reflector and improves the operating bandwidth to a little over 3.2 GHz which is even

better than the case with no reflector. The radiation patterns have been plotted in Fig. 6.17 and all the parameters being studied has been summarized in Table 6.4. The improvement in the radiation characteristics is exactly as seen in the previous section. Gain and directivity improvement of about 0.5 dB is seen. SLLs at the lower end of the frequency are higher by 5 dB and the beam is slightly narrower at some frequencies.

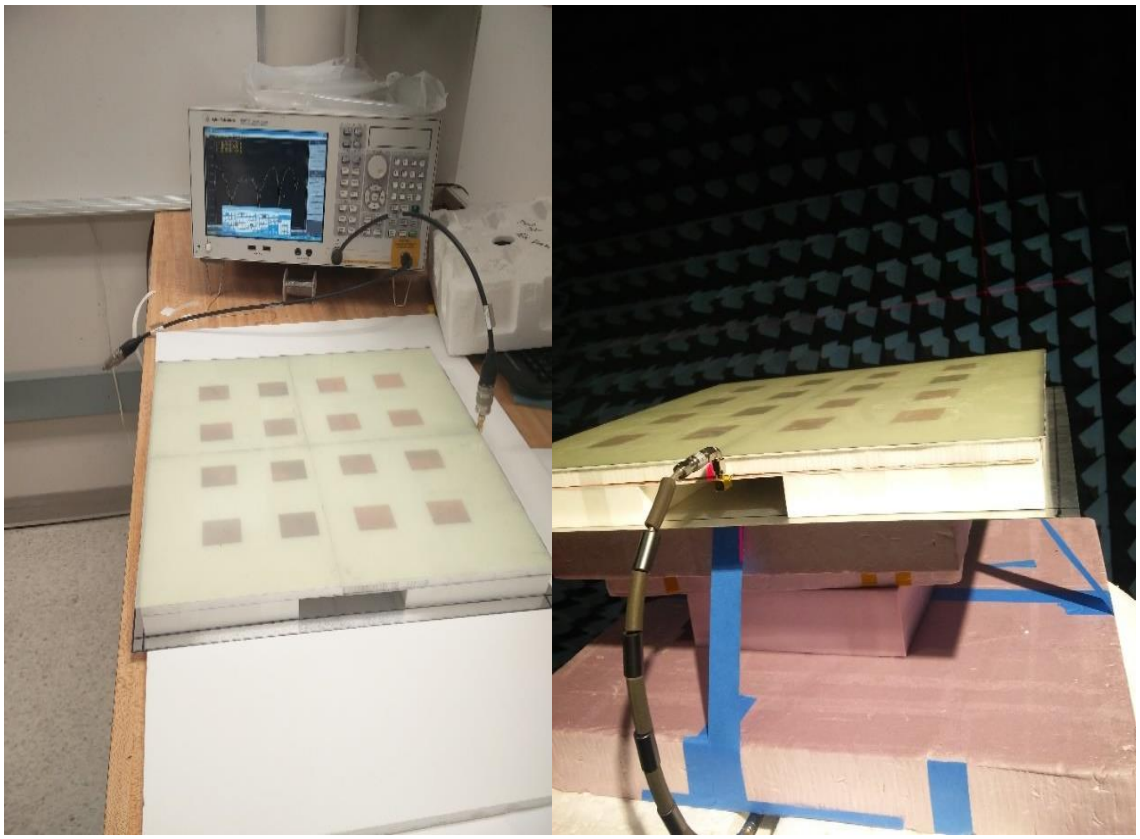

Fig. 6.15: S_{11} and radiation pattern measurement setup for array with superstrate and reflector.

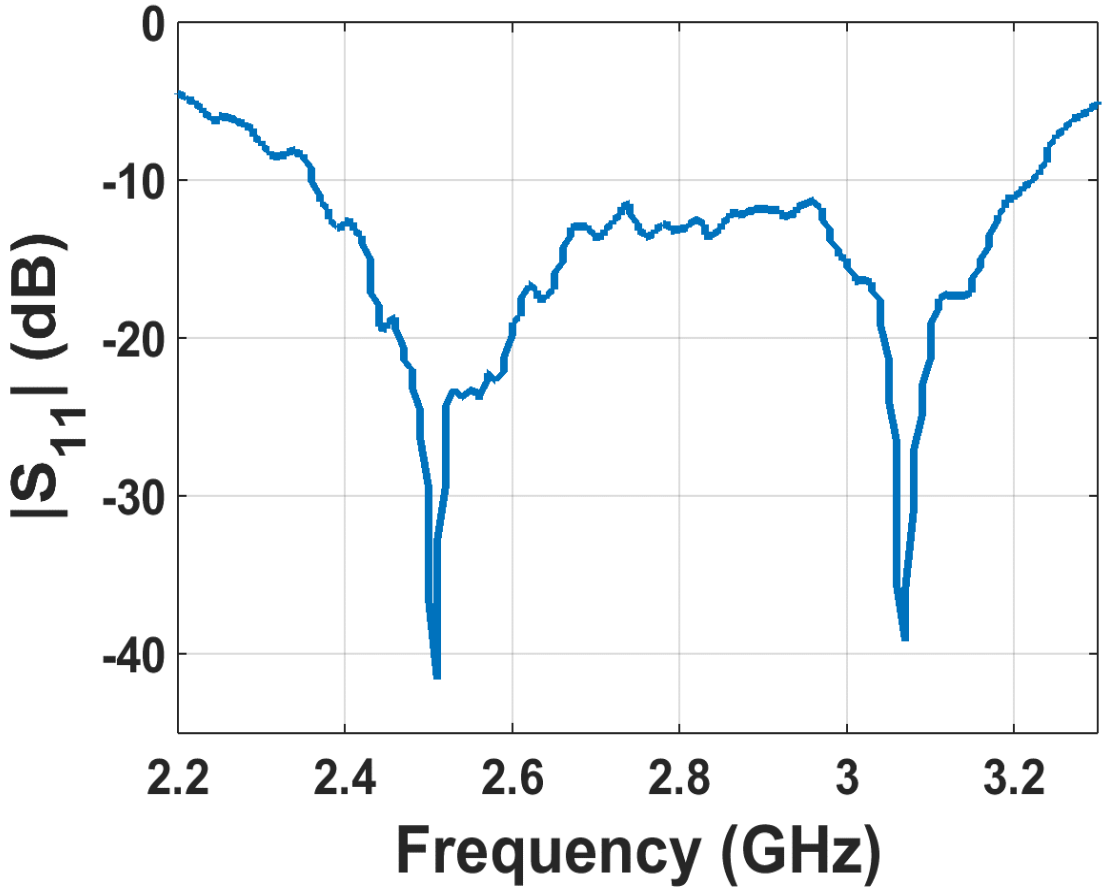

Fig. 6.16: Measured S_{11} performance of 4X4 array with superstrate and reflector.

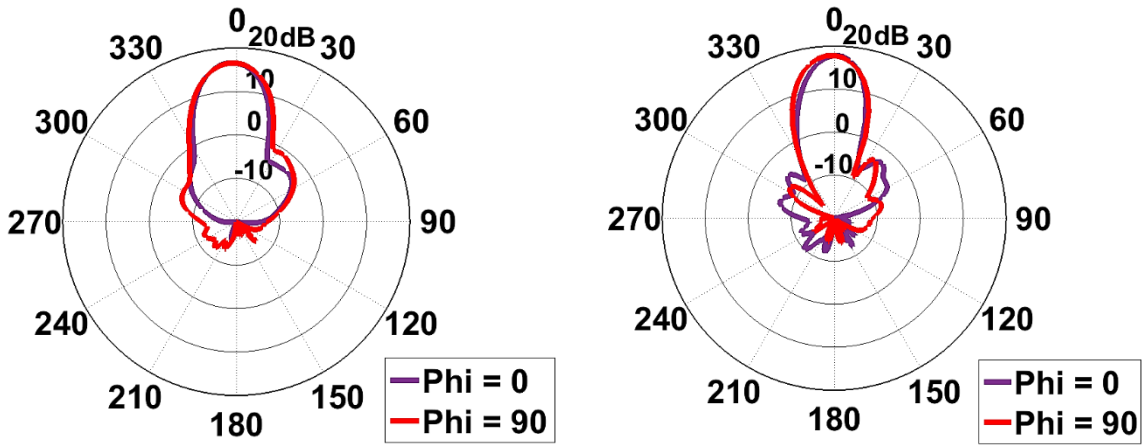

(a) (b)

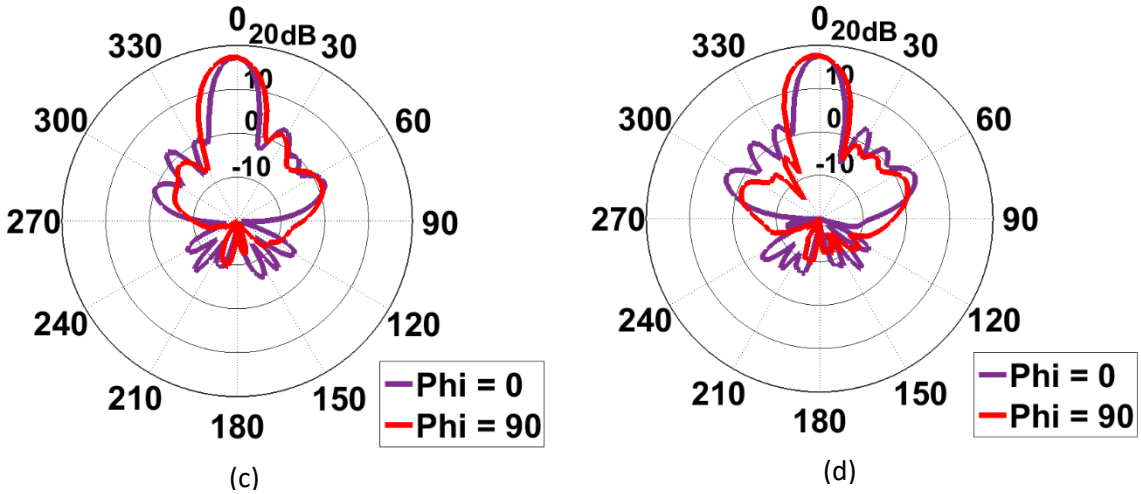

Fig. 6.17: Measured radiation pattern plots for array with superstrate and reflector at (a) 2.45 GHz, (b) 2.65 GHz, (c) 3 GHz, (d) 3.1 GHz.

Table 6.4: Measured data for 4X4 array with superstrate and reflector.

Frequency (GHz)	**Realized Gain (dBi)**	**SLL (dB)**	**F/B (dB)**	**Directivity (dBi)**	**HPBW (Degrees)**
2.45	16.6	20.4	37.8	18.1	< 21
2.65	17.8	20.9	44	19.5	< 21
3	17.3	16.7	36.7	19.8	< 15
3.1	17.6	13.8	37.7	19.9	< 18

Chapter 7: Phased Array

7.1 Introduction

The simulation results for a 4X4 planar phased array antenna have been presented in this chapter. It also goes over the requirements that need to be met in order to achieve beam steering, the maximum angle that an array can be electronically steered without creating significant sidelobes and the phase difference required to achieve this. Possible solutions to practically implementing this design was looked into, mainly by using a Monolithic Microwave Integrated Circuit. After surveying the various available options in the market, the analog phase shifter IC HMC928LP5E [42] seemed like a good fit for the 4X4 planar array considering its wideband response, ease of integration, low insertion loss and linear phase response. Implementation has been left for future work.

7.2 Beam Steering

Beam steering in antenna arrays is achieved by adjusting the phase difference between successive antenna elements. By controlling the progressive phase shift along the x-axis we can move the main beam maximum along the x-axis and similarly by controlling the progressive phase shifts along the elements lying on the y-axis we can control where along the y-axis the beam ends up radiating and by simultaneously controlling the phase excitations we can move the beam to any position we desire. This is

how we control the azimuth (Φ) and elevation (θ) angles of a phased array antenna. The required phase difference can be found by examining the array factor of a planar array antenna. As described in Chapter 3 the array factor for a planar array can be written as [9],

$$AF(\theta,\varphi) = \left\{\frac{\mathrm{Sin}\left(\left(\psi_x\frac{M}{2}\right)\right)}{M\mathrm{Sin}\left(\left(\frac{\psi_x}{2}\right)\right)}\right\}\left\{\frac{\mathrm{Sin}\left(\left(\psi_y\frac{N}{2}\right)\right)}{N\mathrm{Sin}\left(\left(\frac{\psi_y}{2}\right)\right)}\right\} \quad \ldots (7.1)$$

Here, ψ_x and ψ_y are defined as follows,

$$\psi_x = kd_x\sin\theta\cos\phi + \beta_x \quad \ldots (7.2)$$

$$\psi_y = kd_y\sin\theta\sin\phi + \beta_y \quad \ldots (7.3)$$

The phases β_x and β_y are independent and can be controlled separately as mentioned earlier. To determine the phase shifts we equate ψ_x=0 and ψ_y=0 to obtain,

$$\beta_x = -kd_x\sin\theta\cos\phi \quad \ldots (7.4)$$

$$\beta_y = -kd_y\sin\theta\sin\phi \quad \ldots (7.5)$$

Where,

$$k = \frac{2\pi}{\lambda}$$

$$d_x = d_y = 83.3\ mm$$

The above set of equations help us determine the phase progressions needed in order to steer the antenna beam. Before proceeding to find this phase difference, one main concern regarding phased array antennas must be discussed, and that is grating lobes. Usually for linear broadside and standard planar array grating lobes appear when the inter-element spacing is a multiple of the wavelength. But in the case of phased array antennas grating lobes can appear when the "look angle" i.e. the angle the main beam points to is increased beyond a certain point. This look angle can be determined by the relation given below,

$$d = \frac{\lambda}{1+\mathrm{Sin}\theta} \quad \ldots (7.6)$$

So when,

$$d = 83.3\ mm$$

$$\theta = \begin{cases} 30^o\text{, at } 2.45\mathrm{GHz} \\ 21^o\text{, at } 2.65\mathrm{GHz} \\ 15.3^o\text{, at } 2.85\mathrm{GHz} \\ 10.4^o\text{, at } 3.05\mathrm{GHz} \end{cases} \quad \ldots (7.7)$$

Due to the wideband nature of the antenna, the look angle, i.e. the angle within which the antenna mainlobe can be steered varies from 30^o at 2.45 GHz to a very narrow 10.4^o at 3.05 GHz. The only way to improve the scanning range for these kinds of planar array antennas is to decrease the inter-element separation and in the current array design a smaller distance between array elements causes a higher level of mutual coupling as was demonstrated in Chapter 4. The phase difference required between elements to achieve beam steering will also be a function of frequency. So the progressive phase shifts between the successive antenna elements has to be adjusted accordingly. Say the antenna

main beam needs to be steered to $\theta = +30^o, \Phi = 90^o$, then this will only be possible for frequencies below 2.45 GHz and the required phase difference can be found by calculating β_x and β_y from the aforementioned equations. To move the main beam to $\theta = +30^o, \Phi = 90^o$ a successive phase difference of $\beta_y = -122.6^o$ and $\beta_x = 0^o$ must been maintained between the antenna elements.

Simulations were performed by assigning the required phases to the respective antenna elements in the 16 element planar array. The radiation pattern at 2.45 GHz has been shown below in Fig. 7.1. The realized gain at this position is seen to 17.6 dBi and the backlobe radiation is at -12 dB. This puts the F/B at 29.6 dB and the SLL is measured to be 7.6 dB which is considerable high. This is due to the fact that the antenna is being steered at the maximum possible look angle for this frequency which causes the grating lobe to be significant. As we decrease the look angle, this lobe which is seen between 310^o to 320^o also decreases. This becomes evident in Fig. 7.2. In Fig. 7.2 the antenna main beam is steered to $\theta = +10^o, \Phi = 90^o$. All four frequencies within the bandwidth can be steered to at least 10^o.

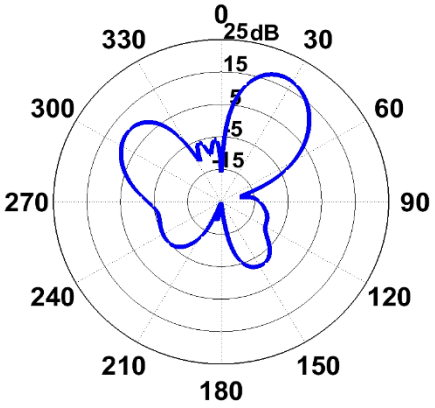

Fig. 7.1: Radiation pattern with main beam at $\theta = +30^o, \Phi = 90^o$ and 2.45 GHz.

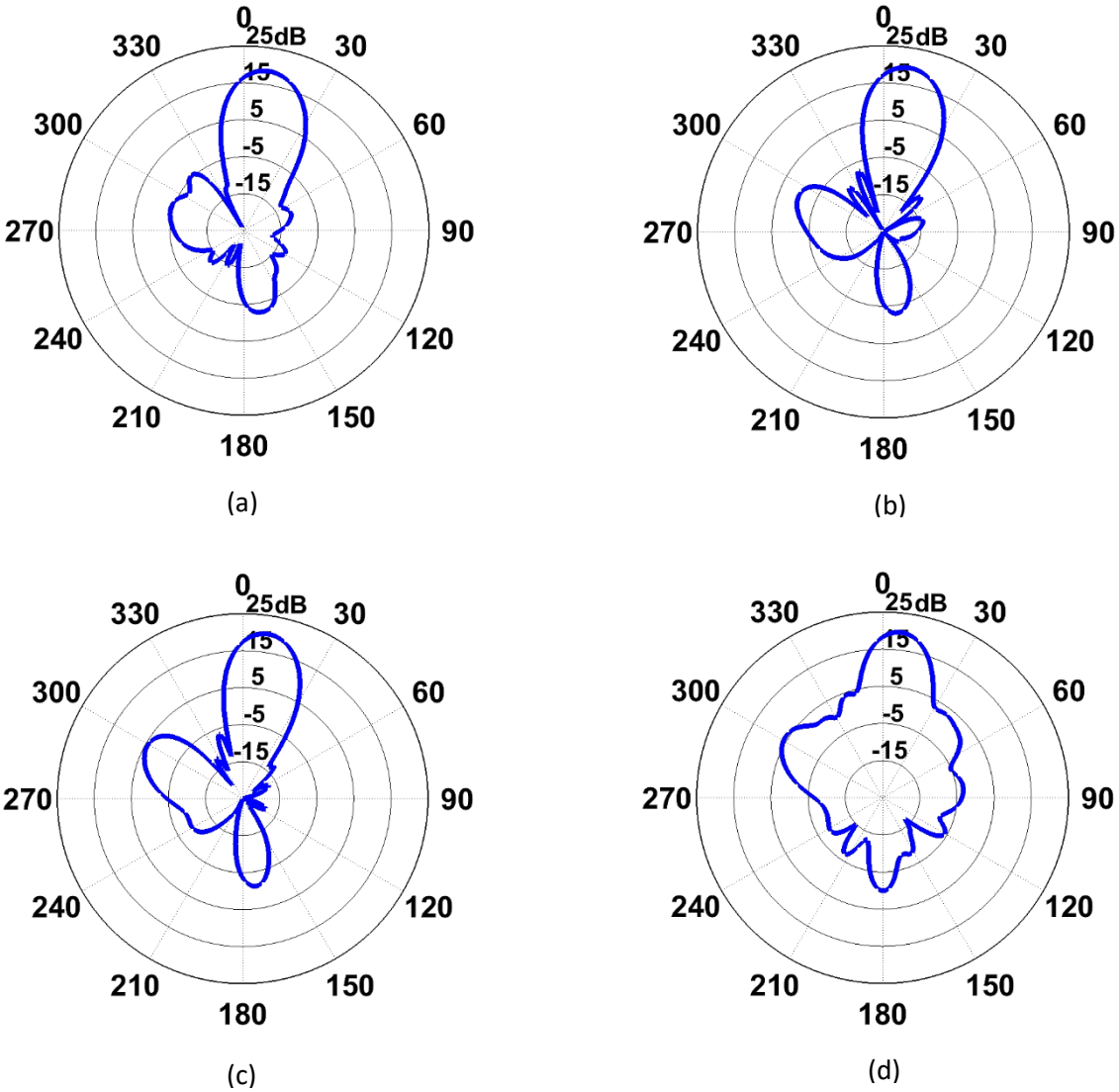

Figs. 7.2: Radiation pattern with main beam at $\theta = +10^o, \Phi = 90^o$ (a) 2.45 GHz, (b) 2.65 GHz, (c) 2.85 GHz, (d) 3.05 GHz.

The realized gain, SLL, F/B and HPBW data for the radiation pattern plots presented in Fig. 7.2 are summarized in Table 7.1.

Table 7.1: Summary of radiation pattern data with main beam at $\theta = +10^o, \Phi = 90^o$.

Frequency (GHz)	**Realized Gain (dBi)**	**SLL (dB)**	**F/B (dB)**	**Directivity (dBi)**	**HPBW (Degrees)**
2.45	18.6	23	35.4	18.7	22

2.65	19.6	19.9	34.4	19.8	22
2.85	19.9	15.5	33.9	20.5	20
3.05	19.7	13.9	29	17.6	20

All of the above radiation pattern plots are steered towards the $\Phi = 90^o$ plane which is the H-plane. The radiation characteristics are better, i.e. more directive and have lower HPBWs in the H-plane when compared to the radiation pattern characteristics observed in the E-plane. Figs. 7.3, 7.4 and 7.5 show the 3D radiation patterns at 2.45 GHz in a linear scale when the main beam is directed towards, $\theta = +20^o, \Phi = 0^o$; $\theta = +20^o, \Phi = 45^o$ and $\theta = +20^o, \Phi = 90^o$ respectively. The 3D patterns represent the axis and help visualize the radiation patterns and the beam steering. The radiation patterns seen at $\theta = -20^o$ for the various values of Φ are almost identical due to the symmetry of the array.

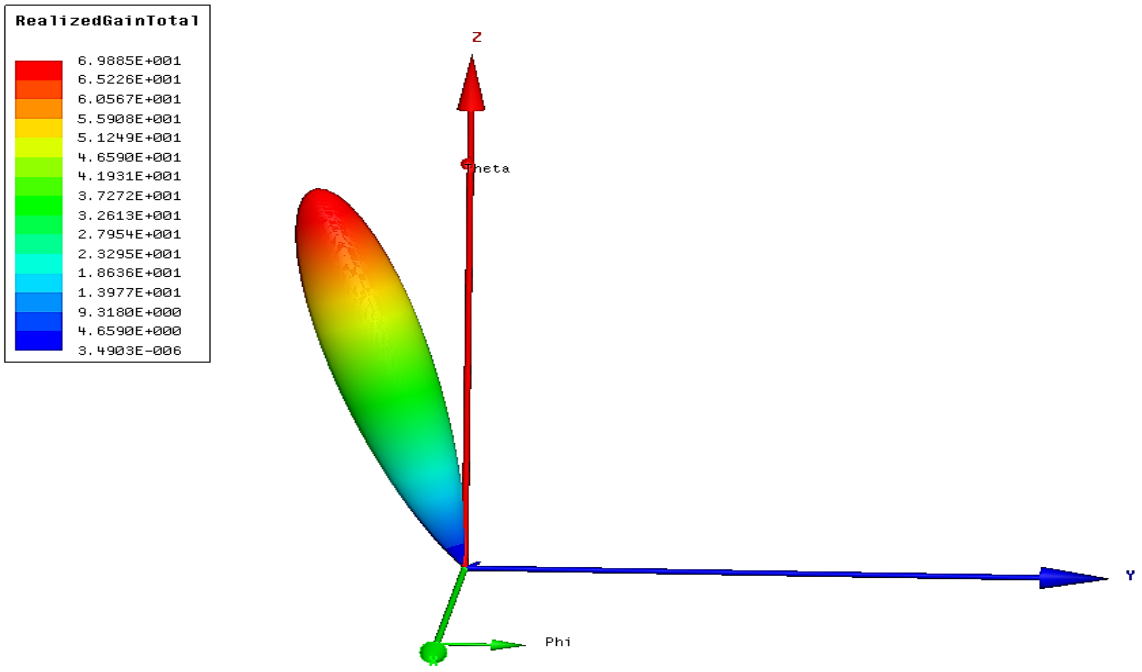

Fig. 7.3: 3D radiation pattern at, $\theta = +20^o, \Phi = 0^o$ and 2.45 GHz.

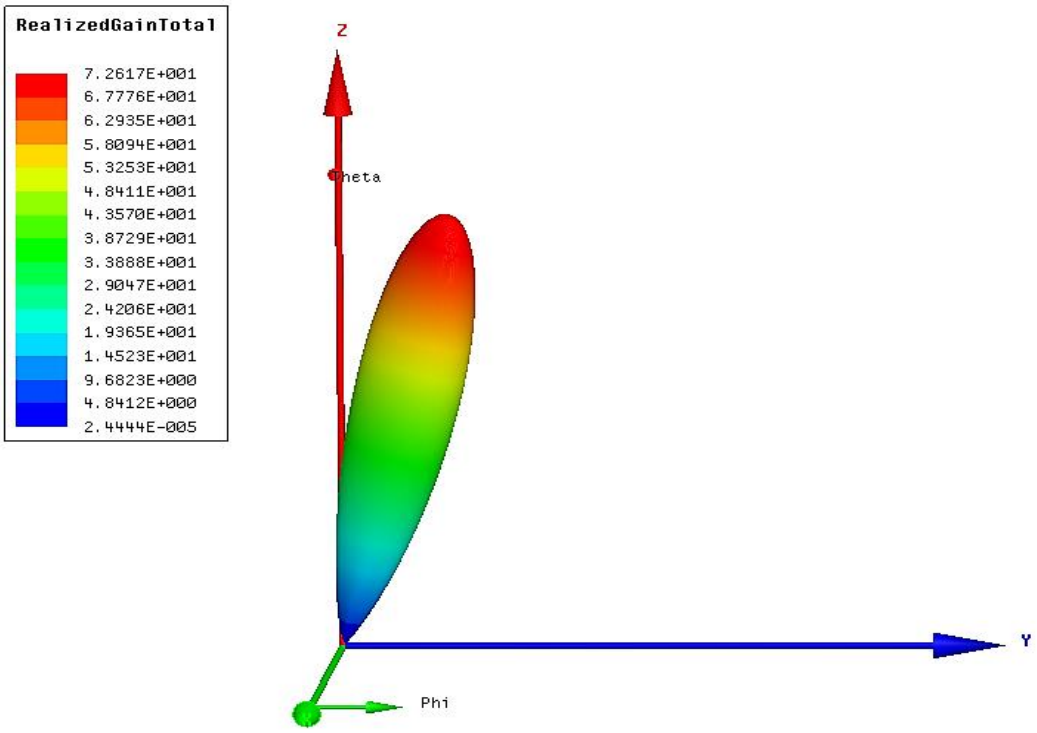

Fig. 7.4: 3D radiation pattern at, $\theta = +20^{o}, \Phi = 45^{o}$ and 2.45 GHz.

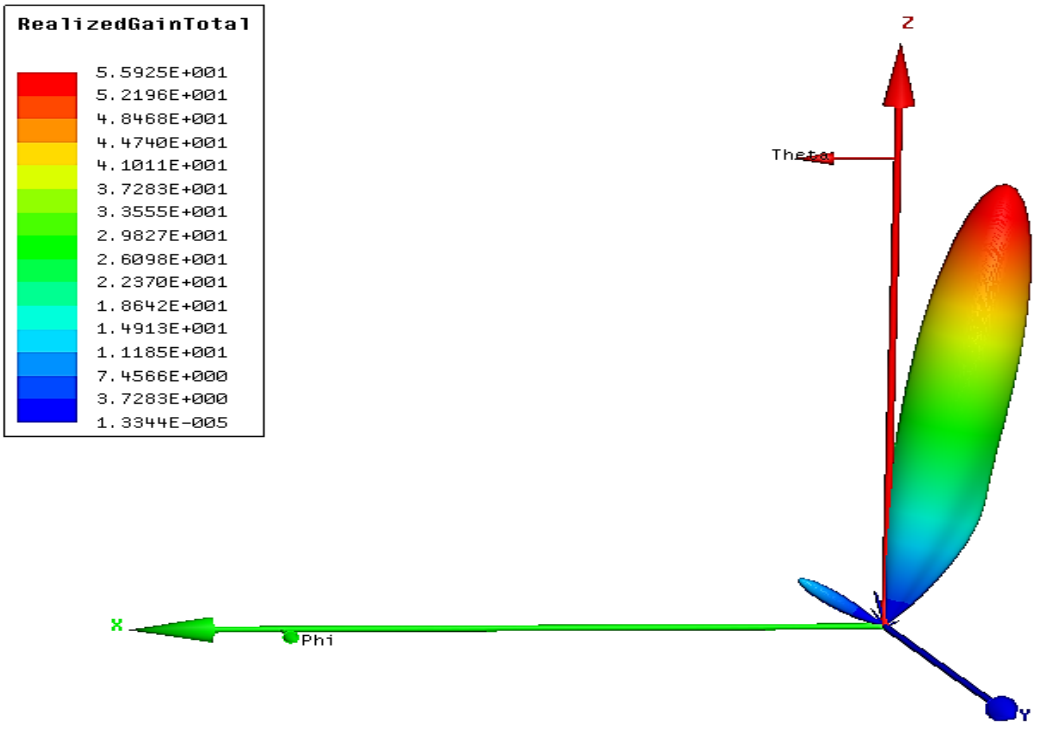

Fig. 7.5: 3D radiation pattern at, $\theta = +20^{o}, \Phi = 90^{o}$ and 2.45 GHz.

The radiation pattern plots at these three positions have been shown in the figures below. Only frequencies below 2.65 GHz can be steered to $\theta = +20^o$, hence radiation patterns are plotted for only 2.45 GHz and 2.65 GHz. Fig. 7.5 shows the radiation patterns when the main beam is directed towards $\theta = +20^o, \Phi = 0^o$.

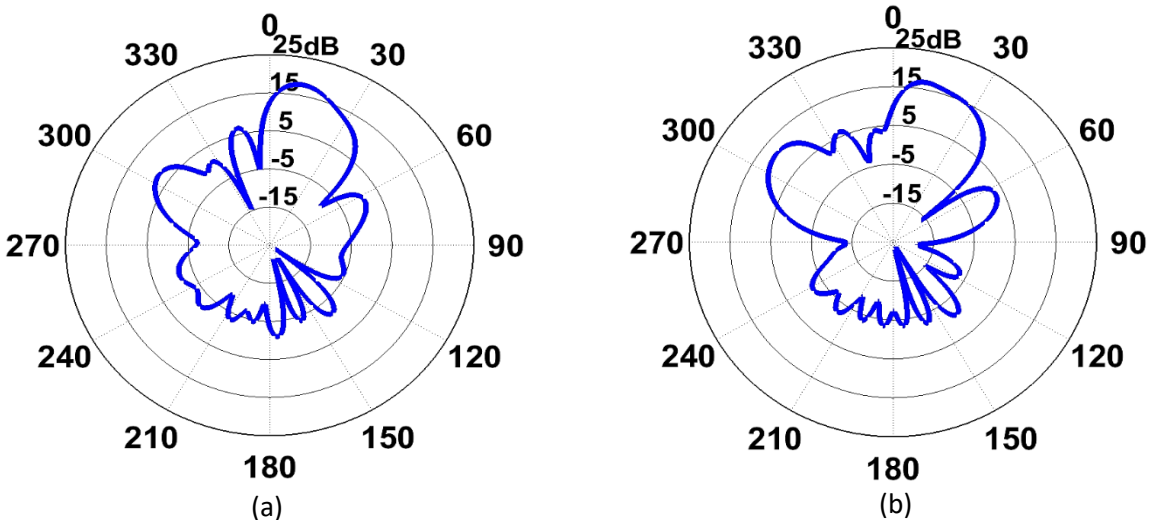

Figs. 7.6: Radiation pattern with main beam at $\theta = +20^o, \Phi = 0^o$ (a) 2.45 GHz, (b) 2.65 GHz.

Similarly, the plots for $\Phi = 45^o$ and $\Phi = 90^o$ have been shown in Figs. 7.7 and 7.8 below.

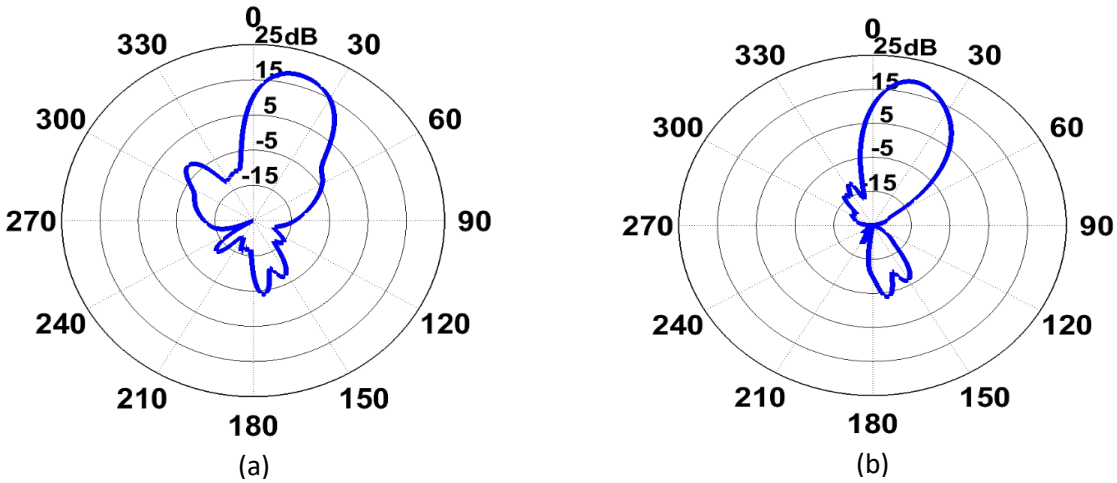

Figs. 7.7: Radiation pattern with main beam at $\theta = +20^o, \Phi = 45^o$ (a) 2.45 GHz, (b) 2.65 GHz.

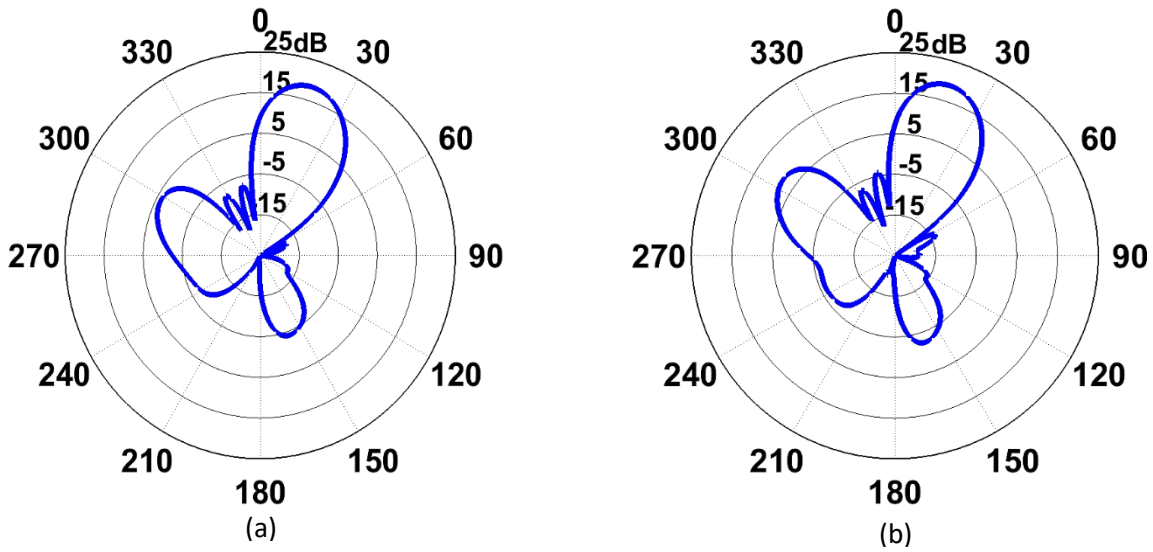

Figs. 7.8: Radiation pattern with main beam at $\theta = +20^o, \Phi = 90^o$ (a) 2.45 GHz, (b) 2.65 GHz.

The trend seen from the six plots shown above is that the realized gain steadily improves as we move the main beam towards $\Phi = 90^o$ i.e. away from the E-plane and toward the H-plane. For the array at 2.45GHz the realized gains are 17.4, 17.8 and 18.6 dBi at $\Phi = 0^o$, $\Phi = 45^o$ and $\Phi = 90^o$ respectively. And at 2.65 GHz, the realized gains are seen to be 16, 18.2 and 18.9 dBi at $\Phi = 0^o$, $\Phi = 45^o$ and $\Phi = 90^o$ respectively and the directivity and backlobe radiation follows the same trend. But the SLL is least when the beam is pointing towards $\Phi = 45^o$ and has value of 19.8 and 32.1 dB at 2.45 and 2.65 GHz.

Chapter 8: Conclusion and Future Work

8.1 Conclusion

A 4X4 aperture coupled planar antenna array was designed, implemented and tested for operation in the 2.3 to 3.1 GHz frequency range. The array offers high gain, low SLL and high F/B all of which are greatly desired in many communication and radar systems. Starting from the design of a single element aperture coupled patch the design focused on (1) a separately fed 4 element linear patch array design and their mutual coupling calculation, (2) a 4 by 4 separately fed planar array design, (3) a corporate-fed 4 by 4 planar array design, (4) an amplitude tapered low SLL corporate fed array design, (5) an experimental prototype build and test of the array, and finally the simulation studies of (6) a separately fed phased array of the antenna. The prototype array fabricated was measured in four different configurations: no reflector, with reflector, no superstrate but with reflector, and with superstrate and with reflector. Measured realized gain observed in the tests were between 16 to 20 dBi depending on the frequency of operation. The measured F/B was in fact better than what was expected from simulation for the reason that the Satimo near-field measurement system lacks the capability to probe the fields within a narrow cone of angle. Simulated F/B was nearly 22 dB in the presence of a reflector nearby. Sidelobe reduction was achieved using an amplitude tapered corporate feed network. Although the theoretical SLL expected was 25 dB measured SLL was in

the vicinity of 20 dB. The deterioration in the SLL can be mainly attributed to manufacturing difficulties which led to the thinner microstrip line sections to be non-uniform due to over-etching in certain sections, hence affecting the power division and match at the T-junctions, which are essential for the required SLLs to be achieved. Another source of error is the misalignment of the four boards while piecing them together to form the array and minor misalignments between the feedlines and apertures. Finally, the proposed array was simulated in a phased array setting which showed that the array beam could be steered at $\pm 30^{o}$ in the lower end of the operating band, while still keeping the grating lobes in check.

8.2 Future Work

Future work should include the integration of phase shifters with the proposed array. A phase shifter called HMC298LP5E could be used for that purpose. This phase shifter has wideband performance which makes it compatible to the proposed wideband array. The main problem one may encounter while trying to develop a PCB for the corporate feed network with the MMIC included would be the small size of the phase shifter. The input, output and control lines that the component requires is only 0.3 mm wide due to its small pad size which is too thin for in house etching. However, such a design can easily be sent to a board house and fabricated. Also, more work can be done to improve the bandwidth of the array by using other substrate and by optimizing the array dimensions. This thesis very briefly goes over the effect of a superstrate/radome structure on antenna radiation and bandwidth. Further research can be done regarding the superstrate materials and the effects of their size, relative permittivity and loss can be

investigated. Finally, the beam scanning at wider scanning angles and throughout the frequency range can be attempted.

References

[1] G. A. Deschamps, “Microstrip Microwave Antennas,” Presented at the Third USAF Symposium on Antennas, 1953.

[2] H. Gutton and G. Baissinot, “Flat Aerial for Ultra High Frequencies,” French Patent No. 703 113, 1955.

[3] R. E. Munson, “Conformal Microstrip Antennas and Microstrip Phased Arrays,” *IEEE Trans. Antennas Propagat.,* Vol. AP-22, No. 1, pp. 74-78, January 1974.

[4] A. G. Derneryd, “Linearly Polarized Microstrip Patch Antennas,” *IEEE Trans. Antennas Propagat.,* Vol. AP-24, No. 6, pp. 846-851, November 1976.

[5] J. W. Howell, “Microstrip Antennas,” *IEEE Trans. Antennas Propagat.,* Vol. AP-23, No. 1, pp. 90-93, January 1975.

[6] D. M. Pozar, “Microstrip antennas”, in *Proceedings of the IEEE*, vol. 80, no. 1, pp. 79-91, Jan 1992.

[7] D. M. Pozar, “A Microstrip Antenna Aperture Coupled to a Microstrip Line”, *Electronics Letters*, Vol. 21, pp. 49-50, Jan 17, 1985.

[8] D. M. Pozar, “A Review of Aperture Coupled Microstrip Antennas: History, Operation, Development, and Applications”, Dept. of Elect. And Comp. Eng., Univ. of Massachusetts at Amherst, Amherst, May 1996.

[9] C. A. Balanis, "*Antenna Theory: Analysis and Design*, 3rd Edition," John Wiley and Sons, Inc., Hoboken, New Jersey, 2005.

[10]Georg Splitt, "Eziente Rechenverfahren zur Analyse von komplexen Einzel- und Gruppenantennen in Streifenleitungstechnik" PhD thesis, Deutsche Forschungsan-stalt fur Luft- und Raumfahrt, 1990.

[11] Georg Splitt, "Guidelines for design of electromagnetically coupled microstrip patch antennas on two-layer substrates," *IEEE Trans. Antennas Propagat.*, AP-38 (7): 1136-1140, July 1990.

[12] S. D. Targonski, R. B. Waterhouse, and D. M. Pozar, "Wide-band aperture-coupled stacked patch antenna using thick substrate," *Electron. Lett.*, vol. 32, no. 21, pp. 1941–1942, Nov. 1996.

[13] J.-F. Zurcher, "The SSFIP: a global concept for high-performance broadband planar antennas," *Electron. Lett, U.K.*, vol. 24, no. 16, pp. 1433–1435, Nov, 1988.

[14]http://www.rohacell.com/sites/lists/RE/DocumentsHP/ROHACELL-HF-mechanical-electrical-properties-EN.pdf

[15] "The Array Factor," http://www.antenna-theory.com/arrays/arrayfactor.php

[16] "Two Dimensional Phased Arrays," http://www.antennatheory.com/arrays/weights/twoDuniform.php

[17] Hubregt J. Visser, "*Array and Phased Array Antenna Basics*," John Wiley and Sons, Inc., Hoboken, New Jersey, 2005.

[18] P. S. Hall and C. M. Hall, "Coplanar corporate feed effects in microstrip patch array design," *in IEE Proceedings H - Microwaves, Antennas and Propagat.*, vol. 135, no. 3, pp. 180-186, Jun 1988.

[19] P.S. Hall, J.S. Dahele and J.R. James, "Design principles of sequentially fed, wide bandwidth, circularly polarised microstrip antennas," *in IEE Proceedings H - Microwaves, Antennas and Propagat.*, Volume 136, Issue 5, p. 381 –389.

[20] David M. Pozer, "*Microwave Engineering,* 4th edition," John Wiley and Sons, Inc., Hoboken, New Jersey, 2012.

[21] F. Yang, X,-X. Zhang, X Ye, and Y. Rahmat-Samii, "Wide-Band E-Shaped Patch Antennas for Wireless Communications," *IEEE Trans. Antennas and Propagat.*, Vol. 49, No. 7, July 2001. Pp. 1094-110.

[22] H. Alias, M. T. Ali, S. S. N. Ramli, M. A. Sulaiman and S. Kayat, "A back lobe reduction of aperture coupled microstrip antenna using DGS," *2013 10th International Conference on Electrical Engineering/Electronics, Computer, Telecommunications and Information Technology*, Krabi, 2013, pp. 1-5.

[23] D. M. Pozar, "A Microstrip Antenna Aperture Coupled to a Microstrip Line", *Electronics Letters*, Vol. 21, pp.49-50, Jan 17, 1985.

[24] P. Sharma and S. Gupta, "Bandwidth and Gain Enhancement in Microstrip Antenna Array for 8 GHz Frequency Applications," *Students Conference on Engineering and Systems (SCES)*, pp. 1-6, 28-30 May 2014.

[25] N.K. Mishra and S. Das, "Investigation of Binomial & Chebyshev Distribution on Dielectric Resonator Antenna Array," *International Conference on Electronic Systems, Signal Processing and Computing Technologies*, 9-11 Jan 2014.

[26] J. F. D. Essiben , M. P. M. Zanga , E. R. Hedin , and Y. S. Joe, "Design of Non-Uniform Linear Antenna Arrays Using Dolph-Chebyshev and Binomial Methods," *Int. Journal of Engineering Research and Applications*, ISSN: 2248-9622, Vol. 5, Issue 8, (Part - 5) Aug 2015, pp.187-195.

[27] http://www.antenna-theory.com/arrays/weights/dolph.php - Dolph-Chebyshev weights.

[28] B. Goswami and D. Mandal, "A genetic algorithm for the level control of nulls and side lobes in linear antenna arrays," *Journal of King Saud University – Computer and Information Sciences*, May 25, 2013, 117-126.

[29] R. L. Haupt and D. H. Werner, "Genetic Algorithms in Electromagnetics," *IEEE Press Wiley-Inter science, 2007.*

[30] F. Harrou, B. Bouyeddou, S. A. Djennas, and L. Merad, "Synthesis and Optimization of Printed Linear Antennas arrays by the Minima Method," *Proc. 5th International Conference: Sciences of Electronic, Technologies of Information and Telecommunications*, Tunisia, 2009, 1-9.

[31] G. Ridha, G. Ali, F. Najib, and R. Mohamed, "Synthesis of the radiation pattern of a linear antennas arrays by the Dolph-Tchebyscheff method," *Proc. 4th International*

Conference: Sciences of Electronic, Technologies of Information and Telecommunications, Tunisia, 2007, 1-4.

[32] W. P. M. N. Keizer, "Fast low sidelobe synthesis for large planar array antennas utilizing successive fast Fourier transforms of the array factor," *IEEE Trans. Antennas Propagat.*, vol. 55, no. 3, pp. 715-722, March 2007.

[33] W. P. M. N. Keizer, "Element failure correction for a large monopulse phased array antenna with active amplitude weighting," *IEEE Trans. Antennas Propagation.*, vol. 55, no. 8, pp. 2211-2218, August 2007.

[34] P. Cardieri and T. S. Rappaport, "Application of narrow-beam antennas and fractional loading factor in cellular communication systems," *IEEE Transactions on Vehicular Technology*, vol. 50, no. 2, pp. 430-440, Mar 2001.

[35] https://www.fcc.gov/general/specific-absorption-rate-sar-cellular-telephones

[36] G. V. Trentini, "Partially reflecting sheet arrays," *IEEE Trans. Antennas Propagat.*, vol. 4, no. 4, pp. 666–671, Oct. 1956.

[37] B. Sasser, "A highly thinned array using the image element*," Proc. Antennas Propagat. Society Int. Symp.,* Jun. 1980, vol. 18, pp. 150–153.

[38] D. Jackson and N. Alexopoulos, "Gain enhancement methods for printed circuit antennas," *IEEE Trans. Antennas Propag.*, vol. 33, pp. 976–987, Sep. 1985.

[39] Christopher J. Meagher, and Satish Kumar Sharma, "A Wideband Aperture-Coupled Microstrip Patch Antenna Employing Spaced Dielectric Cover for Enhanced Gain

Performance," *IEEE Trans. Antennas Propagat.*, VOL. 58, NO. 9, pp. 2802- 2810, Sep 2010.

[40] D. R. Jackson and A. A. Oliner, "A leaky-wave analysis of the high gain printed antenna configuration," *IEEE Trans. Antennas Propagat*., vol. 36, no. 7, pp. 905–910, Jul. 1988.

[41] H. Ostner, J. Detlerfsen, and D. R. Jackson, "Radiation from one-dimensional dielectric leaky-wave antennas," *IEEE Trans. Antennas Propagat.*, vol. 43, no. 4, pp. 331–339, Apr. 1995.

[42] http://www.analog.com/media/en/technical-documentation/data-sheets/hmc928.pdf